Characteristics of Welded-Wire Fabric as Concrete Reinforcement

by

Andrew Griezic

May 1992

Department of Civil Engineering and Applied Mechanics

McGill University, Montréal

A THESIS SUBMITTED TO THE FACULTY OF GRADUATE STUDIES AND RESEARCH IN PARTIAL FULFILMENT FOR THE DEGREE OF MASTER OF ENGINEERING

© ANDREW GRIEZIC, 1992

Abstract

Sixteen tension tests, performed on specimens having cold-rolled, Grade 500, deformed welded-wire fabric and companion specimens reinforced with hot-rolled, Grade 400 steel, show the improved cracking behaviour and the less ductile response of the specimens with welded-wire fabric. An expression for the minimum reinforcement ratio for tension specimens is presented and the influence of high strength concrete on the response is examined.

Two full-scale beams, having welded-wire fabric U-stirrups, were tested to assess the service and ultimate load performance of the welded-wire fabric. By comparing the responses of these beams with two companion beams, reinforced with hot-rolled Grade 400 stirrups, it was demonstrated that the use of welded-wire fabric resulted in better diagonal crack control and enabled large strains to be developed in the stirrups. These tests demonstrated that the full yield stress of the Grade 500 reinforcement can be developed in the stirrups.

Résumé

Seize essais en traction de spécimens de béton, armés d'un treillis d'acier crénelé à mailles soudées, de nuance 500, et sur des spécimens armés de barres de nuance 400 démontrent la meilleure résistance à la fissuration et le comportement moins ductile du spécimen armé d'acier à haute résistance. Une expression pour le pourcentage d'armature minimum est présentée pour le béton armé en traction, et le comportement du béton à haute résistance soumis à un effort normal est examiné.

Deux poutres grandeur réelle, ayant des étriers en U, formés d'un treillis d'acier crénelé à mailles soudées, ont été testées afin de déterminer le comportement du treillis métallique soudé sous l'action des charges prévues et ultimes. Une comparaison de la réponse de ces deux poutres à celles des deux autres ayant des étriers en U, de nuance 400, a démontré que les treillis métalliques soudés ont amélioré la résistance à la fissuration diagonale et ont permis d'atteindre des déformations unitaires élevés dans les étriers. Ces essais ont démontré qu'il est possible de développer la limite d'élasticité de l'acier d'armature de nuance 500.

Acknowledgements

The author would like to express his appreciation to Professor D. Mitchell for his encouragement and skilful guidance throughout this research project. The author would also like to thank Dr. W.D. Cook for his advice and support.

The efforts of Ron Sheppard and John Bartczac in preparing the tests and Jamie Mitchell, Kent Harries and Robert Katz in testing the specimens are greatly appreciated.

The financial support of the Natural Sciences and Engineering Research Council of Canada is gratefully acknowledged.

Table of Contents

Abstract i
Résumé ii
Acknowledgements iii
List of Figures vi
List of Tables ix
List of Symbols x

Chapter 1 Introduction 1
1.1 Welded-Wire Fabric 1
1.1.1 Advantages of Welded-Wire Fabric 1
1.1.2 Material Properties of Welded-Wire Fabric 2
1.2 High Performance Concrete 3
1.3 Behaviour of Reinforced Concrete Under Axial Tension 5
1.3.1 Crack Widths and Crack Spacings 6
1.3.2 Minimum Reinforcement for Crack Control 8
1.4 Shear Tests 9
1.4.1 CSA Standard Code Requirements for Welded-Wire Fabric as Shear Reinforcement 9
1.4.2 The Compression Field Theory 10
1.4.3 The Modified Compression Field Theory 14
1.4.4 The Staggering Concept for Shear Design 17
1.4.5 Previous Research on Welded-Wire Fabric 18
1.5 Objectives 19

Chapter 2 Experimental Programme 21
2.1 Pure Tension Tests 21
2.1.1 Description of Test Specimens 21
2.1.2 Test Setup 24
2.1.3 Instrumentation 24
2.1.4 Concrete Material Properties 25
2.1.5 Reinforcement Properties 27
2.2 Tee-Beam Tests 29
2.2.1 Description of Test Specimens 29
2.2.2 Test Setup 33
2.2.3 Instrumentation 35
2.2.4 Concrete Material Properties 38
2.2.5 Reinforcement Properties 39

Chapter 3 Measured and Predicted Responses of Pure Tension Specimens 40
3.1 Predicting Responses of the Tension Members 40
3.2 Low-Strength Concrete Tension Tests 41
3.2.1 Specimens T1 (f_y = 589 MPa) and T3 (f_y = 407 MPa) 43
3.2.2 Specimens T2 (f_y = 589 MPa) and T4 (f_y = 407 MPa) 46
3.2.3 Specimens T9 (f_y = 589 MPa) and T10 (f_y = 407 MPa) 49
3.2.4 Specimens T11 (f_y = 589 MPa) and T12 (f_y = 407 MPa) 52

Table of Contents *(cont'd)*

3.3 High-Strength Concrete Tension Tests 55
3.3.1 Specimens T5 (f_y = 589 MPa) and T7 (f_y = 407 MPa) 56
3.3.2 Specimens T6 (f_y = 589 MPa) and T8 (f_y = 407 MPa) 59
3.3.3 Specimens T13 (f_y = 589 MPa) and T14 (f_y = 407 MPa) 62
3.3.4 Specimens T15 (f_y = 589 MPa) and T16 (f_y = 407 MPa) 65

3.4 Influence of Reinforcement Properties, Concrete Strength and Reinforcement Ratio on the Response 68
3.5 Minimum Reinforcement Ratio for Crack Control 74

Chapter 4 Observed Responses of Tee Beams 76
4.1 Tee Beam Subjected to High Shear (TH500) 76
4.2 Tee Beam Subjected to Moderate Shear (TM500) 88
4.3 Comparison of Responses of Beams TH500 and TM500 99

Chapter 5 Predicted Responses of Tee Beams 101
5.1 Analysis Using CSA Standard's Equations 101
5.2 Computer Analysis Using Program "RESPONSE" 102
5.3 Comparison of Strength Predictions with Test Results 104

Chapter 6 Effectiveness of Welded-Wire Fabric as Shear Reinforcement 110
6.1 Measured Responses 112
6.1.1 Load-Deflection Response 12
6.1.2 Stirrup Strains 114
6.1.3 Shear Crack Widths 114
6.2 Predicted Responses 121

Chapter 7 Conclusions 126
7.1 Conclusions 126
7.2 Future Research 128

References 130

Appendix A "RESPONSE" Data Files 132

List of Figures

Chapter 1
1-1 Typical stress-strain characteristics of different types of reinforcement 2
1-2 Typical compressive stress-strain curves for different concrete strengths 4
1-3 Anchorage requirements for smooth welded-wire fabric U-shape stirrups 10
1-4 Equilibrium conditions for the variable-angle truss model 11
1-5 Limiting values of the principal angle of compression for different levels of shear stress 13
1-6 The staggering concept for shear design 17

Chapter 2
2-1 Cross-sectional dimensions and reinforcement details of tension specimens 22
2-2 Photograph of tension test setup 24
2-3 Typical stress-strain response of 70 MPa and 20 MPa concretes 26
2-4 Stress-strain response of Grade 500, welded-wire fabric and Grade 400, hot-rolled reinforcement 28
2-5 Photograph showing prefabricated stirrup cage for beam TH500 32
2-6 Reinforcement details of tee beam specimens TH500 and TM500 30
2-7 Reinforcement details of companion beams tested by Mailhot 31
2-8 Beam loading apparatus used to simulate uniform loading 34
2-9 Assumed and actual loading patterns for tee-beam tests 33
2-10 Overall view of TH500 before loading 35
2-11 Location of Demec targets and strain rosettes 36
2-12 Photograph of Demec targets epoxied directly to the stirrups 37

Chapter 3
3-1 (a) Load versus average strain response of Specimens T1 and T3 44
3-1 (b) Comparison of predicted and measured responses of Specimens T1 and T3 44
3-1 (c) Load versus maximum crack width for Specimen T1 45
3-1 (d) Load versus maximum crack width for Specimen T3 45
3-2 (a) Load versus average strain response of Specimens T2 and T4 47
3-2 (b) Comparison of predicted and measured responses of Specimens T2 and T4 47
3-2 (c) Load versus maximum crack width for Specimen T2 48
3-2 (d) Load versus maximum crack width for Specimen T4 48
3-3 (a) Load versus average strain response of Specimens T9 and T10 50
3-3 (b) Comparison of predicted and measured responses of Specimens T9 and T10 50
3-3 (c) Load versus maximum crack width for Specimen T9 51
3-3 (d) Load versus maximum crack width for Specimen T10 51
3-4 (a) Load versus average strain response of Specimens T11 and T12 53
3-4 (b) Comparison of predicted and measured responses of Specimens T11 and T12 . . . 53
3-4 (c) Load versus maximum crack width for Specimen T11 54
3-4 (d) Load versus maximum crack width for Specimen T12 54
3-5 (a) Load versus average strain response of Specimens T5 and T7 57
3-5 (b) Comparison of predicted and measured responses of Specimens T5 and T7 57
3-5 (c) Load versus maximum crack width for Specimen T5 58
3-5 (d) Load versus maximum crack width for Specimen T7 58

List of Figures *(cont'd)*

3-6 (a) Load versus average strain response of Specimens T6 and T8 60
3-6 (b) Comparison of predicted and measured responses of Specimens T6 and T8 60
3-6 (c) Load versus maximum crack width for Specimen T6 61
3-6 (d) Load versus maximum crack width for Specimen T8 61
3-7 (a) Load versus average strain response of Specimens T13 and T14 63
3-7 (b) Comparison of predicted and measured responses of Specimens T13 and T14 . . . 63
3-7 (c) Load versus maximum crack width for Specimen T13 64
3-7 (d) Load versus maximum crack width for Specimen T14 64
3-8 (a) Load versus average strain response of Specimens T15 and T16 66
3-8 (b) Comparison of predicted and measured responses of Specimens T15 and T16 . . . 66
3-8 (c) Load versus maximum crack width for Specimen T15 67
3-8 (d) Load versus maximum crack width for Specimen T16 67
3-9 Steel stress at cracking as a function of the reinforcing index 68
3-10 Steel stress at cracking as a function of the reinforcement ratio for specimens reinforced with Grade 400, hot-rolled steel 69
3-11 Steel stress at cracking as a function of the reinforcement ratio for specimens reinforced with Grade 500, cold-rolled welded-wire fabric 70
3-12 Cracking patterns of specimens having the lowest and highest reinforcement ratios in the low-strength concrete test series 72
3-13 Cracking patterns of specimens having the lowest and highest reinforcement ratios in the high-strength concrete test series 73

Chapter 4

4-1 Load-deformation response of tee beam subjected to a high shear (TH500) 77
4-2 Crack patterns in west end of beam TH500 80
4-3 Crack patterns in east end of beam TH500 81
4-4 Stirrup strains in the top and bottom of each stirrup for west half of TH500 82
4-5 Stirrup strains in the top and bottom of each stirrup for east half of TH500 83
4-6 Maximum and average stirrup strains measured in each stirrup for west half of TH500 84
4-7 Maximum and average stirrup strains measured in each stirrup for east half of TH500 85
4-8 Load versus maximum shear crack width in west end of TH500 86
4-9 Load versus maximum shear crack width in east end of TH500 86
4-10 Magnitudes and directions of principal strains measured in TH500 near failure 87
4-11 Load-deformation response of tee beam subjected to a moderate shear (TM500) . . . 88
4-12 Crack patterns in west end of beam TM500 91
4-13 Crack patterns in east end of beam TM500 92
4-14 Stirrup strains in the top and bottom of each stirrup for west half of TM500 93
4-15 Stirrup strains in the top and bottom of each stirrup for east half of TM500 94
4-16 Maximum and average stirrup strains measured in each stirrup for west half of TM500 95
4-17 Maximum and average stirrup strains measured in each stirrup for east half of TM500 96
4-18 Load versus maximum shear crack width in west end of TM500 97

List of Figures *(cont'd)*

4-19 Load versus maximum shear crack width in east end of TM500 97
4-20 Magnitudes and directions of principal strains measured in TM500 near failure 98
4-21 Beams TH500 (top) and TM500 (bottom) at respective ultimate loads 100
4-22 Beams TH500 (top) and TM500 (bottom) after removal of loading apparatus 100

Chapter 5
5-1 Discretization of beam cross-section and material stress-strain relationships used in RESPONSE predictions 103
5-2 Comparison of predicted and experimental shear and moment diagrams at failure for TH500 105
5-3 Comparison of predicted and experimental shear and moment diagrams at failure for TM500 106

Chapter 6
6-1 Load deformation responses of beams subjected to a high shear 113
6-2 Load deformation responses of beams subjected to a moderate shear 113
6-3 (a) Maximum strains measured in the stirrups at service and ultimate load levels in the west half of the beams subjected to a high shear 115
6-3 (b) Maximum strains measured in the stirrups at service and ultimate load levels in the east half of the beams subjected to a moderate shear 115
6-4 (a) Maximum strains measured in the stirrups at service and ultimate load levels in the west half of the beams subjected to a high shear 116
6-4 (b) Maximum strains measured in the stirrups at service and ultimate load levels in the east half of the beams subjected to a moderate shear 116
6-5 Maximum shear crack widths in west end of beams subjected to a high shear 117
6-6 Maximum shear crack widths in east end of beams subjected to a high shear 118
6-7 Maximum shear crack widths in west end of beams subjected to a moderate shear . . 119
6-8 Maximum shear crack widths in east end of beams subjected to a moderate shear . . 120
6-9 Comparison of predicted and experimental shear and moment diagrams at failure for Beam A 123
6-10 Comparison of predicted and experimental shear and moment diagrams at failure for Beam B 124

List of Tables

Chapter 1
1-1 Values of β and θ for design using the Modified Compression Field Theory 16

Chapter 2
2-1 Description of pure tension test specimens 23
2-2 Material properties of concrete batches for tension specimens 25
2-3 Mix design for 70 MPa concrete 27
2-4 Mix design for 20 MPa concrete 27
2-5 Properties of reinforcement for tension specimens 28
2-6 Material properties of concrete for beam specimens 38
2-7 Mix design for 30 MPa concrete 38
2-8 Properties of reinforcement for beam specimens 39

Chapter 3
3-1 Summary of low-strength concrete tension tests 41
3-2 Crack characteristics of low-strength concrete specimens 42
3-3 Summary of high-strength concrete tension tests 55
3-4 Crack characteristics of high-strength concrete specimens 55

Chapter 4
4-1 Comparison of shear response characteristics in west halves of TH500 and TM500 ... 99

Chapter 5
5-1 Strength predictions using the Compression Field Theory 102
5-2 Predicted failure loads from combined shear and moment analyses using RESPONSE with Modified Compression Field Model for shear 104
5-3 Comparison of test results and shear strength predictions 107
5-4 Predicted and measured strains at service load levels 108
5-5 Strength predictions using nominal yield and maximum yield 109

Chapter 6
6-1 Design parameters and reinforcement details of the four tee beams 111
6-2 Comparison of the measured responses of the beams reinforced with WWF stirrups and the beams with hot-rolled stirrups 112
6-3 Strength predictions using the Compression Field Theory 121
6-4 Predicted failure loads from combined shear and moment analyses using RESPONSE with Modified Compression Field Model for shear 122
6-5 Comparison of test results and shear strength predictions 125

List of Symbols

a	maximum aggregate size
A	effective area of concrete surrounding each reinforcing bar
A_c	net area of concrete
$A_{c,ef}$	area of effective embedment zone of the concrete where the reinforcing bars can influence the crack widths
A_s	cross-sectional area of steel reinforcement
A_v	cross-sectional area of stirrup reinforcement
b_v	minimum effective web width
b_w	effective web width
c	clear concrete cover
D	principal diagonal compressive force
d_b	diameter of reinforcing bar
d_c	distance from extreme tension fibre to centre of the closest bar
d_v	effective shear depth
E_c	modulus of elasticity of concrete
E_s	modulus of elasticity of reinforcing steel
f_c	concrete stress
f'_c	compressive strength of concrete
f_{cr}	direct tensile strength of concrete
f_r	modulus of rupture of concrete
f_s	steel stress
$f_{s,cr}$	stress in the reinforcing steel at a crack
f_{sp}	average split cylinder strength of concrete
f_u	tensile strength of the reinforcement
f_y	yield stress of reinforcing steel
f_2	diagonal compressive stress
f_{2max}	compressive strength of diagonally cracked concrete
k_1	coefficient that characterizes bond properties of reinforcing bars
k_2	coefficient to account for strain gradient
ℓ_n	clear span
M_{cr}	cracking moment resistance of concrete
M_f	factored moment
M_r	factored moment resistance
M_u	maximum measured applied moment
N	applied axial tension
N_f	factored axial tension
N_v	longitudinal tensile force
P_{cr}	axial load at first cracking
P_u	applied axial load at ultimate
s	maximum distance between longitudinal reinforcing bars ($s \leq 15\ d_b$)
s	spacing of stirrups
s_m	mean crack spacing
$s_{m\theta}$	mean crack spacing of the inclined shear cracks
V	applied shear force
V_c	shear resistance provided by the concrete
V_{cr}	cracking shear resistance of concrete
V_f	factored shear force
V_r	factored shear resistance
V_s	shear capacity of the stirrups

List of Symbols *(cont'd)*

V_{se}	shear at service load level
V_{supp}	shear force at support face
V_u	maximum shear observed
w	crack width, equal to $\epsilon_1 s_{m\theta}$
w_f	factored applied uniform load
w_m	mean crack width
w_{max}	maximum crack width
w_r	uniform load corresponding to the predicted capacity
w_{se}	service load
w_u	maximum measured applied uniform load
α_1	factor accounting for bond characteristics of reinforcement
α_2	factor accounting for sustained or repeated loading
β	factor accounting for strain gradient
β	residual tensile stress factor
ϵ	average member strain, for a reinforced concrete section in tension
ϵ_c	strain in the concrete
ϵ'_c	peak strain corresponding to f'_c
ϵ_{cf}	strain in concrete caused by stress
ϵ_{meas}	maximum strain in the stirrups at service load
ϵ_{rupt}	strain in reinforcing bar at rupture
ϵ_s	strain in the reinforcing steel
ϵ_{se}	predicted tensile strain in transverse reinforcement due to service load
$\epsilon_{s,cr}$	strain in the reinforcing bar at a crack location
ϵ_{sh}	shrinkage strain of concrete, shrinkage negative
ϵ_t	transverse strain, tension positive
ϵ_u	average strain in reinforced concrete section, corresponding to P_u
ϵ_x	longitudinal strain at mid-depth of the web, tension positive
ϵ_1	principal tensile strain, tension positive
ϵ_2	principal compressive strain, compression negative
θ	angle of inclination of diagonal compressive stresses measured from the longitudinal axis
of the	member, degrees
θ_{min}	minimum angle of principal compression, degrees
θ_{max}	maximum angle of principal compression, degrees
λ	factor accounting for the density of concrete
ρ	reinforcement ratio, equal to A_s / A_c
ρ_{ef}	$A_s / A_{c,ef}$
ρ_{min}	minimum reinforcement ratio required for crack control
ϕ_c	resistance factor for concrete, equal to 0.6
ϕ_s	resistance factor for reinforcing steel, equal to 0.85

Chapter 1

Introduction

This research program was undertaken in order to examine the properties of welded-wire fabric used in reinforced concrete construction and its suitability in tension specimens and as shear reinforcement in beams.

1.1 Welded-Wire Fabric

Welded-wire fabric is assembled with a series of longitudinal and transverse cold-rolled deformed steel wires, resistance welded at their intersections. The longitudinal wires are fed into an automatic welding machine which positions, then welds the transverse wires at the specified spacings. Welded-wire fabric is a versatile type of reinforcement since it can be used as a flat sheet for slab reinforcement or can be bent into a variety of shapes to serve as stirrup or column cages. A bending machine with many mandrel sizes is used to obtain the desired bend angle while providing the required bend radius.

1.1.1 Advantages of Welded-Wire Fabric

Welded-wire fabric has been used successfully in precast concrete construction and slabs on grade, but is not as common in cast-in-place construction in North America. Welded-wire fabric is used more extensively in Europe. Significant savings of labour costs could be realized if welded-wire fabric were used as reinforcement in cast-in-place structural members, such as slabs, beams and columns. Studies have shown (Ref. 1 and Ref. 2) that time savings of 70%

were realized by placing prefabricated welded-wire fabric stirrup cages versus assembling conventional stirrup cages on site. Furthermore, the well controlled fabrication process results in better dimensional tolerances in the placement of the reinforcement.

The nominal yield strength of welded-wire fabric is 500 MPa as compared to 400 MPa for normal reinforcing bars. Substituting the higher strength steel for standard reinforcement can also result in savings on the total amount of reinforcement required.

1.1.2 Material Properties of Welded-Wire Fabric

The cold-rolled deformed wire that constitutes welded-wire fabric has a specified minimum yield strength (Ref. 3) of 485 MPa and a minimum tensile strength of 550 MPa.

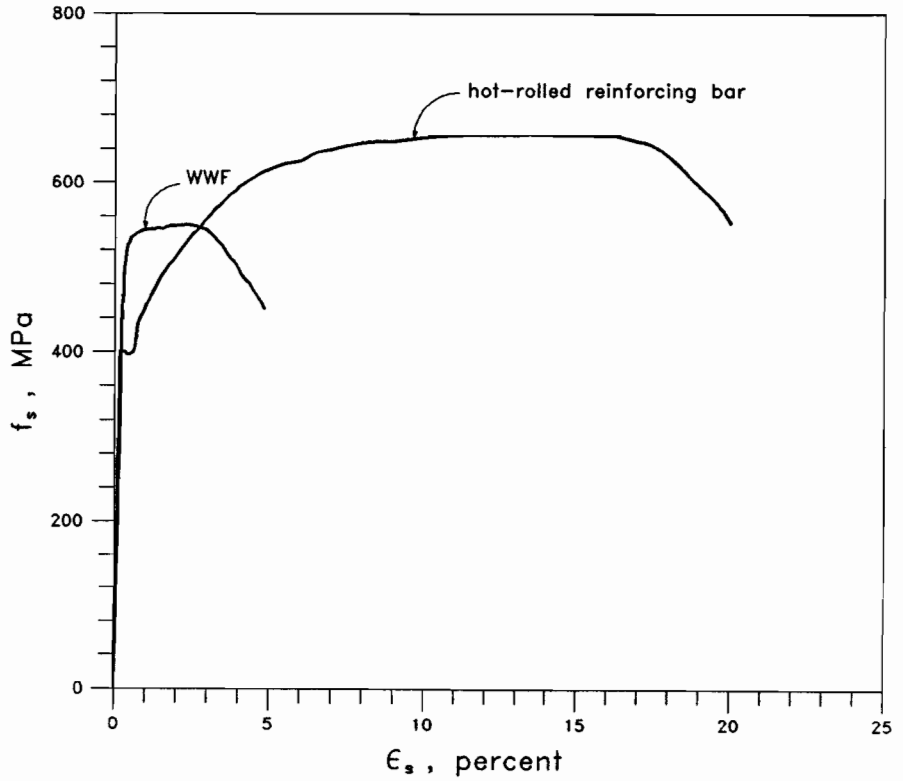

Figure 1-1 Typical stress-strain characteristics of different types of reinforcement

As shown in Fig. 1-1, cold-rolled welded-wire fabric does not have a definite yield point and typically has a higher yield stress but a lower ultimate stress than Grade 400 hot-rolled reinforcing

bars. The increased yield strength is usually accompanied by a reduction in ductility. This inherent reduction in ductility is a major concern to engineers since the desired mode of failure of reinforced concrete members, is yielding of the tension steel, followed by crushing of the concrete, as this type of response warns of impending failure. The validity of the ultimate elongation as a measure of the ductility of deformed wire was challenged by Dove (Ref. 4) and it was suggested that the true indicator of the ductility of cold-drawn wire is the bend test, in which the wire is bent through 90 degrees. In this bend test, as specified in G30.14-M83 (Ref. 3), the outermost tension fibre of the wire must undergo an elongation of 50% without cracking on the outside of the bent portion. Dove also proposed that the amount of reduction of area at fracture is a better measure of ductility than the elongation at rupture, since the amount of local plastic deformation under triaxial stresses is determined at the point where necking occurs.

The sheets of welded-wire fabric and the strength of the welds must conform to G30.15-M83 (Ref. 5). In the past, welded-wire fabric, when tested in tension, would fail at the cross tie location. However, using electric resistance welding has succeeded in causing a tension specimen to fail away from the cross-ties. A metallurgical investigation was performed (Ref. 6), which involved the microhardness testing of the heat-affected zones at the cross-ties, and determined that the welds are not prone to brittle fracture.

1.2 High Performance Concrete

By using lower water/cement ratios, it is possible to produce high strength concrete having compressive strengths in excess of 40 MPa. Reducing the quantity of water used in a concrete mix reduces the spacing between cement particles, thus creating a more dense, stronger material. As the compressive strength of the concrete is increased, the aggregate strength eventually governs the maximum strength that the concrete can achieve, since the cementious paste becomes stronger than the aggregates.

Typical compressive stress-strain curves for high strength and normal strength concretes

are shown in Fig. 1-2. The high strength concrete has a much stiffer response under a compressive load than the normal strength concrete. The modulus of elasticity of normal weight concrete is typically given as:

$$E_c = 5000\sqrt{f'_c} \quad , MPa \tag{1-1}$$

where f'_c is the compressive strength of concrete in MPa units.

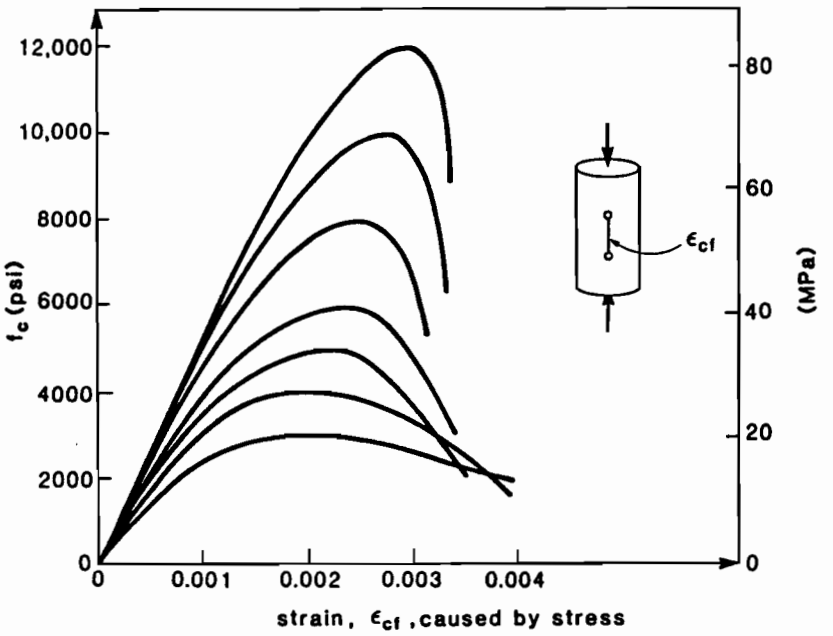

Figure 1-2 Typical compressive stress-strain curves for different concrete strengths, tested by Nilson (Ref. 7). From Ref. 10.

Carrasquillo, Nilson and Slate (Ref. 8) found that Eq. 1-1 overestimates the stiffness of normal-weight concretes having compressive strengths greater than 40 MPa and suggested the following relationship between the modulus of elasticity of concrete and its compressive strength:

$$E_c = 3320\sqrt{f'_c} + 6900 \ , \ MPa \tag{1-2}$$

The direct tensile strength of the concrete, f_{cr}, is normally taken as $0.33\sqrt{f'_c}$ MPa for all concrete

strengths (Ref. 9). It can also be seen in Fig. 1-2 that high strength concrete reaches a greater peak strain, ϵ'_c, than normal strength concrete but exhibits a less ductile response than normal strength concrete.

1.3 Behaviour of Reinforced Concrete Under Axial Tension

The load-strain response of a reinforced concrete member can be determined using the approach developed by Collins and Mitchell (Ref. 10). The tensile load carried by a reinforced concrete section is given by:

$$N = A_c f_c + A_s f_s \tag{1-3}$$

where: N = applied axial tension
A_c = net area of concrete
f_c = concrete stress
A_s = area of steel reinforcement
f_s = steel stress.

Before cracking, the stress-strain relationship for the concrete is assumed to be linear where:

$$f_c = E_c \epsilon_{cf} \tag{1-4}$$

where: E_c = secant modulus of elasticity of the concrete
ϵ_{cf} = strain in the concrete caused by stress.

Once the specimen cracks, the steel stress at the crack increases suddenly. At the crack, the load must be transferred from the exposed bar to the concrete. Goto (Ref. 11) demonstrated that the load is transferred from the reinforcing bar to the surrounding concrete through inclined radial forces. The overall stiffness of a reinforced concrete member must therefore depend on the bond characteristics of the reinforcement.

At cracking, the average stress in the concrete is equal to f_{cr}. After cracking, the magnitude of the average tensile stress in the concrete decreases with increasing levels of axial strain and is given by (Ref. 10 and 12):

$$f_c = \frac{\alpha_1 \alpha_2 f_{cr}}{1 + \sqrt{500 \epsilon_{cf}}} \qquad (1\text{-}5)$$

where: α_1 = factor accounting for bond characteristics of reinforcement
α_1 = 1.0 for deformed reinforcing bars
α_1 = 0.7 for plain bars, wires, or bonded strands
α_2 = 1.0 for short-term monotonic loading
f_{cr} = direct tensile strength of concrete.

The complete response of a member subjected to axial tension is determined by an iterative procedure which involves first assuming a total concrete strain, ϵ_c. In order to determine the corresponding stress in the concrete, the strain, ϵ_{cf}, caused by stress, must first be determined. The strain caused by stress is given by:

$$\epsilon_{cf} = \epsilon_c - \epsilon_{sh} \qquad (1\text{-}6)$$

where ϵ_{sh} = shrinkage strain of concrete (negative quantity).

For this given strain, the average stress in the concrete can be determined from either Eq. 1-4, if ϵ_{cf} is less than the cracking strain, ϵ_{cr}, or from Eq. 1-5, if ϵ_{cf} exceeds ϵ_{cr}. Due to compatibility of strains and assuming perfect bond between the steel and the concrete, the strain in the steel, ϵ_s, is equal to ϵ_c. At a crack location, the tensile stress in the concrete is zero and the axial tension must be carried solely by the reinforcement. Hence, for a concrete member reinforced with steel having a bi-linear stress-strain relationship, the maximum load carrying capacity is governed by the yield force of the steel, $A_s f_y$.

1.3.1 Crack Widths and Crack Spacings

Tension tests have been carried out to determine the influence of longitudinal and transverse reinforcement on the distance between cracks in reinforced concrete members. Concrete can only withstand a small tensile strain before it cracks. Because cracks do not form at equal spacings, the crack widths will vary in size and it is therefore appropriate to define the

mean crack width, w_m, as a function of the axial strain in the member such that:

$$w_m = \epsilon_{cf} s_m \tag{1-7}$$

where: s_m = the mean crack spacing
ϵ_{cf} = strain in the concrete caused by stress.

The maximum crack width, w_{max}, can be predicted according to the CEB-FIP Code expression (Ref. 13) from:

$$w_{max} = 1.7\, w_m \tag{1-8}$$

where w_m is the mean crack width from Eq. 1-7.

In Equation 1-7, the mean crack spacing, s_m, is given by:

$$s_m = 2\left(c + \frac{s}{10}\right) + k_1 k_2 \frac{d_b}{\rho_{ef}} \tag{1-9}$$

where: c = clear concrete cover
s = maximum spacing between longitudinal reinforcing bars but shall not be taken as greater than 15 d_b
d_b = diameter of reinforcing bar
$\rho_{ef} = A_s / A_{c,ef}$
A_s = area of steel considered to be effectively bonded to the concrete
$A_{c,ef}$ = area of effective embedment zone of the concrete where the reinforcing bars can influence the crack widths
k_1 = coefficient that characterizes bond properties of reinforcing bars
k_1 = 0.4 for deformed bars
k_1 = 0.8 for plain bars
k_2 = coefficient to account for strain gradient
$k_2 = 0.25\ (\epsilon_1 + \epsilon_2)/2\ \epsilon_1$
(ϵ_1 and ϵ_2 are the largest and the smallest tensile strains in the effective embedment zone).

The maximum crack widths can also be estimated using the Gergely-Lutz expression (Ref. 14), given by:

$$w_{max} = 2.2 \beta \epsilon_{s,cr} \sqrt[3]{d_c A} \tag{1-10}$$

where: β = factor accounting for strain gradient, 1.0 for uniform strains
$\epsilon_{s,cr}$ = strain in the reinforcing bar at a crack location
d_c = distance from extreme tension fibre to centre of the closest bar

A = effective area of concrete surrounding each bar, taken as the total area of concrete in tension which has the same centroid as the tension reinforcement, divided by the number of bars.

In the Gergely-Lutz expression, the strain in the reinforcement at a crack is computed as:

$$\epsilon_{s,cr} = \frac{N}{E_s} \qquad (1\text{-}11)$$

where E_s = modulus of elasticity of steel.

Tension tests were performed by Rizkalla, Hwang and El Shahawi (Ref. 15) to determine the influence of transverse reinforcement on crack spacings. They found that if a concrete section which contains no transverse reinforcement is subjected to an axial load, the cracks formed at random spacings along the member. Transverse reinforcement acts as a crack initiator by reducing the net area of concrete at a section and causing an increased stress. Their research found that if the spacing of the transverse reinforcement is similar to the average crack spacing, s_m, the cracks would form at the location of the cross bars. These cross-bars would therefore act as crack initiators and result in an almost uniform crack distribution along the length of the member.

1.3.2 Minimum Reinforcement for Crack Control

Axially loaded reinforced concrete members crack once the average stress exceeds the direct tensile strength of the concrete, f_{cr}. Once a crack forms, the stress in the reinforcing steel at the crack, $f_{s,cr}$, increases suddenly. The ability of the steel to carry the applied load at a crack determines the crack control characteristics of the member.

Williams (Ref. 16) tested reinforced concrete sections in pure tension that had reinforcement ratios ranging from 0.24% to 2.30%. According to his results, a reinforcement ratio of 0.24% did not provide adequate crack control and a ratio of 0.38% only offered marginal crack control. If the concrete cracked before the average stress in the section reached the yield strength of the steel, adequate crack control was provided. For a reinforced concrete member

subjected to axial tension and reinforced with steel having a bi-linear stress-strain relationship, the steel must be capable of resisting the cracking load of the concrete. Hence:

$$A_c f_{cr} = A_{s,min} f_y \tag{1-12}$$

Rearranging Eq. 1-12 yields an expression for the minimum reinforcement ratio, ρ_{min}, required for crack control such that:

$$\rho_{min} = \frac{A_{s,min}}{A_c} = \frac{f_{cr}}{f_y} \tag{1-13}$$

Supplying the minimum amount of steel reinforcement as given by Eq. 1-13 will ensure that cracking will occur below the yield strength of the steel and hence provide adequate crack control.

1.4 Shear Tests

1.4.1 CSA Standard Requirements for Welded-Wire Fabric as Shear Reinforcement

The maximum yield strength to be used in shear design calculations is limited to 400 MPa (Ref. 17, §11.2.2.5), in order to avoid a sudden, brittle shear failure. Hence, using Grade 500 welded-wire fabric instead of Grade 400 reinforcing bars as stirrups, would not lead to a reduction of the amount of stirrups required.

Clause 11.2.2.1 (Ref. 17) allows welded-wire fabric to be used as shear reinforcement if a tension specimen, which includes at least one transverse wire, can undergo a minimum elongation of 4% over a gauge length of 100 mm. This requirement was included in the CSA Standard (Ref. 17), in addition to the requirements of CSA standard G30.14 (Ref. 3), to ensure that the deformed wire stirrups are capable of developing significant strains prior to failure.

No specific requirement is given in the CSA Standard for the anchorage of deformed welded-wire fabric U-shape stirrups. The anchorage requirement given by Clause 12.13.2 (c) (Ref. 17) for smooth welded-wire fabric U-stirrups is shown in Fig. 1-3. Mansur et al. (Ref. 18)

determined that two cross wires having the same diameter as the stirrups and welded at the top of the stirrup cage provide adequate anchorage for deformed welded-wire fabric U-stirrups.

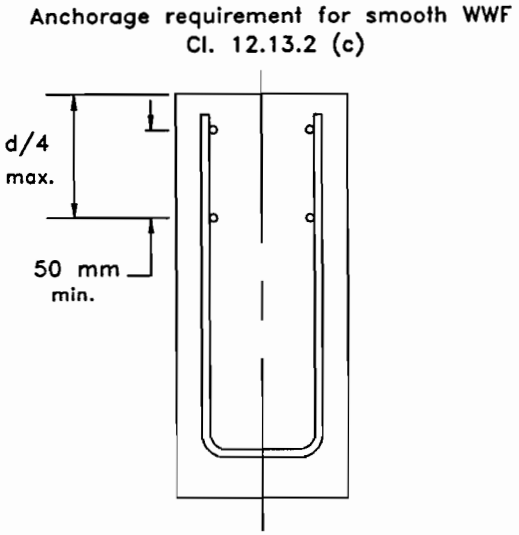

Figure 1-3 Anchorage requirements for smooth welded-wire fabric U-shape stirrups

1.4.2 The Compression Field Theory

The Compression Field Theory (Ref. 19) is based on the variable angle truss model which assumes that the shear is carried by diagonal compressive struts, inclined at an angle, θ, to the horizontal axis. The equilibrium conditions that exist at a section of the beam are shown in Fig. 1-4b. In order to equilibrate the shear, V, the diagonal compressive force is equal to V/sin θ. The magnitude of the principal compressive force, D, is given by:

$$D = f_2 b_w d_v \cos\theta \qquad (1\text{-}14)$$

where: f_2 = diagonal compressive stress
b_w = effective web width
d_v = effective shear depth
θ = angle of inclination of the diagonal compressive stresses to the longitudinal axis of the member, degrees.

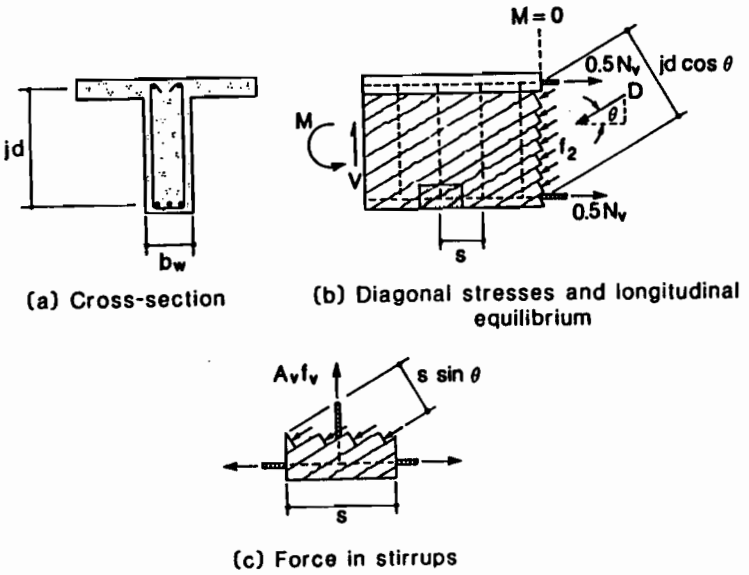

Figure 1-4 Equilibrium conditions for the variable-angle truss model. Taken from Ref. 10.

Substituting V=sin θ into Eq. 1-14 yields the magnitude of the principal compressive stress as:

$$f_2 = \frac{V}{b_w d_v} \frac{1}{\sin\theta\cos\theta} \tag{1-15}$$

The horizontal component of the diagonal compressive force must be balanced by a longitudinal tensile force, N_v, given as:

$$N_v = \frac{V}{\tan\theta} \tag{1-16}$$

The vertical component of the diagonal compression must be balanced by a tensile force in the stirrups, which at yield is $A_v f_y$. From the free-body diagram shown in Fig. 1-4c, it can be seen that the amount of stirrups required to resist the shear can be determined from:

$$\frac{A_v f_y}{s} = V\frac{\tan\theta}{d_v} \tag{1-17}$$

where: A_v = cross-sectional area of stirrups
f_y = yield stress of stirrup reinforcement
s = spacing of stirrups.

A method of determining the principal angle of compression is required in order to apply the above equilibrium equations in shear design. The Compression Field Theory, as given in the 1984 CSA Standard, assumes that after cracking, the concrete does not carry any tension and that the shear is carried by a field of diagonal compression. This theory utilizes strain compatibility to relate the angle of principal compression, θ, to the strains as follows (Ref. 19):

$$\tan^2\theta = \frac{\epsilon_x - \epsilon_2}{\epsilon_t - \epsilon_2} \qquad \textbf{(1-18)}$$

where: ϵ_x = longitudinal strain at mid-depth of the web, tension positive
ϵ_t = transverse strain, tension positive
ϵ_2 = principal compressive strain, compression negative.

The stress-strain relationship for the diagonally cracked concrete web differs from that determined from a compressive cylinder test, due to the tensile straining of the concrete in a direction perpendicular to the principal compressive stress. As a result of tests on reinforced concrete shear panels, Vecchio and Collins (Ref. 12 and Ref. 20) suggested the following relationship for the compressive strength of diagonally cracked concrete, f_{2max}:

$$f_{2max} = \frac{f'_c}{0.8 - 0.34\frac{\epsilon_1}{\epsilon'_c}} \leq f'_c \qquad \textbf{(1-19)}$$

By examining Eq. 1-19, it can be seen that the diagonal compressive strength depends on the magnitude of the principal tensile strain, ϵ_1. It is possible to determine the shear strength of a reinforced concrete beam by applying the above equilibrium equations, the compatibility equation for the strains and by determining the crushing strength of the concrete with Eq. 1-19.

The CSA Standard (Ref. 17) suggests two methods of designing members for shear and torsion, the Simplified Method and the General Method. The General Method for shear design is based on the compression field theory and offers some simplifications for design. In order to provide a ductile shear response, a minimum value of θ can be chosen such that crushing of the

diagonally cracked concrete does not occur, that is $f_2 \leq f_{2max}$. The limiting values of θ can be determined from Eqs. 1-15, 1-18 and 1-19 and can be plotted as a function of the applied shear stress level as well as the longitudinal strain, ϵ_x (see Fig. 1-5).

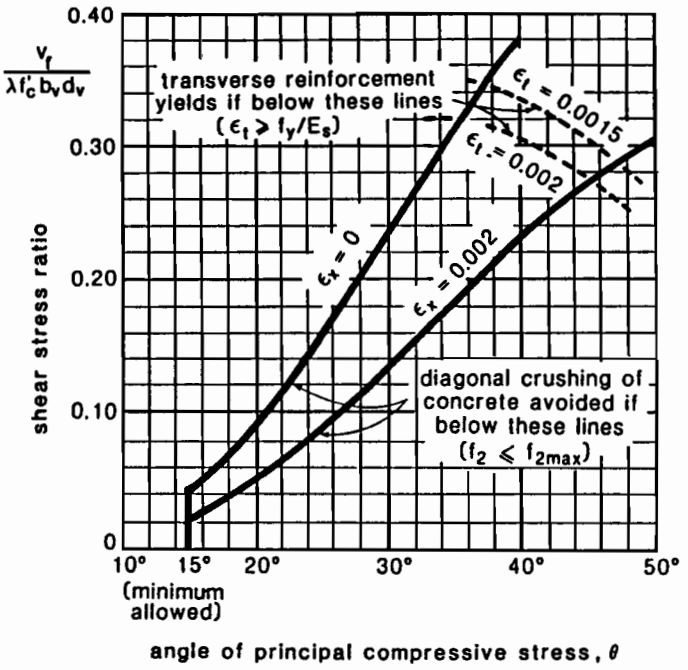

Figure 1-5 Limiting values of the principal angle of compression for different levels of shear stress. From Ref. 21.

The following equation (Ref. 21) offers an approximation to the minimum angle of principal compression, θ_{min} given as:

$$\theta_{min} = 15 + (65 + 25000\epsilon_x)\frac{V_f}{\lambda \phi_c f'_c b_v d_v} \qquad (1\text{-}20)$$

where: θ_{min} = minimum angle of principal compression, degrees
ϵ_x = longitudinal strain at mid-depth of the member
V_f = factored applied shear force at the support face
λ = factor accounting for the density of concrete
ϕ_c = resistance factor for concrete, equal to 0.6
f'_c = compressive strength of concrete
b_v = minimum effective web depth
d_v = effective shear depth.

In order to ensure that the stirrups yield before diagonal crushing of the concrete occurs, it is necessary to keep θ below a maximum value, θ_{max}. Hence from Eq. 1-18, the maximum angle of principal compression can be determined by substituting ϵ_t with the yield strain of the stirrups to give:

$$\theta_{max} = \tan^{-1}\sqrt{\frac{\epsilon_x + 0.002}{\frac{f_y}{E_s} + 0.002}} \qquad (1\text{-}21)$$

where: θ_{max} = maximum angle of principal compression, degrees
f_y = yield stress of stirrup steel
E_s = modulus of elasticity of stirrup steel.

The minimum angle, θ_{min}, is typically chosen as the design angle since the amount of transverse reinforcement required is minimized. The CSA Standard further simplifies the task of determining θ by allowing ϵ_x to be taken as 0.002 (§11.4.2.5). The diagonal compressive stress, f_2, given by Eq. 1-15, is limited by the diagonal crushing strength of the concrete, f_{2max}, which is given by:

$$f_{2max} = \frac{\lambda \phi_c f'_c}{(0.8 + 170\epsilon_1)} \leq \lambda \phi_c f'_c \qquad (1\text{-}22)$$

1.4.3 The Modified Compression Field Theory

The Modified Compression Field Theory (Ref. 10, 12 and 22) accounts for the tensile stresses carried by the concrete after cracking and therefore offers a better prediction of the response than the Compression Field Theory.

Prior to cracking, the principal compressive and tensile stresses carry equal amounts of the applied shear. After cracking, tensile stresses are still present in the concrete between cracks, which contribute to the shear strength of a section. As in the Compression Field Theory, the cracks are considered to be inclined at an angle θ to the horizontal. The magnitude of the tensile stress carried by the concrete decreases with increasing shear stresses. From equilibrium,

any reduction in the tensile stress carried by the concrete must be balanced by an increase in the stirrup stress. The ability of cracked concrete to transfer shear stresses across a crack depends on the magnitude of the principal tensile strain, ϵ_1, since the crack width also depends on ϵ_1. The Modified Compression Field Theory assumes that the shear stresses are uniform over the shear depth, d_v. The magnitude of the longitudinal strain, ϵ_x, at the centroid of the longitudinal tension steel, is determined as:

$$\epsilon_x = \frac{\frac{M_f}{d_v} + 0.5N_v + 0.5\frac{V_f}{\tan\theta}}{E_s A_s} \qquad (1\text{-}23)$$

where: M_f = factored moment
N_f = factored axial tension
V_f = factored shear.

Strain compatibility yields the value of the principal tensile strain, ϵ_1, as:

$$\epsilon_1 = \epsilon_x + (\epsilon_x - \epsilon_2)\cot^2\theta \qquad (1\text{-}24)$$

With increasing loads, θ becomes smaller and ϵ_x increases, the principal tensile strain increases, thus reducing the concrete's ability to transmit shear stresses across a crack. The shear capacity of a section, V_r, can be written as the sum of a concrete contribution, V_c, and a steel contribution, V_s, such that:

$$\begin{aligned} V_r &= V_c + V_s \\ &= \phi_c \beta \sqrt{f'_c} b_v d_v + \frac{\phi_s A_v f_y}{s}\frac{d_v}{\tan\theta} \end{aligned} \qquad (1\text{-}25)$$

where: β = residual tensile stress factor
ϕ_s = resistance factor for reinforcing steel, equal to 0.85.

The value of the residual tensile stress factor is given by the following expressions, in MPa units:

$$\beta = \frac{\alpha_1 \alpha_2 0.33\cot\theta}{1 + \sqrt{500\epsilon_1}} \quad , MPa \qquad (1\text{-}26)$$

$$\beta \leq \frac{0.18}{0.3 + \frac{24w}{a+16}} \quad , MPa \qquad (1\text{-}27)$$

where: w = crack width, in mm
a = maximum aggregate size, in mm.

Eq. 1-26 is based on the assumption that the concrete has a direct tensile strength of $0.33\sqrt{f'_c}$ MPa and is reduced for increasing values of principal tensile strain, ϵ_1. The magnitude of the tensile stress in the concrete may be governed by the concrete's ability to transmit the shear stress across the crack, which is a function of the crack width and the maximum aggregate size (Eq. 1-27). The crack width is assumed to be equal to $\epsilon_1 s_{m\theta}$ where $s_{m\theta}$ is the mean crack spacing of the inclined shear cracks. For design, the values of θ and β can be expressed as functions of the applied shear stress level and value of ϵ_x. Table 1-1 (Ref. 22) gives such a design table.

v/f'_c		Longitudinal Strain $\epsilon_x \times 1000$				
		0	0.5	1.0	1.5	2.0
≤ 0.05	β	0.437	0.251	0.194	0.163	0.144
	θ	28°	34°	38°	41°	43°
0.10	β	0.226	0.193	0.174	0.144	0.116
	θ	22°	30°	36°	38°	38°
0.15	β	0.211	0.189	0.144	0.109	0.087
	θ	25°	32°	34°	34°	34°
0.20	β	0.180	0.174	0.127	0.090	0.093
	θ	27°	33°	34°	34°	37°
0.25	β	0.189	0.156	0.121	0.114	0.110
	θ	30°	34°	36°	39°	42°

Table 1-1 Values of β and θ for design using the Modified Compression Field Theory (Refs. 10 and 22).

In order to avoid yielding of the longitudinal reinforcement due to the combined actions of moment, axial load and shear, the following must be satisfied:

$$\phi_s A_s f_y \geq \frac{M_f}{d_v} + 0.5 N_f + (V_f - 0.5 V_s)\cot\theta \qquad \textbf{(1-28)}$$

1.4.4 The Staggering Concept for Shear Design

The staggering concept for shear design (Ref. 19) separates the beam into design regions of length $d_v / \tan\theta$. Fig 1-6 shows a section of a uniformly loaded beam with the stirrups positioned at a constant spacing, s.

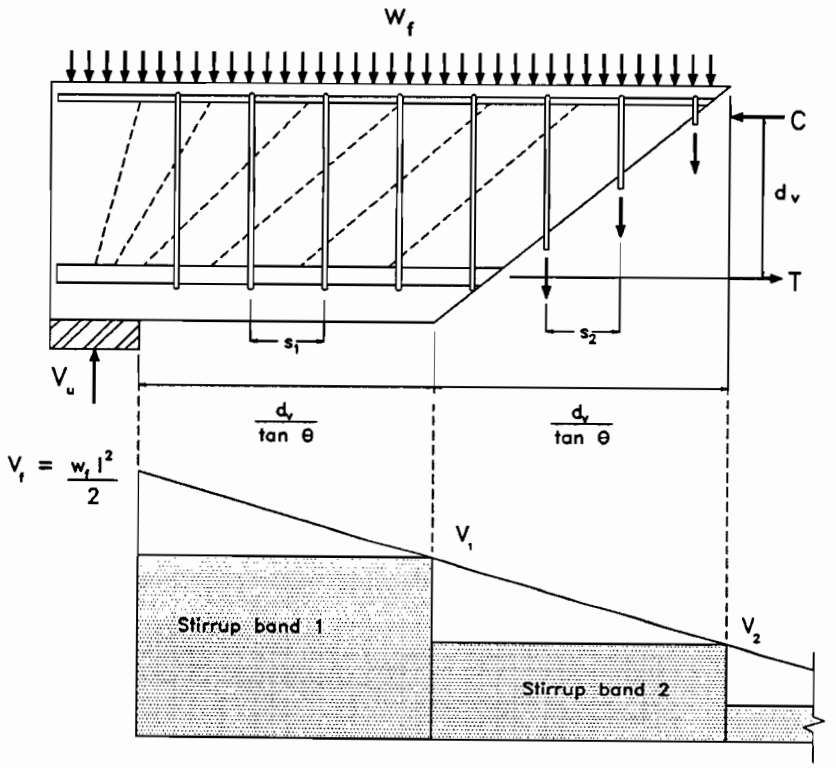

Figure 1-6 The staggering concept for shear design

The shear force that the stirrups in the length $d_v / \tan\theta$ must resist, is equal to the support reaction, V_u, minus the uniform load, w_f, acting over the region under consideration. This shear

force, V_1, corresponds to the shear force applied at a distance $d_v / \tan\theta$ from the support face.

The CSA Standard (Ref. 17) recognizes the staggering concept and requires (§11.4.4.10) that for uniformly, top-loaded beams, the stirrups be capable of resisting the smallest shear within a distance $d_v / \tan\theta$. The shear capacity can be determined from:

$$V_r = \frac{\phi_s A_v f_y}{s} \frac{d_v}{\tan\theta} \qquad (1\text{-}29)$$

where: A_v = area of stirrup reinforcement within a distance s
s = spacing of stirrups.

Using this method to design the stirrup reinforcement results in bands of uniformly distributed stirrups along the beam.

1.4.5 Previous Research on Welded-Wire Fabric

Early research on the use of welded-wire fabric focused on the effectiveness of smooth welded-wire fabric as shear reinforcement and its crack control characteristics. Leonhardt and Walther (Ref. 23) and Taylor and El-Hammasi (Ref. 24) both determined that smooth welded-wire fabric is suitable for shear reinforcement and that it is effective for crack control, as long as it is properly anchored.

More recently, researchers have been trying to determine whether deformed wire fabric further improves the crack control of reinforced concrete tee-beams. Mansur et al. (Ref. 25) considered the anchorage of the deformed welded-wire fabric and its behaviour as shear reinforcement. They compared the response of tee-beams reinforced with both smooth and deformed welded-wire fabric to companion beams reinforced with conventional hot-rolled U-stirrups. The smooth wire cages improved the cracking behaviour, resulting in smaller crack widths than the mild steel stirrups. They also found that the deformed wire further reduced the measured maximum crack widths. The smaller cracks in the specimens reinforced with welded-wire fabric was partly due to the fact that these specimens had smaller stirrup spacings and had more stirrup steel than the companion beams.

While Pincheira et al. (Ref. 26) concentrated on monitoring the behaviour of deformed welded-wire fabric under cyclic loading, they also performed some static tests on tee-beams reinforced with deformed welded-wire fabric. The shear reinforcement that was used in their tests consisted of a single sheet of welded-wire fabric designed to replace an arrangement of conventional single-legged stirrups. They offered no direct comparison between the welded-wire fabric and the hot-rolled single-legged stirrups. They concluded that the deformed welded-wire fabric offered a slight improvement of the crack control over conventional U-shaped or single-legged stirrups. Their results substantiate the findings of Mansur et al.

In spite of the research that has been carried out there are three questions that remain unanswered. One question is whether or not conventional 400 Grade stirrups can be replaced with 500 Grade deformed welded-wire fabric having an equal yield force. In addition, it should be determined whether or not welded-wire fabric can adequately control cracking and whether it can exhibit sufficient ductility to redistribute the stresses in the stirrups.

1.5 Objectives

The main objective of this research program is to determine the characteristics of welded-wire fabric as reinforcement.

A series of tests were carried out on tension specimens to determine the following:

(i) the ductility of concrete members reinforced with welded-wire fabric,

(ii) to compare the response of concrete members reinforced with Grade 500 welded-wire fabric with the response of companion specimens reinforced with Grade 400 deformed bar,

(iii) an expression for the minimum reinforcement ratio required to provide adequate crack control and a ductile response for reinforced concrete sections subjected to axial tension,

(iv) crack development and crack control characteristics of welded-wire fabric,

(v) the validity of response predictions,

(vi) the influence of concrete strength on the behaviour of specimens subjected to pure tension.

A series of full-scale beams were tested to determine the following:

(i) the adequacy of cold-rolled, Grade 500 welded-wire fabric as shear reinforcement,

(ii) the performance of welded-wire fabric stirrups under moderate and high shear loads,

(iii) the diagonal crack control characteristics of welded-wire fabric U-shaped stirrups,

(iv) the distributions of strains in the stirrups in order to assess the crack control, ductility and effectiveness of stirrup anchorage,

(v) the performance of beams reinforced with welded-wire fabric stirrup cages and compare it with that of companion beams reinforced with hot-rolled, Grade 400, stirrups,

(vi) the validity of the response predictions.

Chapter 2

Experimental Programme

This research project consisted of two parts. In the first, a series of reinforced concrete specimens were tested in pure tension to determine the crack control characteristics, the ductility of the cold-rolled welded-wire fabric (WWF) and to investigate the ability of this steel to redistribute local strains. The second test series consisted of two full-scale tests on tee-beams to assess the performance of cold-rolled welded-wire fabric as shear reinforcement, in terms of the crack control and ductility.

2.1 Pure Tension Tests

2.1.1 Description of Test Specimens

Two tension test series were performed, one using low strength concrete, having a compressive strength of about 20 MPa, and the other using high strength concrete, having a compressive strength of about 70 MPa. For each of these two series, specimens having different cross-sectional dimensions and different types of reinforcement were tested. The performance of specimens reinforced with cold-rolled, Grade 500 welded-wire fabric was compared with the response of companion specimens reinforced with hot-rolled, Grade 400 bars. For the specimens reinforced with Grade 400 bars, the transverse bar was not welded to the longitudinal bar, but was held in place by holes drilled in the sides of the formwork and was tied to the longitudinal bar. Details of the steel reinforcement and the cross-sectional dimensions are shown in Fig. 2-1 and a summary of the sixteen tension specimens is given in Table 2-1. The concrete cover

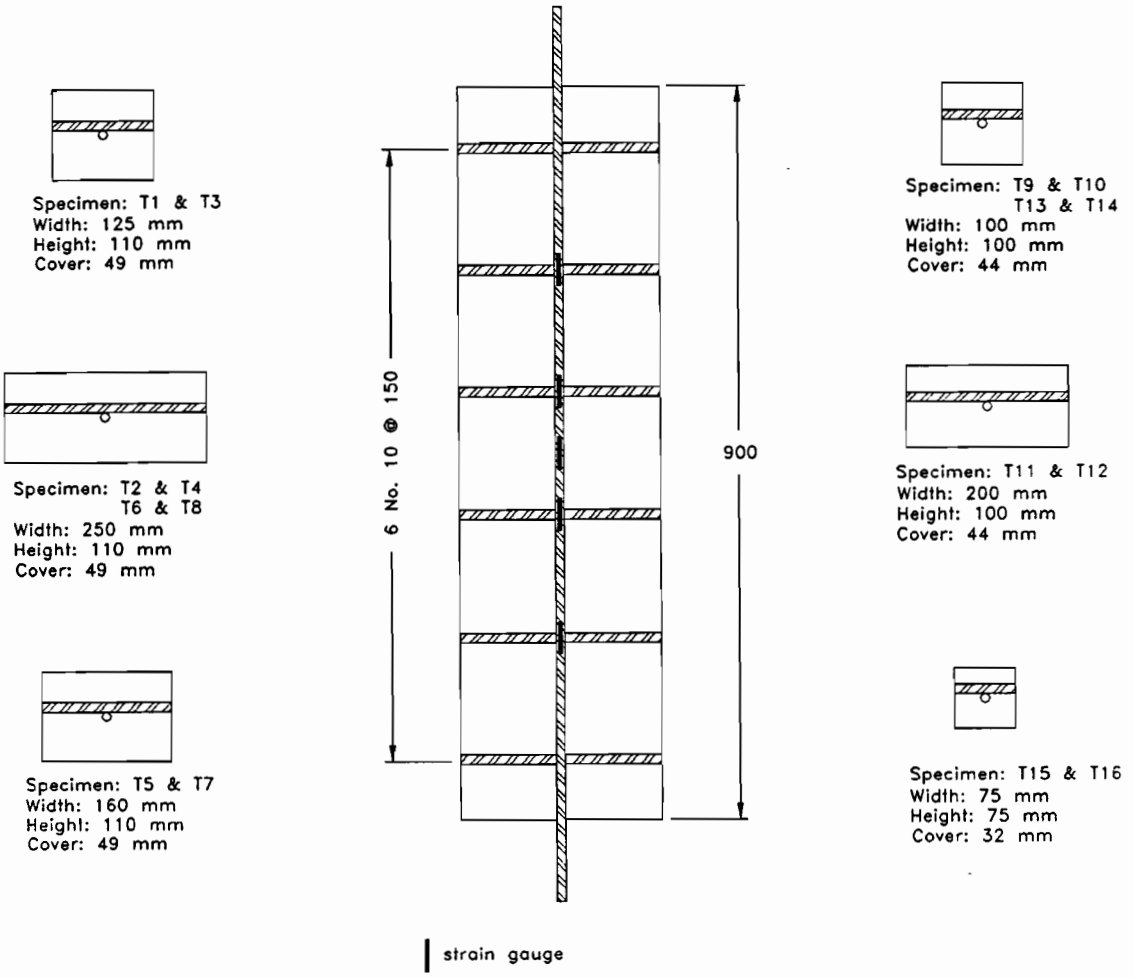

Figure 2-1 Cross-sectional dimensions and reinforcement details of tension specimens

measured from the surface of the bar to the front and back faces is indicated in Fig. 2-1.

The cross-sectional dimensions were determined such that different reinforcement ratios were achieved. As an indication of the significance of the level of the reinforcement ratio, the minimum area of steel, $A_{s,min}$, required such that the yield force of the reinforcement can equilibrate the concrete cracking load can be determined from:

$$A_{s,min} f_y = A_c f_{cr} \tag{2-1}$$

and hence the minimum reinforcement ratio satisfying this criterion is:

$$\rho_{min} = \frac{f_{cr}}{f_y} \tag{2-2}$$

For the preliminary design, the minimum reinforcement ratio was determined using Eq. 2-2, based on the nominal yield strengths of the two different types of steels and taking the cracking strength of the concrete as $0.33\sqrt{f'_c}$ MPa. Some specimens were deliberately designed to have less than the minimum reinforcement ratio, based on the nominal material properties.

Specimen	Reinforcement	Target Concrete Strength	Cross Section Dimensions (mm)
T1	MD100	20 MPa	125 x 110
T2	MD100	20 MPa	250 x 110
T3	No. 10	20 MPa	125 x 110
T4	No. 10	20 MPa	250 x 110
T5	MD100	70 MPa	160 x 110
T6	MD100	70 MPa	250 x 110
T7	No. 10	70 MPa	160 x 110
T8	No. 10	70 MPa	250 x 110
T9	MD100	20 MPa	100 x 100
T10	No. 10	20 MPa	100 x 100
T11	MD100	20 MPa	200 x 100
T12	No. 10	20 MPa	200 x 100
T13	MD100	70 MPa	75 x 75
T14	No. 10	70 MPa	75 x 75
T15	MD100	70 MPa	100 x 100
T16	No. 10	70 MPa	100 x 100

Table 2-1 Description of pure tension test specimens

2.1.2 Test Setup

A loading apparatus was designed to subject the specimens to pure tension as shown in Fig. 2-2. The setup consisted of a hydraulic jack transmitting the load through a 25 mm threaded rod to a set of tension grips, one of which was anchored to the floor of the testing lab. This resulted in the tension being transferred from the steel reinforcing bar to the reinforced concrete section.

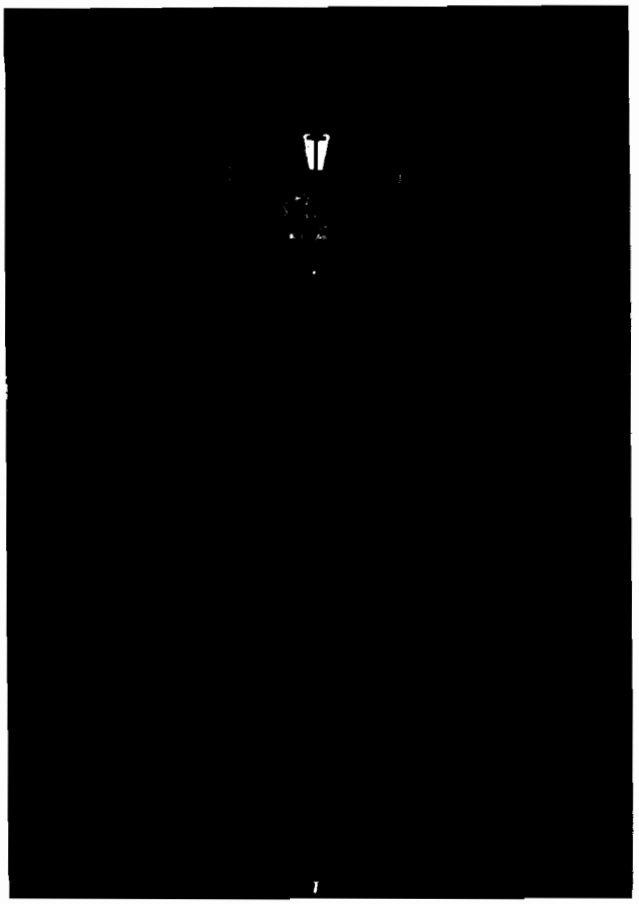

Figure 2-2 Photograph of tension test setup

2.1.3 Instrumentation

Mechanical strain targets, having a gauge length of 100 mm, were epoxied to both the front and the back surfaces of each specimen as shown in Fig. 2-2. These enabled the

measurement of the average strains in different regions of each specimen. A mechanical strain measuring device having an accuracy of $2x10^{-5}$ mm/mm was used. The strain measurements on the front and back surfaces provided a verification of the assumption that very little bending occurred through the thickness of the specimen.

A linear voltage differential transducer (LVDT) was placed along each side of the specimen as shown in Fig. 2-2. These transducers, which were clamped to the steel reinforcing bar just outside of the concrete, measured the specimen's total elongation and enabled the calculation of the average member strain.

Strain gauges were glued to the longitudinal reinforcing bars of Specimens T1 to T8. These gauges, which were located at mid-height and at four of the cross-ties (see Fig. 2-1), were used to measure the local strains at locations where transverse cracks were expected to form.

The crack widths were estimated using a crack width comparator at each load stage. Photographs at key load stages recorded the crack development.

2.1.4 Concrete Material Properties

The properties of the six batches of concrete used for the tension specimens are given in Table 2-2. Three standard 150 by 300 mm cylinders were tested to determine the average

Specimens	ϵ'_c (x 10^3)	f'_c, MPa	f_{sp}, MPa	ϵ_{sh} (x 10^3)
T1-T2	2.43	25.0	2.75	-0.28
T3	2.04	23.5	2.38	-0.06
T4	2.08	20.7	2.18	-0.28
T5-T6	2.77	76.8	4.89	-0.36
T7-T8	2.74	76.3	4.89	-0.36
T9-T12	2.21	17.0	1.89	-0.28
T13-T16	2.22	64.0	4.45	-0.36

Table 2-2 Material properties of concrete batches for tension specimens

compressive strength, f'_c, and the corresponding strain, ϵ'_c. Three additional cylinders were tested to determine the average split cylinder strength, f_{sp}, for each batch. The cylinders were tested on the same day as the testing of the reinforced concrete specimens. Two 100 x 100 x 400 mm shrinkage specimens were cast to measure the average shrinkage strain, ϵ_{sh}.

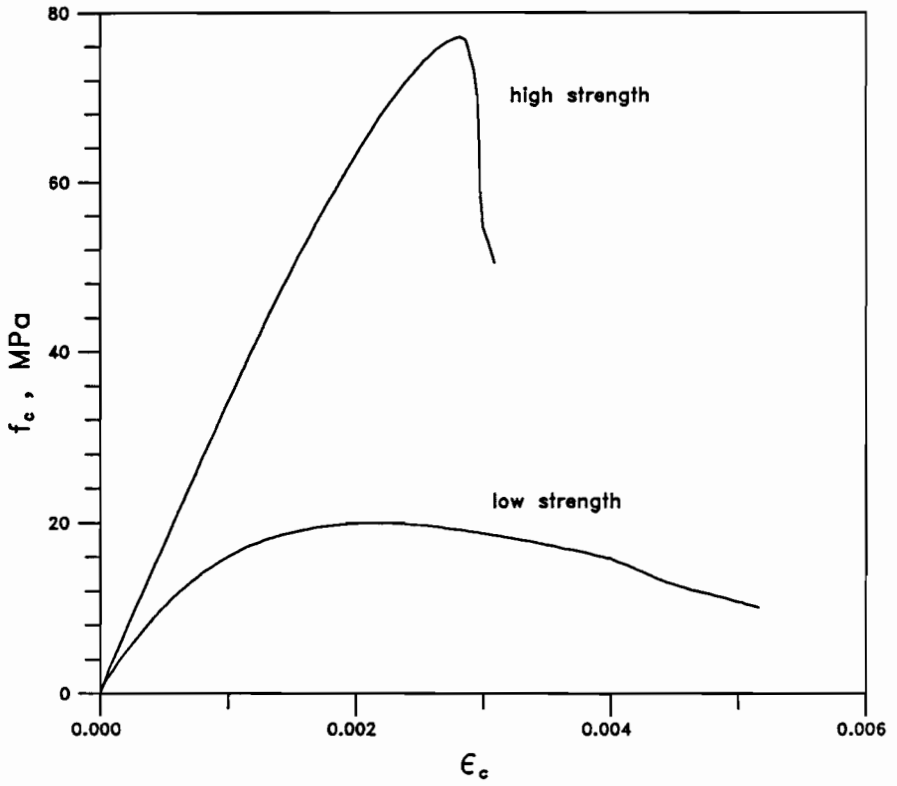

Figure 2-3 Typical stress-strain response of 70 MPa and 20 MPa concretes

Tables 2-3 and 2-4 give the mix designs for the 20 MPa and 70 MPa concretes. Fig. 2-3 shows the typical stress-strain characteristics of the low and high strength concretes. From this figure, it is apparent that the high strength concrete is much less ductile and has a greater modulus than the lower strength concrete. The high strength concrete also reaches a greater peak strain, ϵ'_c, than the low strength concrete.

Ingredients	Type	Quantity kg/m^3
cement	SF	506
fine aggregate		793
coarse aggregate 5-10mm		1015
water (total)		126
total:		2440
chemical admixtures:		
PDA-25XL	WRA-CONCHEM	1305 ml
SPN-superplasticizers	CONCHEM	7.5 l
slump		150-200mm
water/cement ratio		0.27

Table 2-3 Mix design for 70 MPa concrete

Ingredients	Type	Quantity kg/m^3
cement	10	349
fine aggregate		1012
coarse aggregate 5-10mm		907
water (total)		236
total:		2504
slump		150 mm
water/cement ratio		0.68

Table 2-4 Mix design for 20 MPa concrete

2.1.5 Reinforcement Properties

The properties of the reinforcement are summarized in Table 2-5. All of the deformed steel wire conforms to G30.14-M83 (Ref. 3) and the wire mesh conforms to G30.15-M83

(Ref. 5). The strains were measured over a 100 mm gauge length, which included one cross-wire for the welded-wire fabric tension specimen.

Size Designation	Nominal Yield	Area (mm^2)	E_s (MPa)	f_y (MPa)	f_u (MPa)	ϵ_{rupt} (%)
MD100	500	100	200000	589	614	4.75
No. 10	400	100	204600	400	658	20.46

Table 2-5 Properties of reinforcement for tension specimens

The yield stress of the welded-wire fabric reinforcement was determined at a strain of 0.005 (Ref. 3) as 589 MPa from the stress-strain relationship given in Fig 2-4.

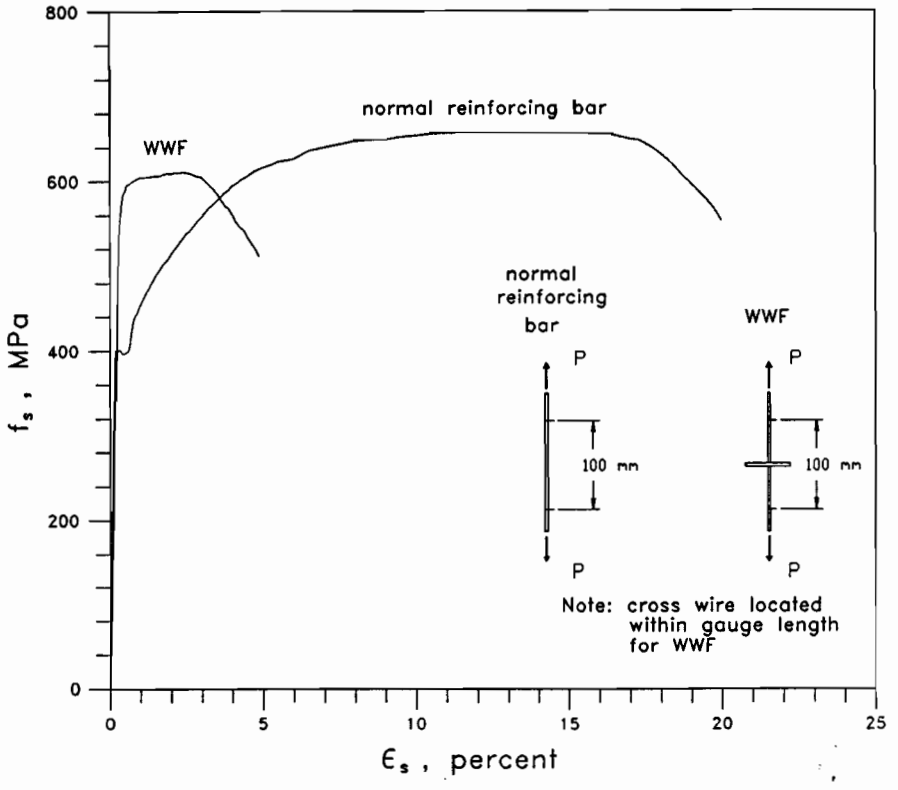

Figure 2-4 Stress-strain response of Grade 500, welded-wire fabric and Grade 400, hot-rolled reinforcement

As can be seen in Fig. 2-4, the welded-wire fabric ruptures at a strain of 4.75% which is considerably less than the rupture strain of 20.5% measured for the 400 MPa steel. The cold-

rolled, Grade 500 welded-wire fabric, also exhibits a small amount of strain hardening and has an ultimate stress which is actually less than the hot-rolled, Grade 400 reinforcement. The average reduction of area was 41% for the deformed wire while it was measured as 40.3% for the 400 MPa sample.

2.2 Tee-Beam Tests

2.2.1 Description of Test Specimens

Two full-scale beams typical of those found in one-way floor slab construction were tested. Beam TM500 was chosen to have a clear span of 4.8 m while Beam TH500 had a clear span of 3.8 m. The flexural span of both specimens, measured to the centre of the roller supports, was 50 mm greater than the clear span due to the support conditions. Beam TM500 was subjected to a moderate level of shear and Beam TH500 to a high shear level. Fig. 2-5 shows the elevation views of both beams and a typical cross section. The shear reinforcement consisted of a stirrup cage constructed from welded-wire fabric. The welded-wire fabric was made with 8 mm diameter, Grade 500, cold-rolled deformed wire which was bent to form the stirrup cages. Anchorage of the stirrups near the top of the beam was provided by two 8 mm diameter deformed wires welded to each stirrup leg, in accordance with the CSA Standard (Ref. 17, §12.3.2 (c)). An additional 8 mm diameter deformed wire was welded to the bottom stirrup legs to keep the shape of the stirrup cage. One of these prefabricated stirrup cages is shown in Fig. 2-6.

The purpose of these tests was to compare their responses with the responses of two companion beams reinforced with Grade 400, hot-rolled 9.5 mm diameter U-shaped stirrups, tested by Mailhot (Ref. 27). The spacings of the stirrups in the different regions of beams TM500 and TH500 were chosen such that they had the same yield force (i.e., the same $A_v f_y/s$) as provided in the companion beams. Figure 2-7 shows the reinforcement details of the companion specimens tested by Mailhot. The measured values of yield stress rather than the nominal values for both types of steel were used in determining the required stirrup spacing.

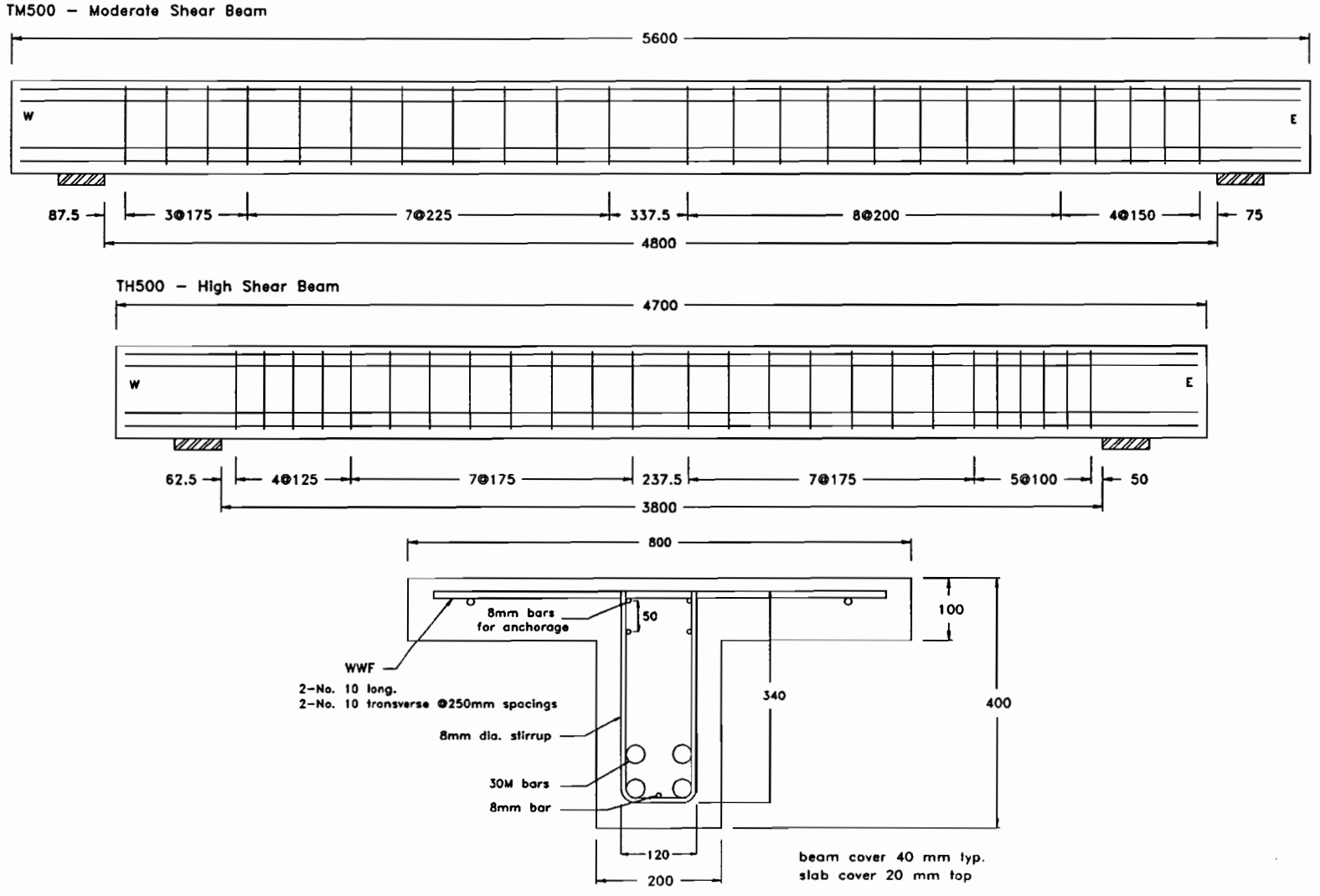

Figure 2-5 Reinforcement details of tee beam specimens TH500 and TM500

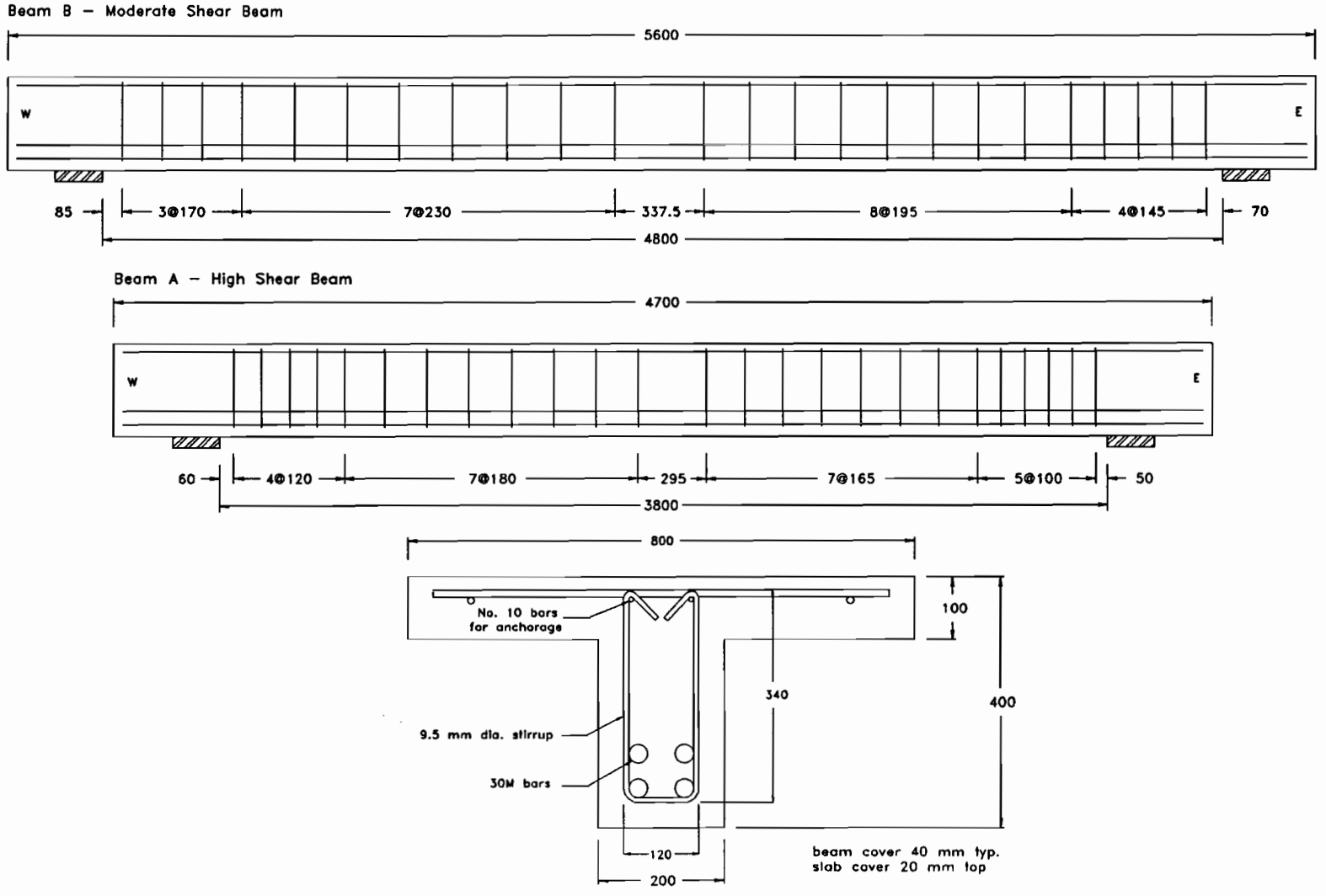

Figure 2-7 Reinforcement details of companion beams tested by Mailhot (Ref. 27)

In order to use the standard fabrication process, the spacing of the stirrups were chosen as multiples of 25 mm. This resulted in a maximum variation of approximately 7 percent from the desired stirrup spacing. For ease of fabrication, the stirrup cages for each beam were fabricated in two pieces.

Figure 2-6 Photograph showing prefabricated stirrup cage for beam TH500

The specimens were designed for flexure and shear in accordance with the CSA Standard (Ref. 17). The longitudinal reinforcement for all the beams consisted of four No. 30 bars having a specified yield stress of 400 MPa. The stirrup reinforcement at the west end of each beam corresponded to the amount of reinforcement determined from the shear strength equations of the code (Eq. 1-29). The amount of stirrup reinforcement in the east half of the beam was increased from that used in the west half in order to satisfy the serviceability requirements of the

CSA Standard.

2.2.2 Test Setup

A loading apparatus was designed to subject the beams to a simulated uniformly distributed loading (see Fig. 2-8). The setup consisted of hydraulic rams transmitting the load through distribution beams under the reaction floor. Each ram loaded four 19 mm diameter threaded tension rods which in turn transmitted the load to four spreader beams seated on eight 100 x 100 mm bearing plates on the top surface of the flange. This resulted in loads being applied at 250 mm intervals along the length of each specimen with each ram loading a 1 m length of beam. This loading pattern produced a relatively uniform loading on the specimen, as can be seen in Fig. 2-9.

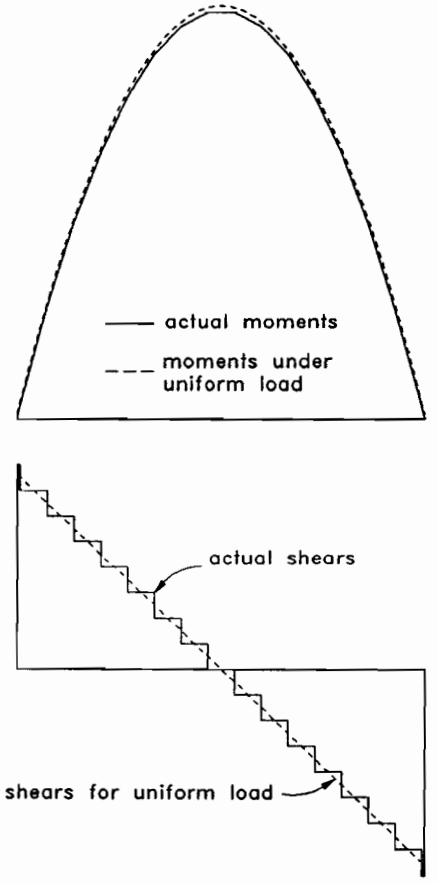

Figure 2-9 Assumed and actual loading patterns for tee-beam tests

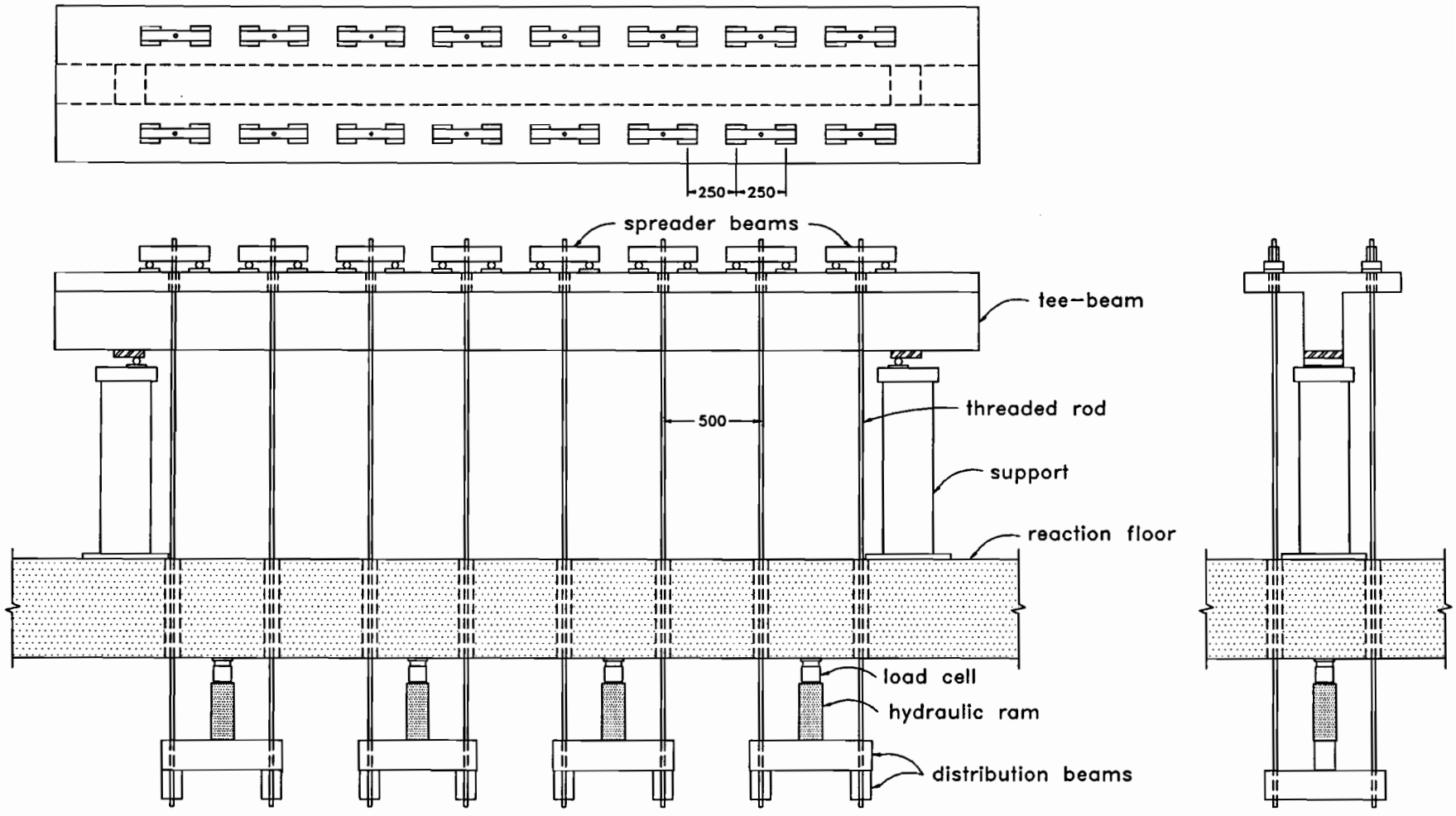

Figure 2-8 Beam loading apparatus used to simulate uniform loading

Transverse reinforcement, perpendicular to the axis of each beam, was provided in the top of the flange to equilibrate the moment produced by bending of the flanges. The flanges were reinforced with a mat of welded-wire fabric having 2-MD100 deformed wires in the longitudinal direction and 2-MD100 wires under each bearing plate (see Fig. 2-5).

Each beam was seated in capping compound on top of two 150 x 200 mm bearing plates which were supported on a fixed roller at one end and on a free roller at the other end in order to prevent longitudinal restraint. Figure 2-10 shows an overall view of specimen TH500 before testing.

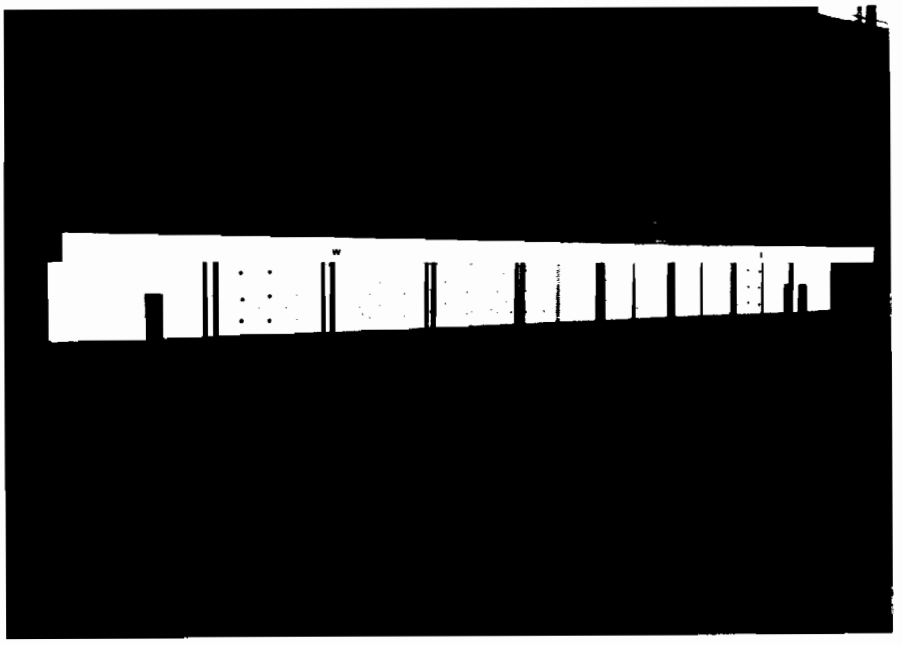

Figure 2-10 Overall view of TH500 before loading

2.2.3 Instrumentation

The beams were heavily instrumented in order to provide detailed strain readings. Mechanical strain targets, having a gauge length of 100 mm, were epoxied to the surface of the concrete web. At the location of each stirrup two vertical strain measurements were taken, in the top and bottom halves of the web (see Fig. 2-11). At every second stirrup, additional targets were provided to form strain rosettes centred about the top and bottom halves of the web in order to

determine the principal strains and the principal angles of compression. The layout of these targets is shown in Fig. 2-11. The above strain measurements were taken using a mechanical gauge having an accuracy of $2x10^{-5}$ mm/mm. Three sets of targets, having a gauge length of 200 mm, were also glued on the top of the slab centred about midspan to monitor the compressive strains in the concrete. One set of targets was located at midspan at the level of the centroid of the bottom layer of longitudinal reinforcement to measure the tensile strain. These strain measurements were taken using a mechanical gauge having an accuracy of $1x10^{-5}$ mm/mm.

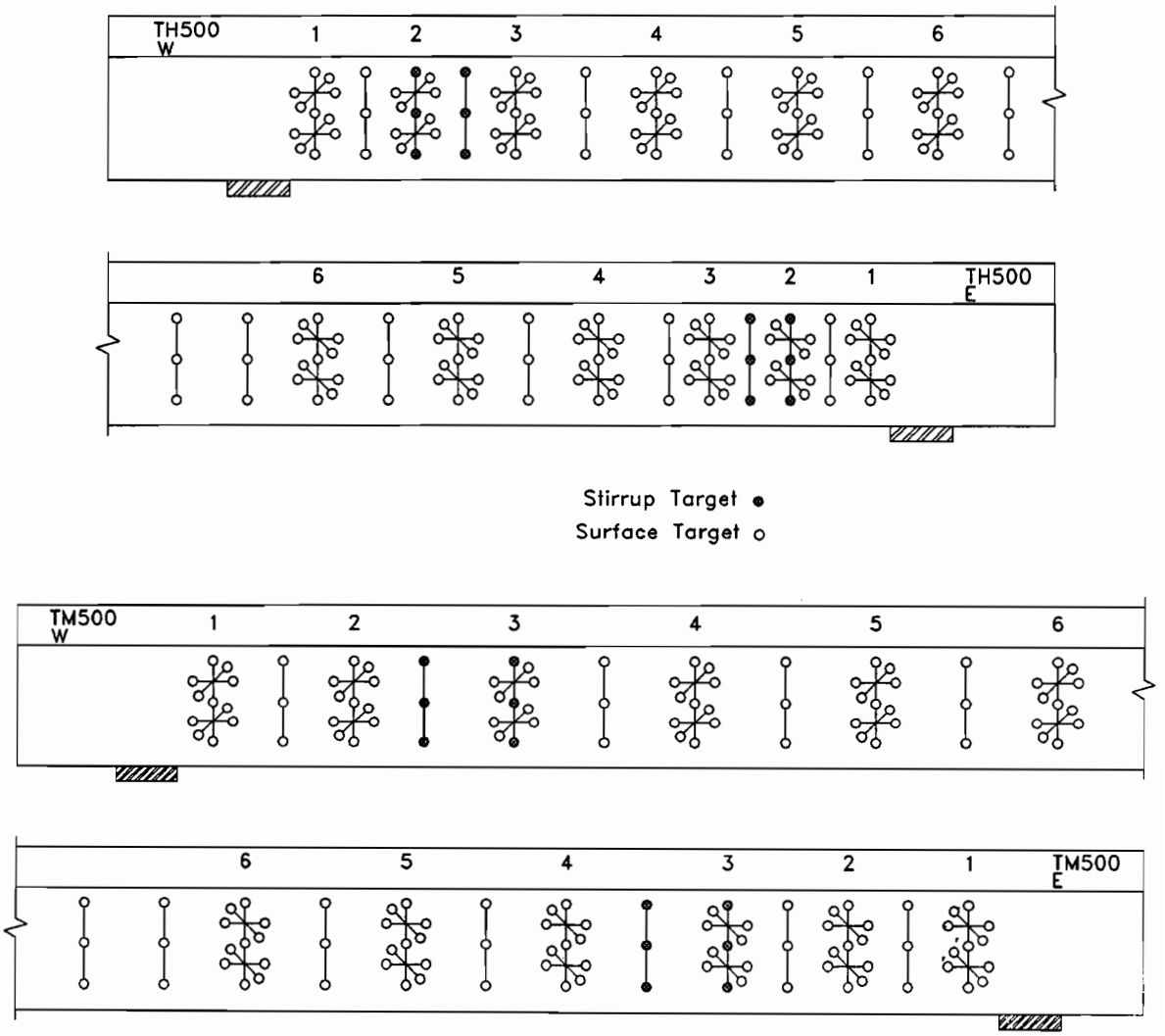

Figure 2-11 Location of Demec targets and strain rosettes

In addition to the targets glued to the surface of the concrete, some targets were epoxied directly to the stirrups with access holes provided by casting removable styrofoam plugs over the targets (see Fig. 2-12). This enabled a direct measurement of the strains in the stirrups. This was done to compare the surface strain measurements with the actual stirrup strains. These strains were measured with a specially designed mechanical gauge having an accuracy of $1x10^{-4}$ mm/mm.

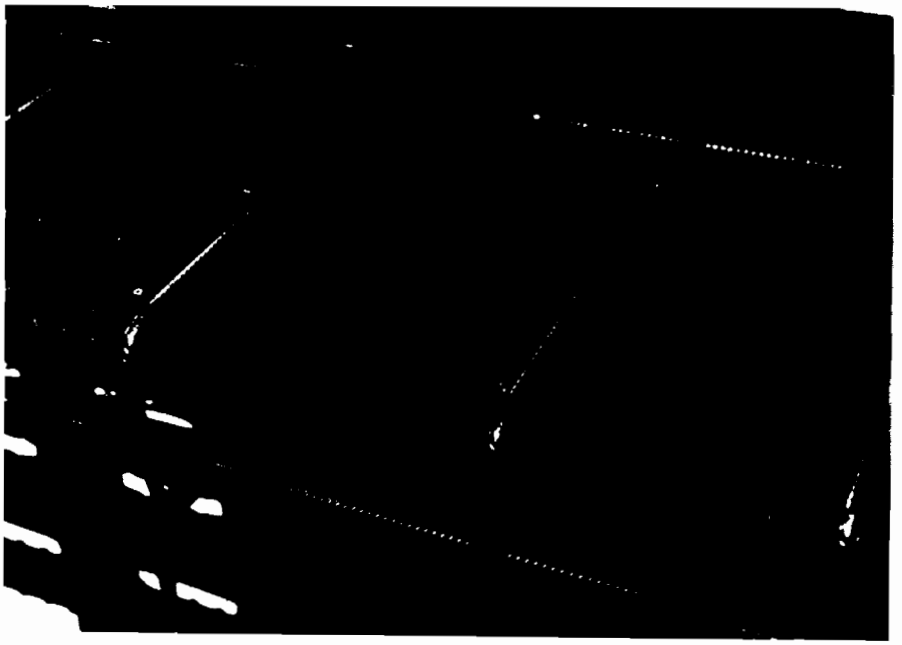

Figure 2-12 Photograph of Demec targets epoxied directly to the stirrups

A linear voltage differential transducer (LVDT) was used to measure the midspan deflection. Two additional LVDTs were used to monitor any support settlements.

For the moderate shear beam, TM500, three 450 kN capacity and two 340 kN capacity load cells were connected to the system in order to measure the applied load. In the case of the high shear beam, TH500, a pair of 450 kN load cells and a pair of 340 kN load cells were placed as shown in Fig. 2-8 to monitor the load.

The crack widths were determined at each load stage using a crack width comparator. Small adhesive labels showing the crack widths were placed beside the cracks thus enabling the

crack width history to be followed by examining photographs of the beams at various stages.

2.2.4 Concrete Material Properties

A single batch of ready-mix concrete having a specified strength of 30 MPa was used to cast both beams. After each beam test, a set of three 150 by 300 mm concrete cylinders was tested to determine the average compressive strength of the concrete (f'_c) and another set was tested to establish its average splitting tensile strength (f_{sp}). Three 400 x 100 x 100 mm flexural beams were tested to determine the concrete's average modulus of rupture, f_r. A summary of the concrete properties can be found in Table 2-6. Table 2-7 gives the mix design for the 30 MPa concrete.

Beam	ϵ'_c (x 10^3)	f'_c, MPa	f_{sp}, MPa	f_r, MPa
TM500	1.99	41.2	3.59	5.35
TH500	1.95	41.4	3.95	5.30

Table 2-6 Material properties of concrete for beam specimens

Ingredients	Type	Quantity kg/m^3
cement	10	355
fine aggregate		790
coarse aggregate 5-20mm		1040
water (total)		160
total:		2345
chemical admixtures:		
PDA-25XL	WRA-CONCHEM	1110 ml
PRO-AIR	AEA-CONCHEM	200 ml
slump		100-120mm
water/cement ratio		0.45

Table 2-7 Mix design for 30 MPa concrete

crack width history to be followed by examining photographs of the beams at various stages.

2.2.4 Concrete Material Properties

A single batch of ready-mix concrete having a specified strength of 30 MPa was used to cast both beams. After each beam test, a set of three 150 by 300 mm concrete cylinders was tested to determine the average compressive strength of the concrete, f'_c, and another set was tested to establish its average splitting tensile strength, f_{sp}. Three 400 x 100 x 100 mm flexural beams were tested to determine the concrete's average modulus of rupture, f_r. A summary of the concrete properties can be found in Table 2-6. Table 2-7 gives the mix design for the 30 MPa concrete.

Beam	ϵ'_c (x 10^3)	f'_c, MPa	f_{sp}, MPa	f_r, MPa
TM500	1.99	41.2	3.59	5.35
TH500	1.95	41.4	3.95	5.30

Table 2-6 Material properties of concrete for beam specimens

Ingredients	Type	Quantity kg/m^3
cement	10	355
fine aggregate		790
coarse aggregate 5-20mm		1040
water (total)		160
total:		2345
chemical admixtures:		
PDA-25XL	WRA-CONCHEM	1110 ml
PRO-AIR	AEA-CONCHEM	200 ml
slump		100-120mm
water/cement ratio		0.45

Table 2-7 Mix design for 30 MPa concrete

2.2.5 Reinforcement Properties

All of the deformed steel wire conforms to G30.14-M83 (Ref. 3) and the wire mesh to G30.15-M83 (Ref. 5). The important properties of the reinforcing steel are shown in Table 2-8.

Size Designation	Area (mm^2)	E_s (MPa)	f_y (MPa)	f_u (MPa)	ϵ_{rupt} (%)	Function
MD50	50	198050	562	595	4.2	Stirrups
MD100	100	200000	596	615	4.4	Tension Ties
No. 30	700	200000	467	712	-	Longitudinal Reinforcement

Table 2-8 Properties of reinforcement for beam specimens

For the welded-wire fabric, the strains were measured over a gauge length of 100 mm, which included one cross-wire. Once again, in comparing the deformed wire stress-strain characteristics to those of hot-rolled deformed reinforcing bars, the deformed wire shows a considerably less ductile response with the 8 mm wire (MD50) reaching a strain at rupture of 4.2% while the 11.3 mm wire (MD100) reached a strain of 4.4% at rupture. The average reduction of area after rupture for the 8 mm and the 11.3 mm diameter deformed wires were 32% and 41%, respectively.

Chapter 3

Measured and Predicted Responses of Pure Tension Specimens

This chapter summarizes the observed behaviour and compares predicted responses with the measured responses of the sixteen tension specimens. Section 3.1 summarizes the procedure used to predict the responses. Sections 3.2 and 3.3 present discussions of the behaviour of the specimens and also compare their predicted and measured responses. In order to facilitate the discussion of the responses, companion specimens having the same concrete strength and percentage of reinforcement are compared. One of the companion specimens contains Grade 400, hot-rolled reinforcement, while the other is reinforced with Grade 500, cold-rolled welded-wire fabric. All of the specimens were reinforced with No. 10 bars or deformed welded wire fabric. A summary of the influence of the reinforcement ratio, ρ, the concrete strength, and the type of steel reinforcement on the behaviour of the specimens is presented in Section 3.4. A recommendation of the minimum reinforcement ratio required to provide crack control is presented in Section 3.5.

3.1 Predicting Responses of the Tension Members

The load-strain response for each specimen was computed using the iterative procedure developed by Collins and Mitchell (Ref. 10), as described in Section 1.3. The measured material properties were used in all of the response predictions. The secant modulus, E_c, was determined

from the measured concrete stress-strain relationship in accordance with ASTM C469-87a (Ref. 28) and the direct tensile strength of the concrete, f_{cr}, was taken as 0.65 times the split cylinder strength, f_{sp}. The modulus of elasticity given by Eq. 1-1 or 1-2 was found to be somewhat greater than the experimentally determined values.

The maximum crack widths were predicted using both the CEB-FIP and the Gergely-Lutz expressions described in Section 1.3.1.

3.2 Low-Strength Concrete Tension Tests

The test results of the tension specimens made with lower strength concrete (17 to 25 MPa) are summarized in Table 3-1. The maximum crack widths and average crack spacings for the specimens are summarized in Table 3-2. The maximum crack widths are given at first cracking and for a service load level assumed to be 0.6 times the measured yield force ($A_s f_y$).

Specimen	Grade	ρ %	f'_c MPa	P_{cr} kN	$f_{s,cr}$ MPa	P_u kN	ϵ_u %	ϵ_r %
T1	500	0.73	25.0	25.2	252	60.8	0.41	0.65
T3	400	0.73	23.5	26.7	267	72.7	7.56	9.59
T2	500	0.36	25.0	50.1	501	59.7	0.16	0.15
T4	400	0.36	20.7	54.2	542	67.8	7.70	9.99
T9	500	1.0	17.0	11.0	110	59.5	0.51	0.67
T10	400	1.0	17.0	12.0	120	68.5	8.47	12.54
T11	500	0.5	17.0	19.2	192	63.7	0.70	0.75
T12	400	0.5	17.0	19.4	194	64.1	8.53	11.26

Table 3-1 Summary of low-strength concrete tension tests

Specimen	Grade	P_{cr} kN	w_{max} @ P_{cr} mm	Service Load $=0.6A_sf_y$ kN	w_{max} @ Service Load mm	Average Crack Spacing mm
T1	500	25.2	0.40	35.3	0.70	225
T3	400	26.7	0.20	24.0	-	150
T2	500	50.1	0.50	35.3	-	900
T4	400	54.2	0.60	24.0	-	300
T9	500	11.0	0.25	35.3	0.40	180
T10	400	12.0	0.15	24.0	0.35	112.5
T11	500	19.2	0.50	35.3	0.50	300
T12	400	19.4	0.75	24.0	0.50	180

Table 3-2 Crack characteristics of low-strength concrete specimens

3.2.1 Specimens T1 (f_y = 589 MPa) and T3 (f_y = 407 MPa)

Specimens T1 and T3 have cross-sectional dimensions of 125 by 110 mm, have reinforcement ratios of 0.73% and have concrete compressive strengths of 25.0 and 23.5 MPa, respectively. As can be seen from Fig. 3-1a, Specimen T3 reached a maximum average strain at rupture, ϵ_r, of 9.59%, displaying considerably greater ductility than Specimen T1 (ϵ_r = 0.65%).

Specimens T1 and T3 both cracked at a load of about 25 kN (see Fig. 3-1b) and hence, the stress in the steel at first cracking, $f_{s,cr}$, was approximately 250 MPa. Since $f_{s,cr}$ was considerably less than the yield stresses of both steels, the specimens were capable of developing loads much greater than the cracking load.

Figure 3-1b compares the predicted responses with the actual responses for Specimens T1 and T3. As can be seen, the predictions are conservative throughout the entire range of the post-cracking responses. The actual cracking loads were somewhat higher than the predicted cracking loads.

Figures 3-1c and 3-1d present the variation of maximum crack widths with loading and compare the results with the predicted values. Immediately after cracking, Specimen T1 had a maximum crack width of 0.4 mm compared with 0.2 mm for Specimen T3. The Gergely-Lutz expression underestimates the maximum crack widths, while the CEB-FIP expression provides conservative estimates. The average crack spacings were 225 mm and 150 mm for Specimens T1 and T3, respectively.

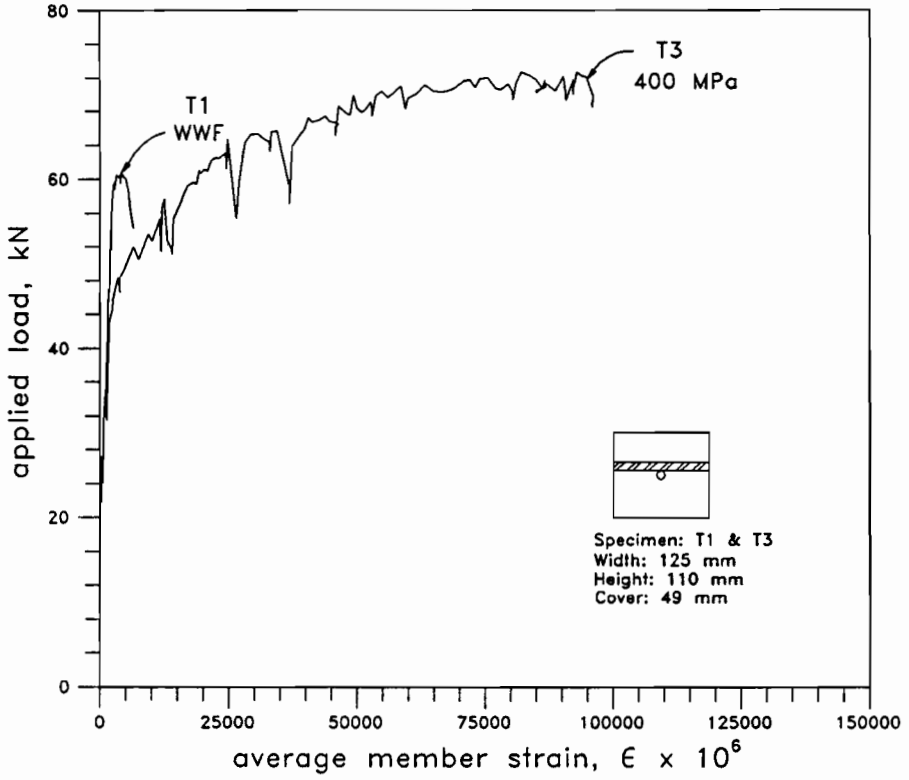

Figure 3-1 (a) Load versus average strain response of Specimens T1 and T3

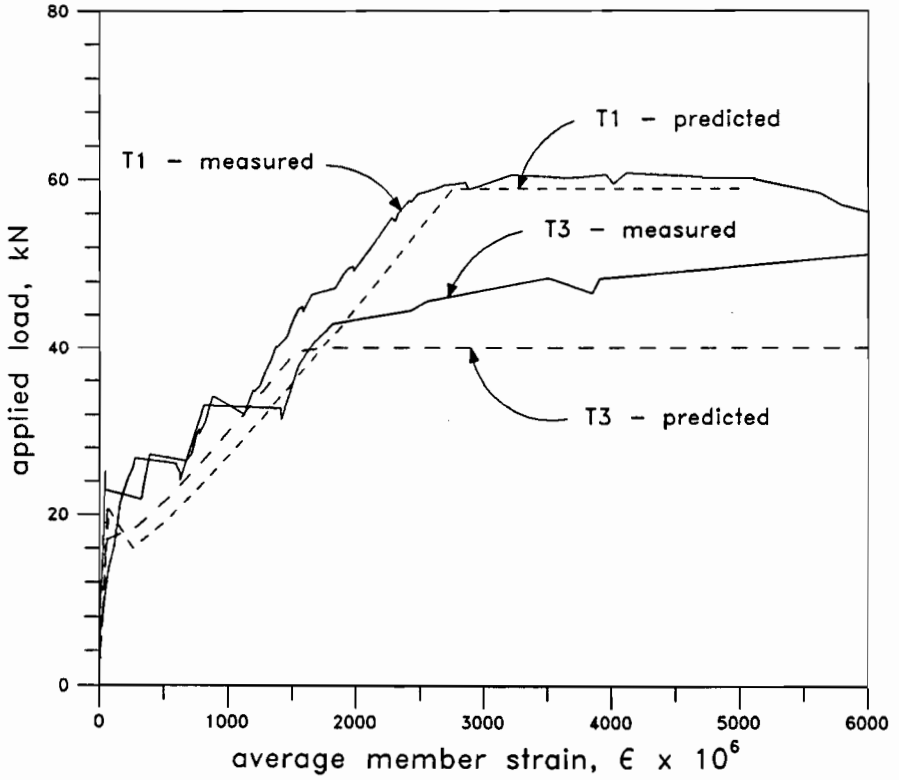

Figure 3-1 (b) Comparison of predicted and measured responses of Specimens T1 and T3

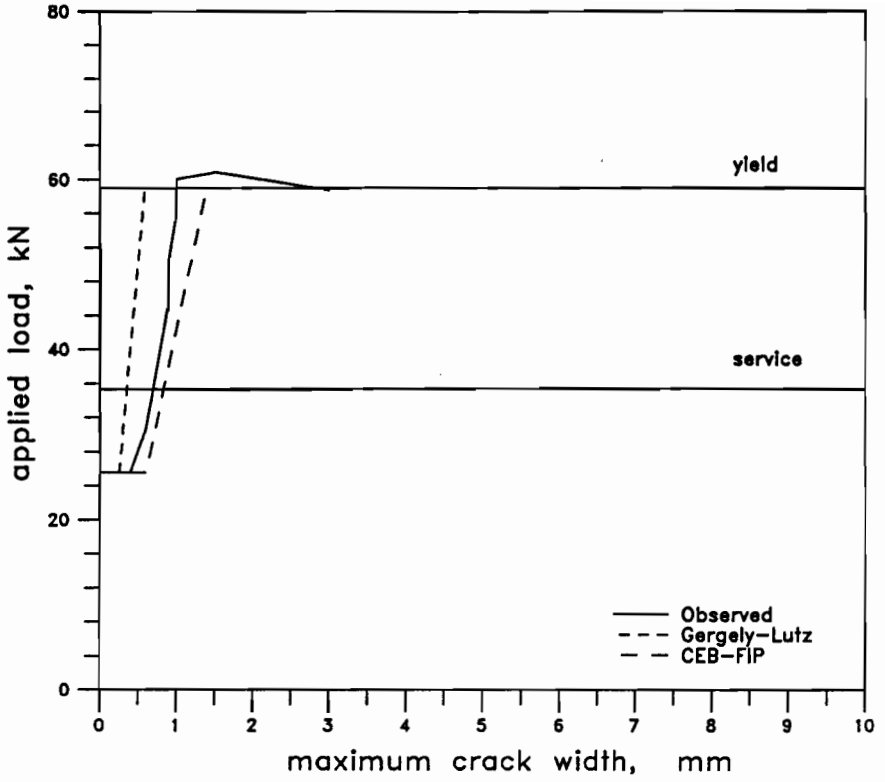

Figure 3-1 (c) Load versus maximum crack width for Specimen T1

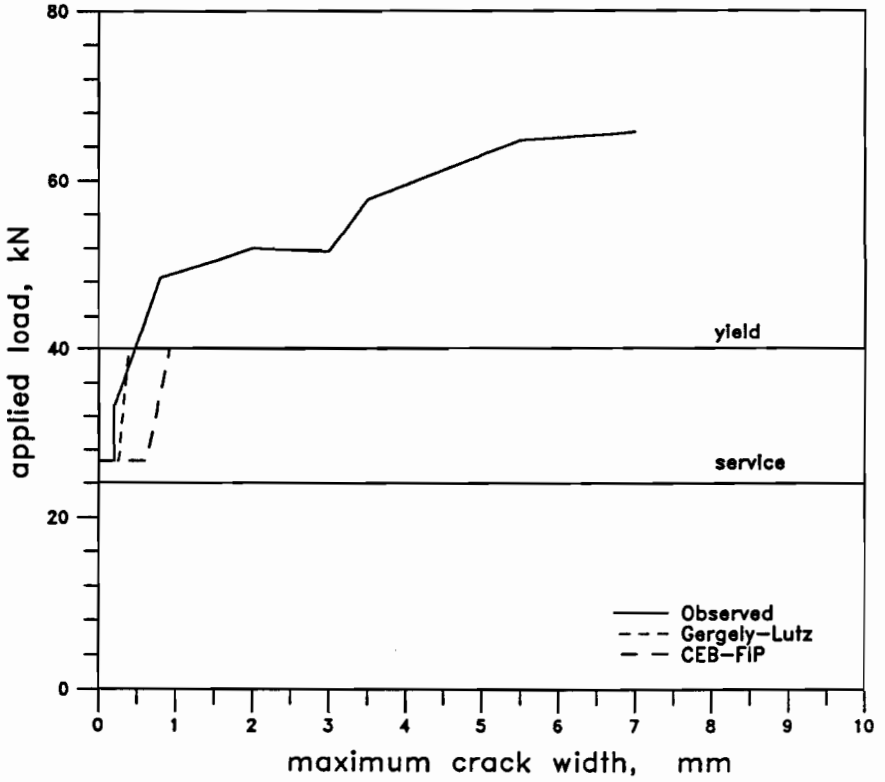

Figure 3-1 (d) Load versus maximum crack width for Specimen T3

3.2.2 Specimens T2 (f_y = 589 MPa) and T4 (f_y = 407 MPa)

Specimens T2 and T4 have a cross section of 250 by 110 mm (ρ = 0.36%) and were cast with 25.0 and 20.7 MPa concrete, respectively. Figure 3-2a shows the load-strain response of these tension specimens. From this figure, it can be seen that Specimen T4 reached a much higher average strain at rupture (ϵ_r = 10%) while Specimen T2 attained a rupture strain of only 0.15%, with failure occurring outside the gauge length.

As shown in Fig. 3-2b, Specimens T2 and T4 cracked at respective loads of 50.1 and 54.2 kN. Specimen T2 cracked at a higher load than predicted, while Specimen T4 cracked before reaching the theoretical cracking load. The post-cracking response predictions are conservative for Specimen T2. However, the actual deformations of Specimen T4 exceed those predicted. The difference between the responses of the two specimens was caused by splitting cracks that formed along their longitudinal axes. New transverse cracks branched out from the longitudinal cracks at the nearest cross-tie. In the case of Specimen T2, the transverse cracks did not reach the extreme fibres of the section. For Specimen T4 on the other hand, these transverse cracks went through the entire cross section causing yielding of the steel at a cross tie location.

The crack development histories are shown in Figures 3-2c and 3-2d for Specimens T2 and T4, respectively. Since the steel stress at cracking was greater than the yield stress of the hot-rolled reinforcement, Specimen T4 underwent significant deformations immediately after cracking, exhibiting a maximum crack width of 0.6 mm. Just after first cracking, the maximum crack width in Specimen T2 was found to be 0.5 mm. The maximum crack widths determined using the Gergely-Lutz expression are smaller than the observed crack widths while the CEB-FIP expression for maximum crack width yields conservative predictions for Specimen T2. No predictions are shown for Specimen T4 since cracking occurred after the yield load was exceeded, at which point the predictions are no longer valid. Specimen T4 displayed a smaller average crack spacing than Specimen T2.

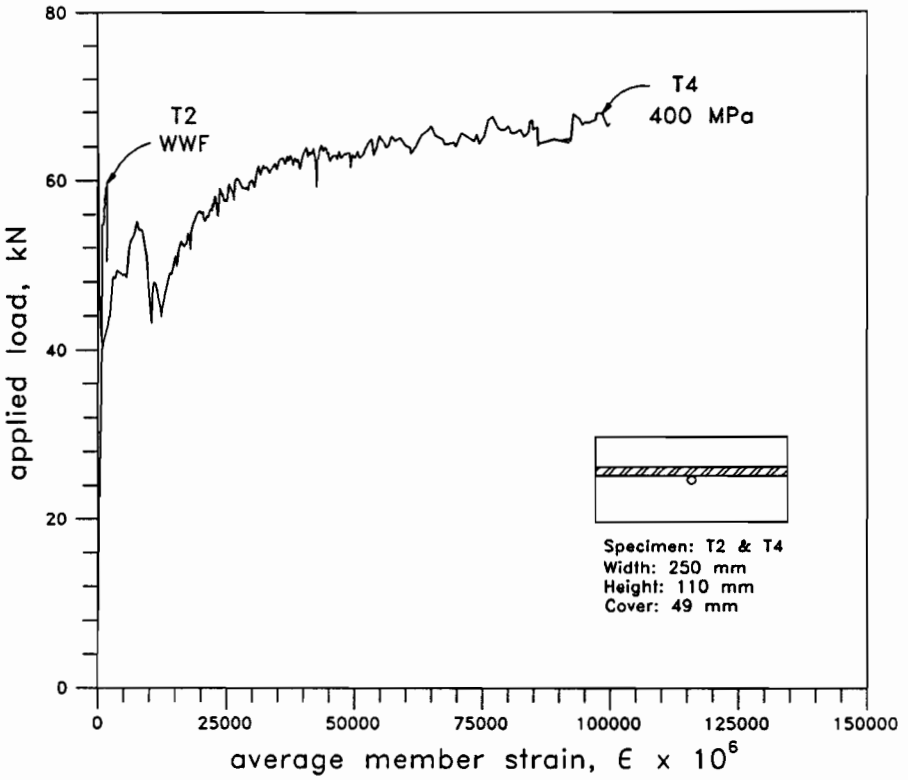

Figure 3-2 (a) Load versus average strain response of Specimens T2 and T4

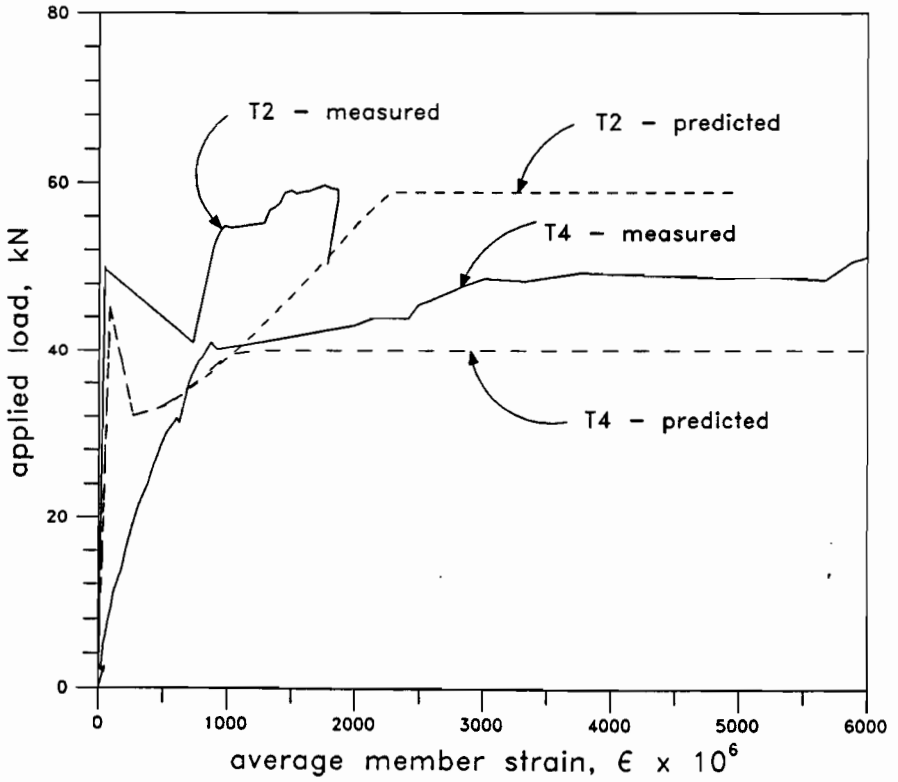

Figure 3-2 (b) Comparison of predicted and measured responses of Specimens T2 and T4

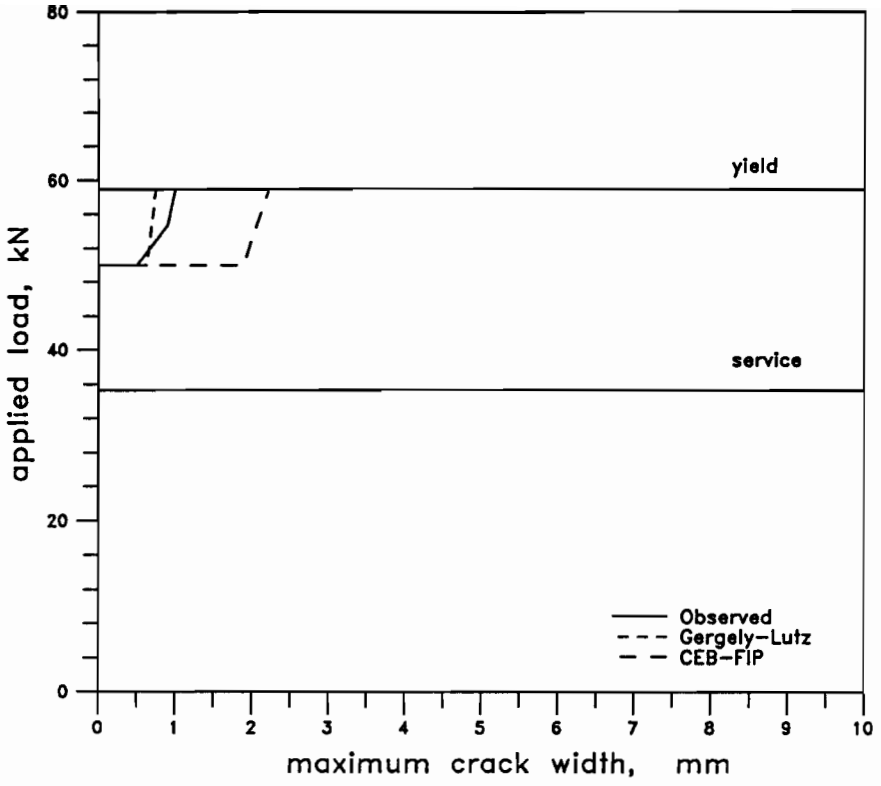

Figure 3-2 (c) Load versus maximum crack width for Specimen T2

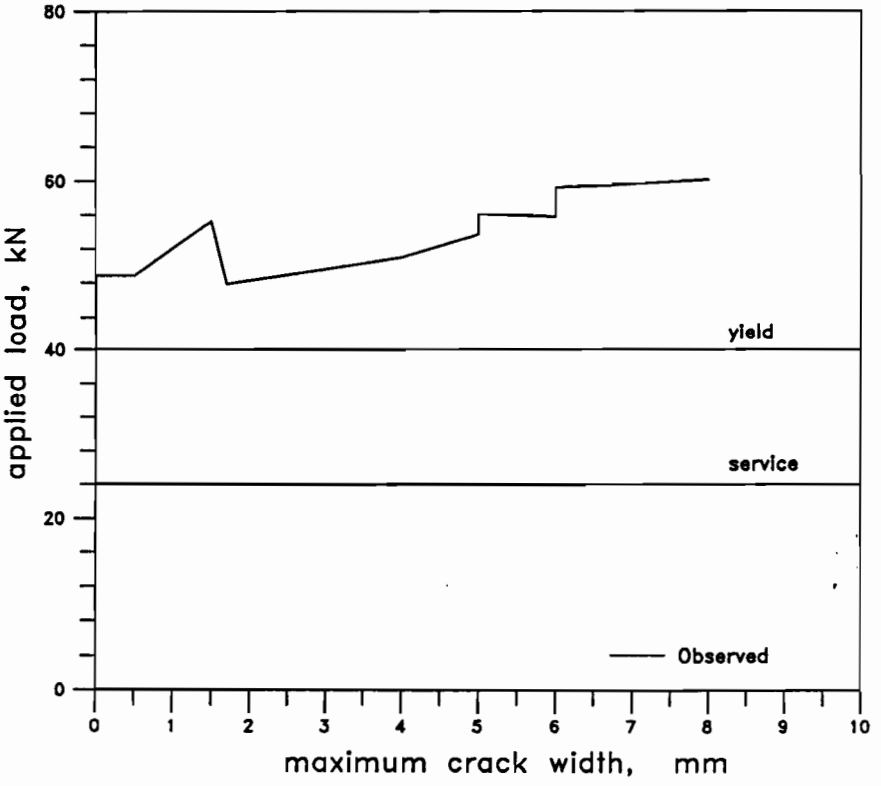

Figure 3-2 (d) Load versus maximum crack width for Specimen T4

3.2.3 Specimens T9 (f_y = 589 MPa) and T10 (f_y = 407 MPa)

Specimens T9 and T10 have cross-sectional dimensions of 100 by 100 mm, have reinforcement ratios of 1.0% and have a concrete compressive strength of 17.0 MPa. Figure 3-3a demonstrates that Specimen T9 ruptured at an average strain of 0.67% and underwent very little plastic deformation, while Specimen T10 deformed plastically to reach an average strain of 12.5% at rupture. Specimen T9 failed outside its gauge length, and hence the average strain at rupture is not representative.

Specimen T9 cracked at a load of about 11 kN and Specimen T10 cracked at a load of 12 kN, as shown in Fig. 3-3b. Since the stress in the steel at first cracking, $f_{s,cr}$ was much less than the yield stress of both types of reinforcement ($f_{s,cr} \approx 110$ MPa), both specimens could develop loads much greater than the cracking load, resulting in a large number of cracks. The average crack spacings were 180 mm and 150 mm for Specimens T9 and T10, respectively.

The predicted responses shown in Fig. 3-3b closely match the observed behaviour of both specimens.

The maximum crack widths corresponding to a given tensile load are shown in Figures 3-3c and 3-3d for Specimens T9 and T10, respectively. The predicted maximum crack widths can also be seen in these figures. At a tension corresponding to service load, Specimen T9 had a maximum crack width of 0.2 mm compared with 0.35 mm for Specimen T10. Once again, the CEB-FIP expression leads to conservative predictions of the maximum crack widths and the Gergely-Lutz expression underestimates the maximum crack widths. These two specimens had approximately the same average crack spacing.

3.2.3 Specimens T9 (f_y = 589 MPa) and T10 (f_y = 407 MPa)

Specimens T9 and T10 have cross-sectional dimensions of 100 by 100 mm, have reinforcement ratios of 1.0% and have a concrete compressive strength of 17.0 MPa. Figure 3-3a demonstrates that Specimen T9 ruptured at an average strain of 0.67% and underwent very little plastic deformation, while Specimen T10 deformed plastically to reach an average strain of 12.5% at rupture. Specimen T9 failed outside its gauge length, and hence the average strain at rupture is not representative.

Specimen T9 cracked at a load of about 11 kN and Specimen T10 cracked at a load of 12 kN, as shown in Fig. 3-3b. Since the stress in the steel at first cracking, $f_{s,cr}$ was much less than the yield stress of both types of reinforcement ($f_{s,cr} \approx$ 110 MPa), both specimens could develop loads much greater than the cracking load, resulting in a large number of cracks. The average crack spacings were 180 mm and 150 mm for Specimens T9 and T10, respectively.

The predicted responses shown in Fig. 3-3b closely match the observed behaviour of both specimens.

The maximum crack widths corresponding to a given tensile load are shown in Figures 3-3c and 3-3d for Specimens T9 and T10, respectively. The predicted maximum crack widths can also be seen in these figures. At a tension corresponding to service load, Specimen T9 had a maximum crack width of 0.4 mm compared with 0.35 mm for Specimen T10. Once again, the CEB-FIP expression leads to conservative predictions of the maximum crack widths and the Gergely-Lutz expression underestimates the maximum crack widths. These two specimens had approximately the same average crack spacing.

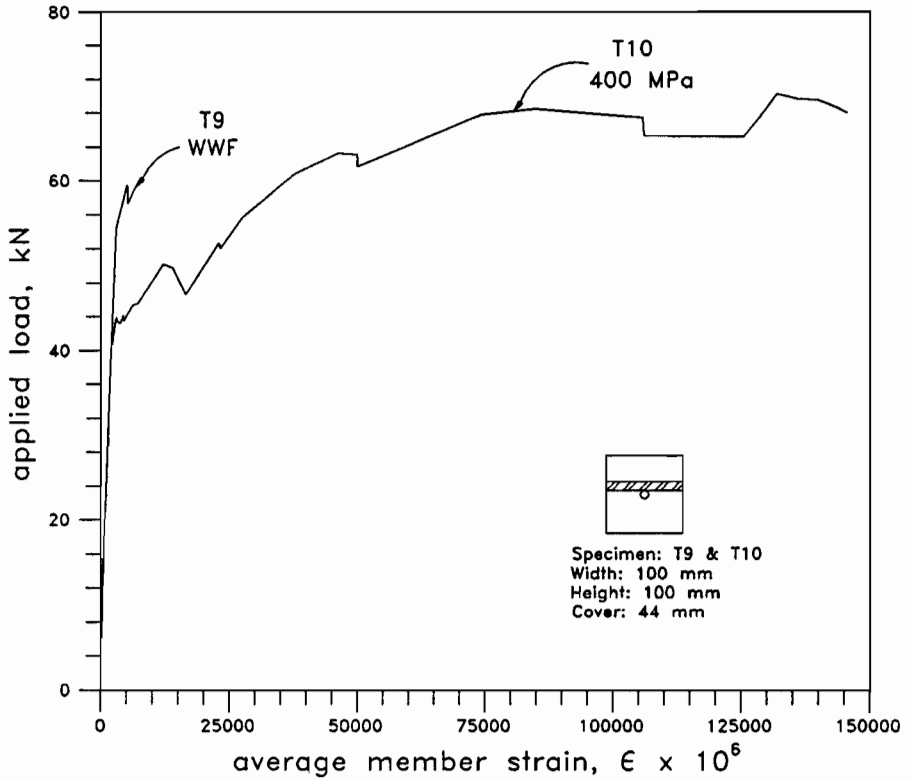

Figure 3-3 (a) Load versus average strain response of Specimens T9 and T10

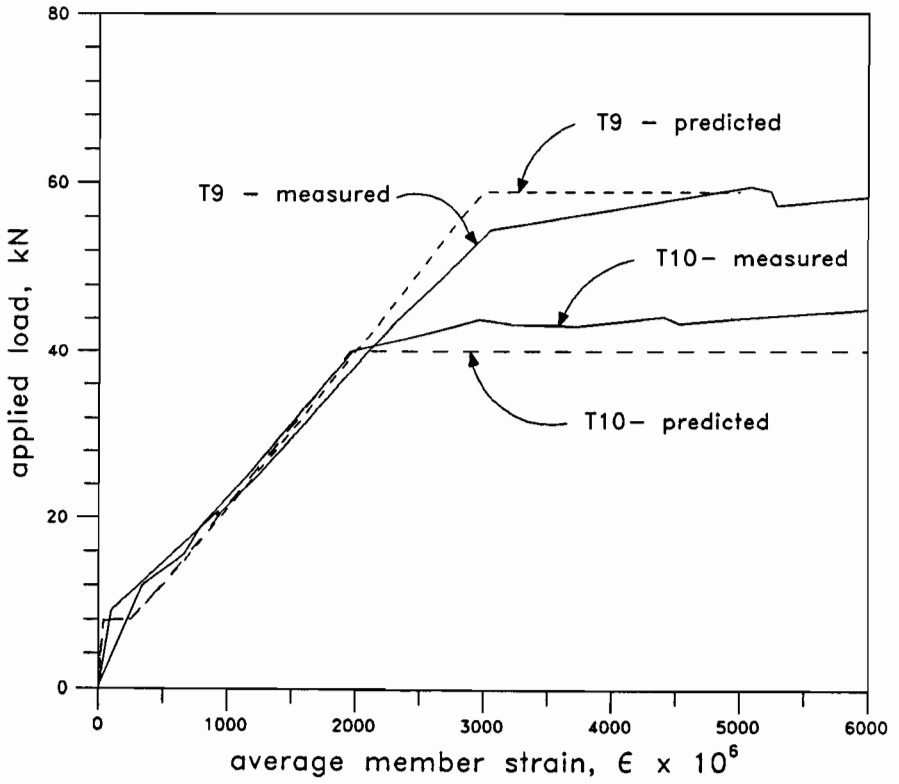

Figure 3-3 (b) Comparison of predicted and measured responses of Specimens T9 and T10

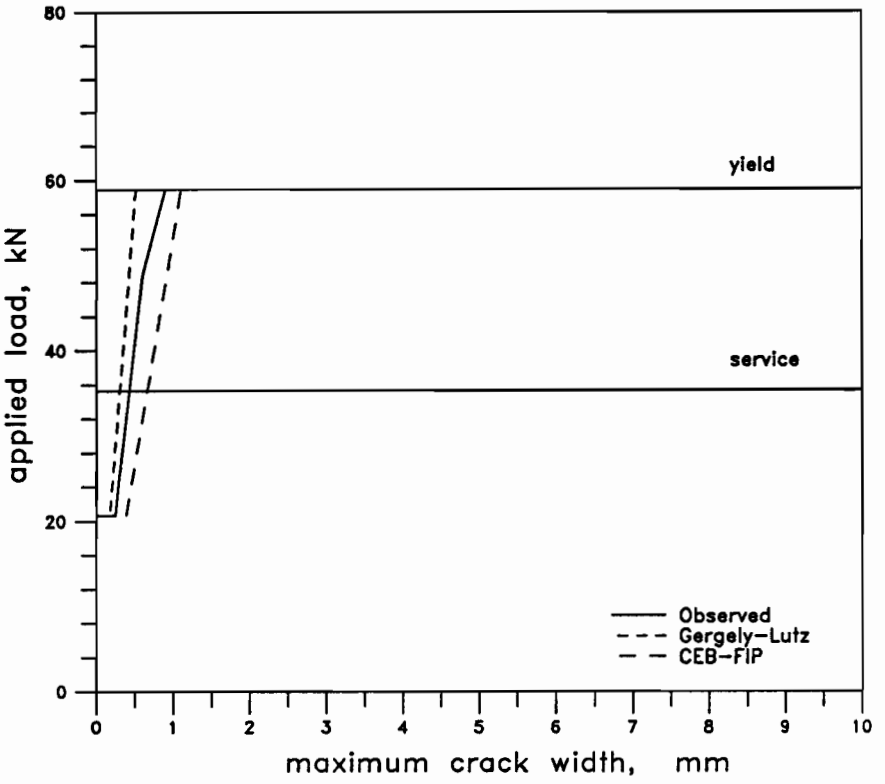

Figure 3-3 (c) Load versus maximum crack width for Specimen T9

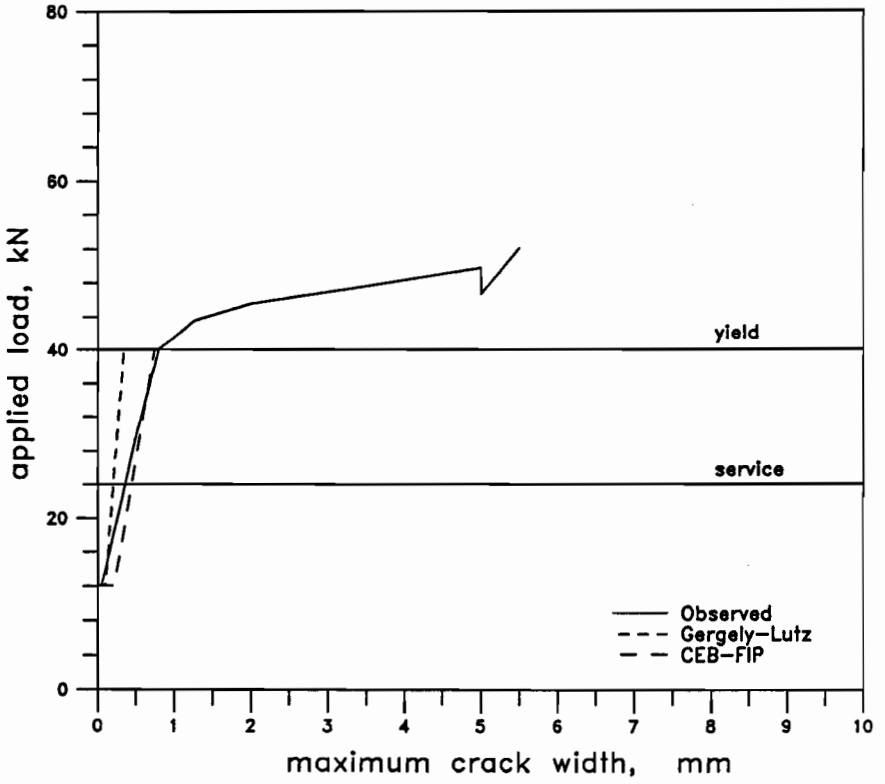

Figure 3-3 (d) Load versus maximum crack width for Specimen T10

3.2.4 Specimens T11 (f_y = 589 MPa) and T12 (f_y = 407 MPa)

Specimens T11 and T12 had cross-sectional dimensions of 100 by 200 mm (ρ = 0.5%) and a concrete strength of 17 MPa. The load-strain responses of these specimens are shown in Fig. 3-4a. Specimen T11 ruptured at a strain, ϵ_r, of 0.75%, while its companion reached an average strain at rupture of 11.3%, after undergoing a significant amount of plastic deformation. Specimen T11 failed outside the gauge length.

Specimen T11 cracked at a load of 19.2 kN while T12 cracked at a slightly higher load of 19.4 kN as shown in Fig. 3-4b. The stress in the steel at first cracking, $f_{s,cr}$, for both specimens was less than their respective yield strengths and they could therefore develop higher loads and allow more cracks to form.

The predicted post-cracking responses of both specimens are conservative (see Fig. 3-4b). In the elastic range, Specimen T12 behaved as predicted. Specimen T11, however, underwent a greater deformation before cracking partly due to localized vertical cracking at the ends of the specimen.

At their respective service load levels, Specimens T11 and T12 both exhibited a maximum crack width of 0.5 mm (see Fig. 3-4c and 3-4d). The CEB-FIP equations yielded conservative estimates of the maximum crack widths up to, and slightly beyond service load, and the Gergely-Lutz expression underestimated the crack widths for both specimens. The average crack spacing in Specimen T11 was 300 mm while it was found to be 180 mm in Specimen T12.

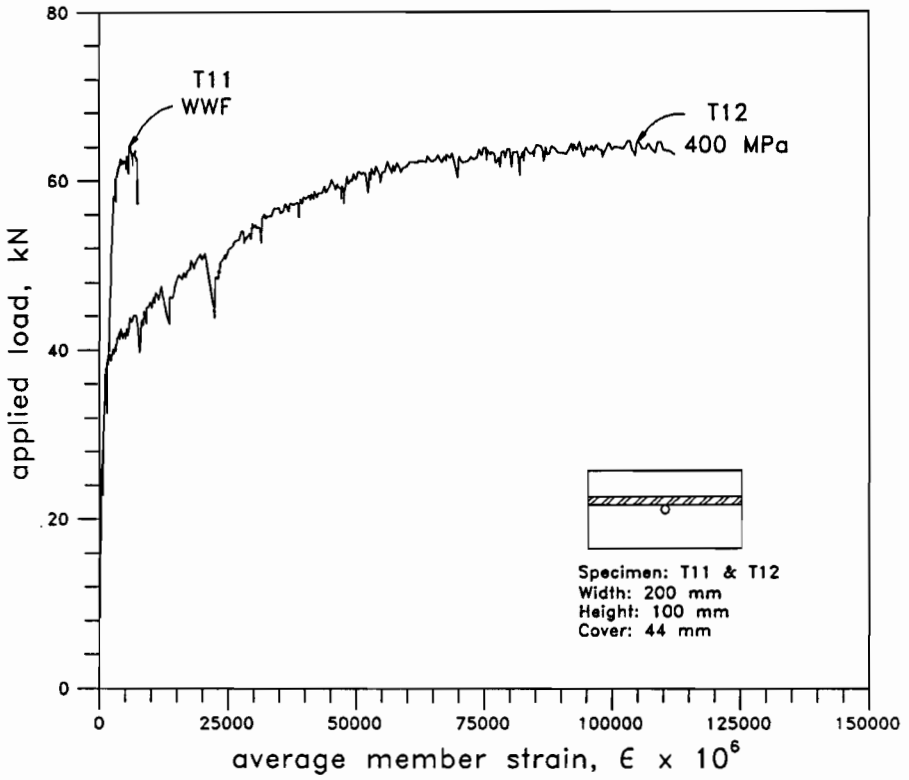

Figure 3-4 (a) Load versus average strain response of Specimens T11 and T12

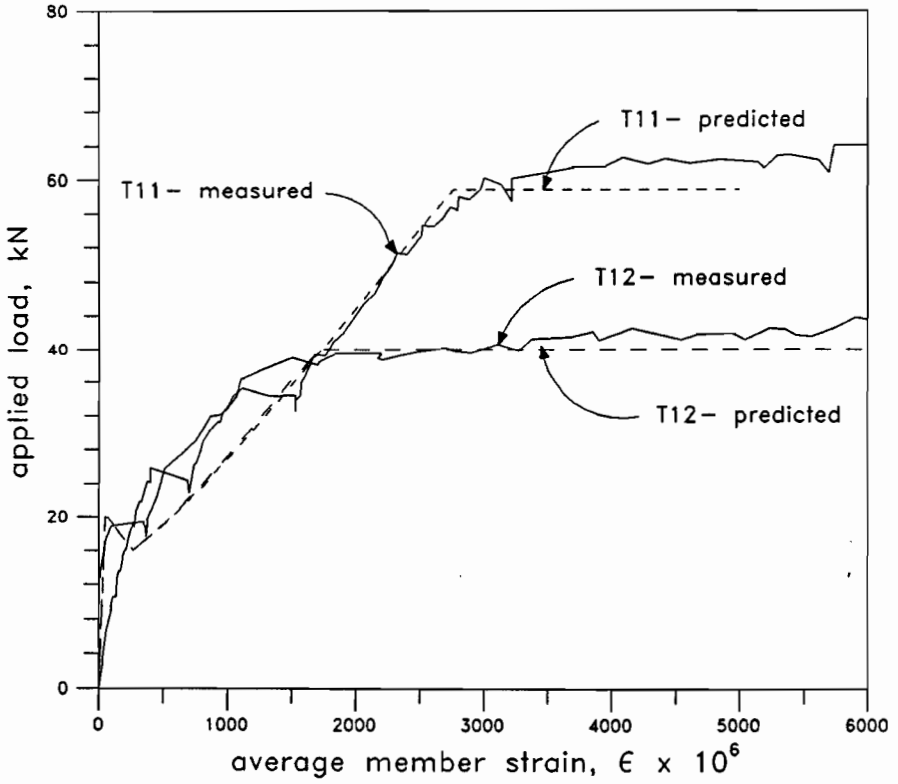

Figure 3-4 (b) Comparison of predicted and measured responses of Specimens T11 and T12

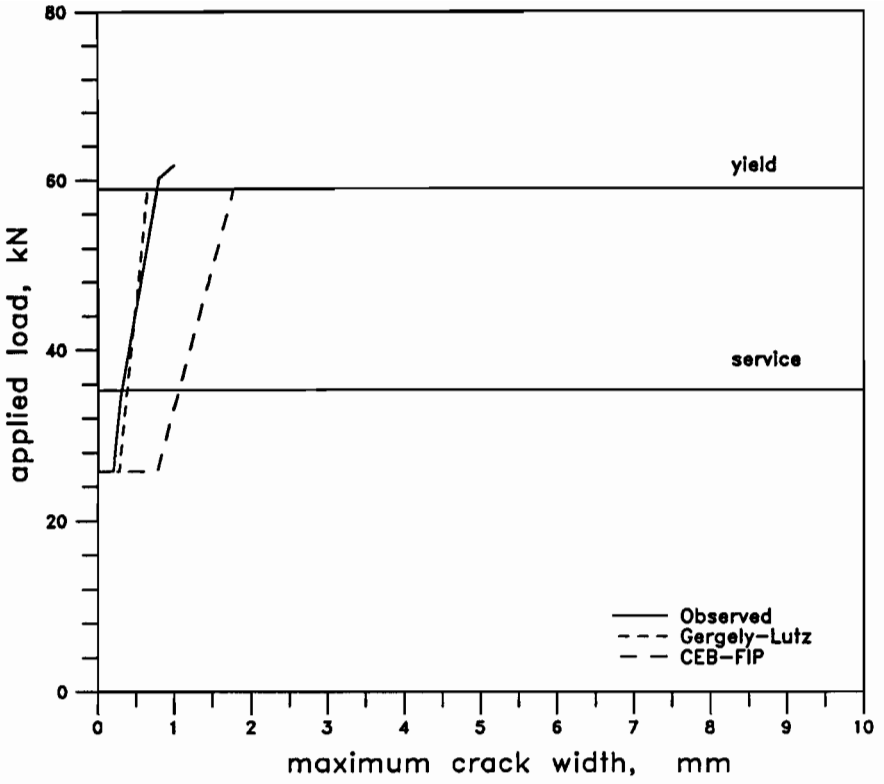

Figure 3-4 (c) Load versus maximum crack width for Specimen T11

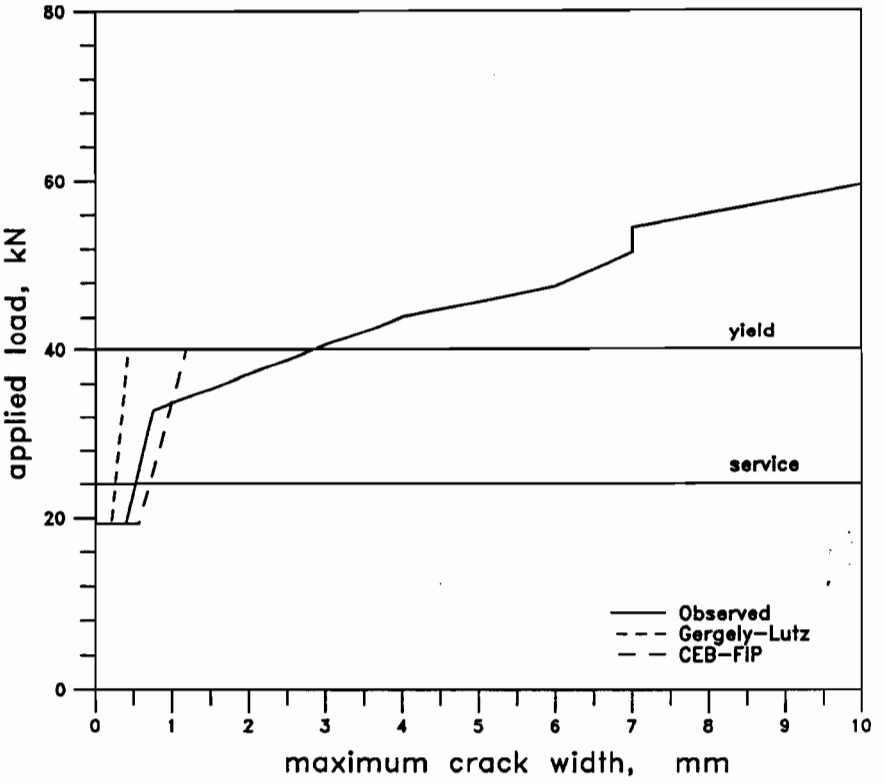

Figure 3-4 (d) Load versus maximum crack width for Specimen T12

3.3 High-Strength Concrete Tension Tests

The results of the high-strength concrete tension tests are summarized in Table 3-3. The maximum crack widths at first cracking are shown in Table 3-4 for the eight high-strength specimens. Table 3-4 also includes the maximum crack widths measured at a service load level of 0.6 times the measured yield load, $A_s f_y$, and the average crack spacings.

Specimen	Grade	ρ %	f'_c MPa	P_{cr} kN	$f_{s,cr}$ MPa	P_u kN	ϵ_u %	ϵ_r %
T5	500	0.568	76.8	47.7	477	61.0	0.76	1.43
T7	400	0.568	76.3	46.5	465	68.5	8.90	13.37
T6	500	0.36	76.8	54.7	547	61.1	0.37	0.45
T8	400	0.36	76.3	52.5	525	69.0	6.06	7.28
T13	500	1.78	64.0	10.4	104	61.2	0.70	1.41
T14	400	1.78	64.0	9.4	94	64.9	7.78	13.74
T15	500	1.0	64.0	24.8	248	62.5	0.67	0.84
T16	400	1.0	64.0	24.4	244	64.0	8.62	11.45

Table 3-3 Summary of high-strength concrete tension tests

Specimen	Grade	P_{cr} kN	w_{max} @P_{cr} mm	Service Load $=0.6A_s f_y$ kN	w_{max} @ Service Load mm	Average Crack Spacing mm
T5	500	47.7	0.50	35.3	-	225
T7	400	46.5	0.90	24.0	-	150
T6	500	54.7	0.50	35.3	-	900
T8	400	52.5	0.60	24.0	-	150
T13	500	10.4	0.05	35.3	0.30	150
T14	400	9.4	0.10	24.0	0.25	82
T15	500	24.8	0.25	35.3	-	150
T16	400	24.4	0.25	24.0	-	90

Table 3-4 Crack characteristics of high-strength concrete specimens

3.3.1 Specimens T5 (f_y = 589 MPa) and T7 (f_y = 407 MPa)

Specimens T5 and T7 were cast with 76.8 and 76.3 MPa concrete, respectively. They had a cross section of 160 by 110 mm and hence a reinforcement ratio, ρ, of 0.57%. As shown in Fig. 3-5a, Specimen T7 ruptured at an average strain of 13.4% and exhibited a more ductile behaviour than Specimen T5 (ϵ_r = 1.4%).

Specimen T5 cracked at a load of approximately 47 kN while T7 cracked at a load of about 40 kN, as shown in Fig. 3-5b. This figure also compares the predicted and actual responses of these two tension specimens. The actual cracking loads differed slightly from the predictions. Splitting cracks formed along the length of the two specimens and caused them to undergo greater deformations than predicted.

The variation of the maximum crack widths with loading are shown in Figures 3-5c and 3-5d for Specimens T5 and T7. The maximum crack widths, predicted for Specimen T5, are shown in Fig 3-5c. The crack widths measured just after cracking were 0.5 mm and 0.9 mm for Specimens T5 and T7, respectively. The average crack spacing along Specimen T5 was 225 mm while Specimen T7 had an average crack spacing of 150 mm.

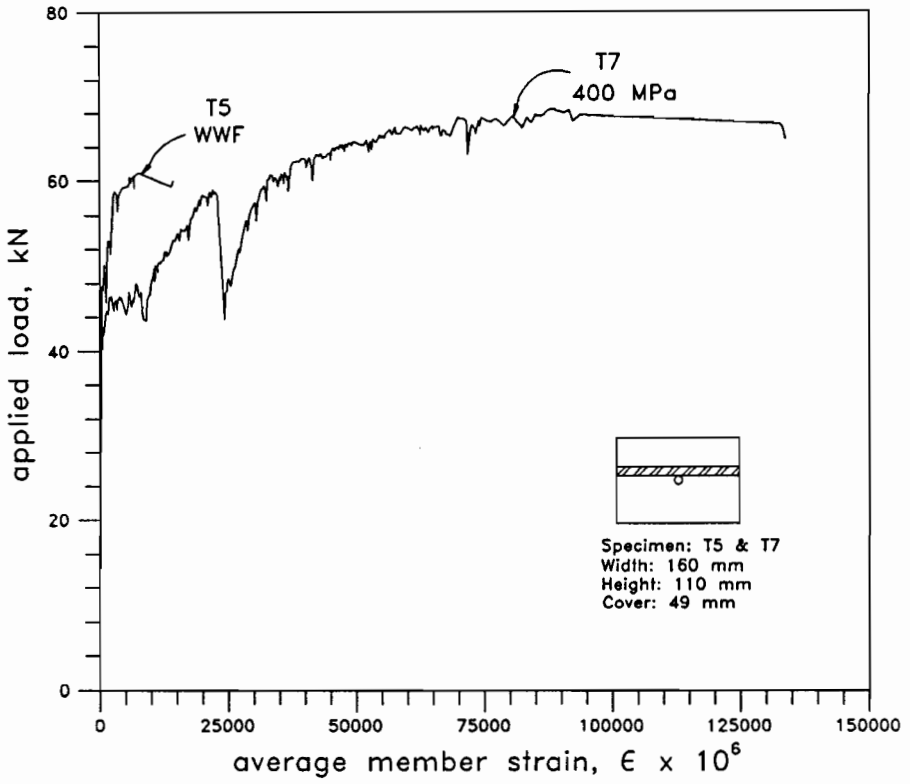

Figure 3-5 (a) Load versus average strain response of Specimens T5 and T7

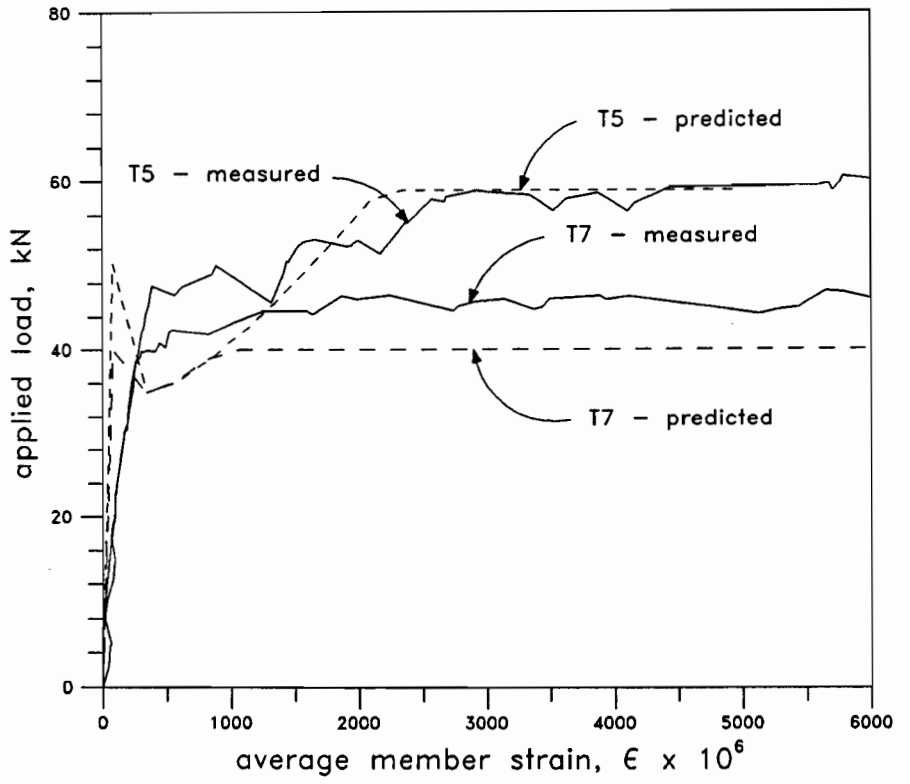

Figure 3-5 (b) Comparison of predicted and measured responses of Specimens T5 and T7

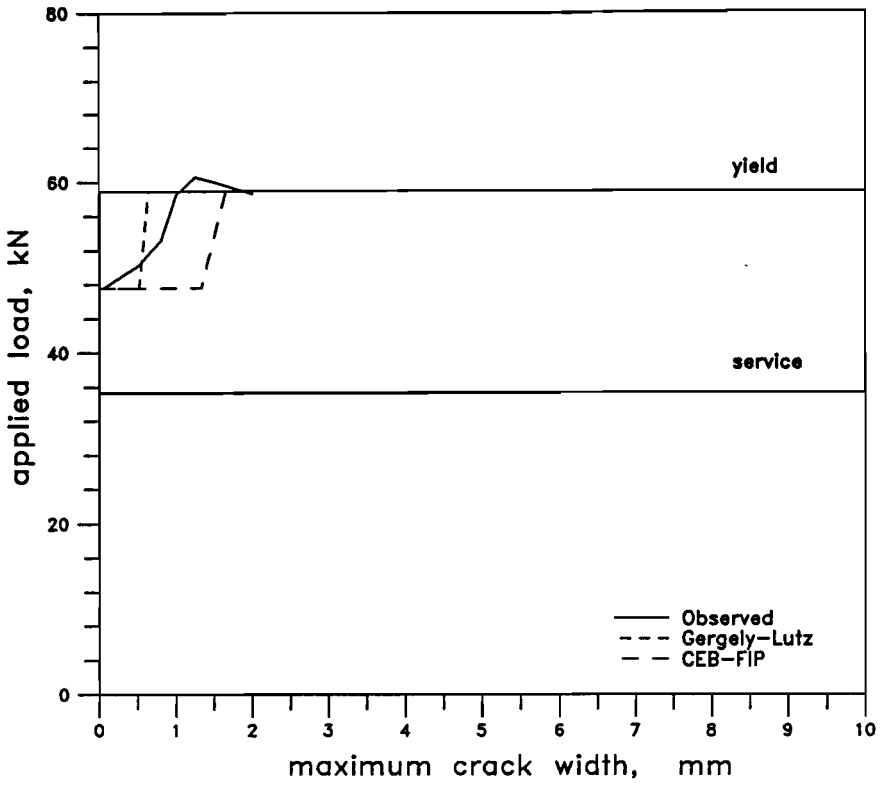

Figure 3-5 (c) Load versus maximum crack width for Specimen T5

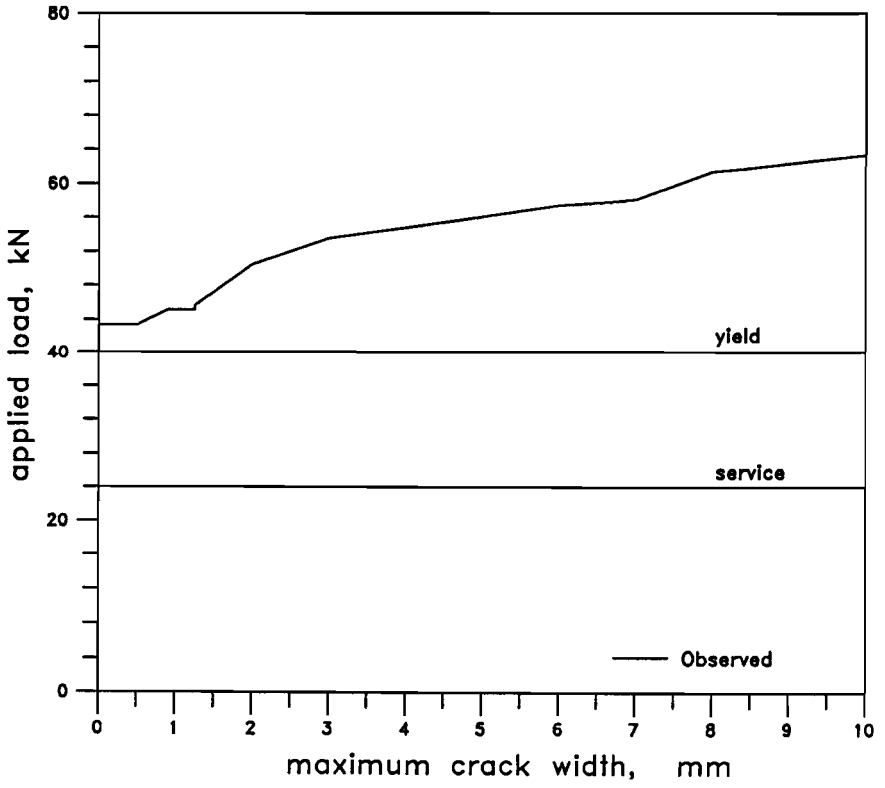

Figure 3-5 (d) Load versus maximum crack width for Specimen T7

3.3.2 Specimens T6 (f_y = 589 MPa) and T8 (f_y = 407 MPa)

Specimens T6 and T8 had cross-sectional dimensions of 250 by 110 mm, a low reinforcement ratio (ρ = 0.36%), and concrete strengths of 76.3 and 76.8 MPa, respectively. Fig. 3-6a shows that Specimen T6 reached a maximum average strain at rupture, ϵ_r, of 0.45%, and exhibited a less ductile response than Specimen T8 which ruptured at a strain of 7.28%. Specimen T6 failed outside its gauge length.

As can be seen in Fig. 3-6b, the predicted cracking loads are greater than the cracking loads of 54.7 and 52.5 kN measured for Specimens T6 and T8, respectively. Since the load required to cause cracking exceeded the yield strength of both steels, localized vertical cracks formed at both ends of the specimens that branched out to form transverse cracks at the cross-ties. This cracking mechanism caused the measured response to be much softer than the predicted response in the elastic range. In the post-cracking range, the predictions are conservative.

Figures 3-6c and 3-6d show the variation of the maximum crack widths with loading. At first cracking, the maximum crack width in Specimen T6 was 0.50 mm while it was measured as 0.60 mm in Specimen T8. The expressions used in predicting the maximum crack widths were not valid for either of the specimens due to the bond initiated cracks and the high cracking load. Specimen T8 had a smaller average crack spacing than Specimen T6.

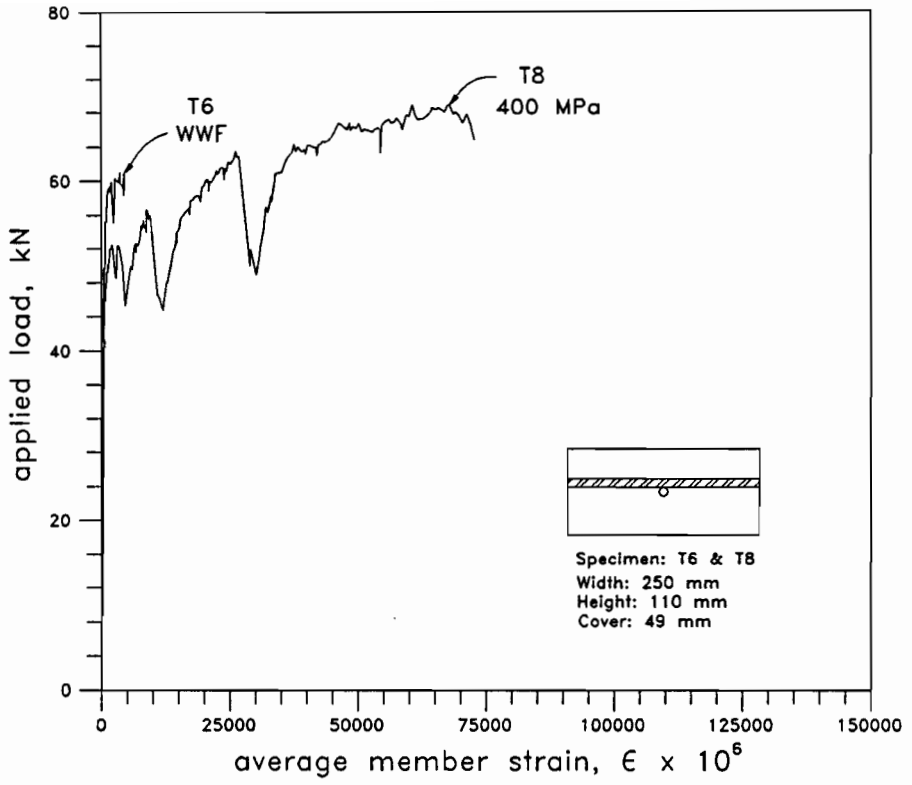

Figure 3-6 (a) Load versus average strain response of Specimens T6 and T8

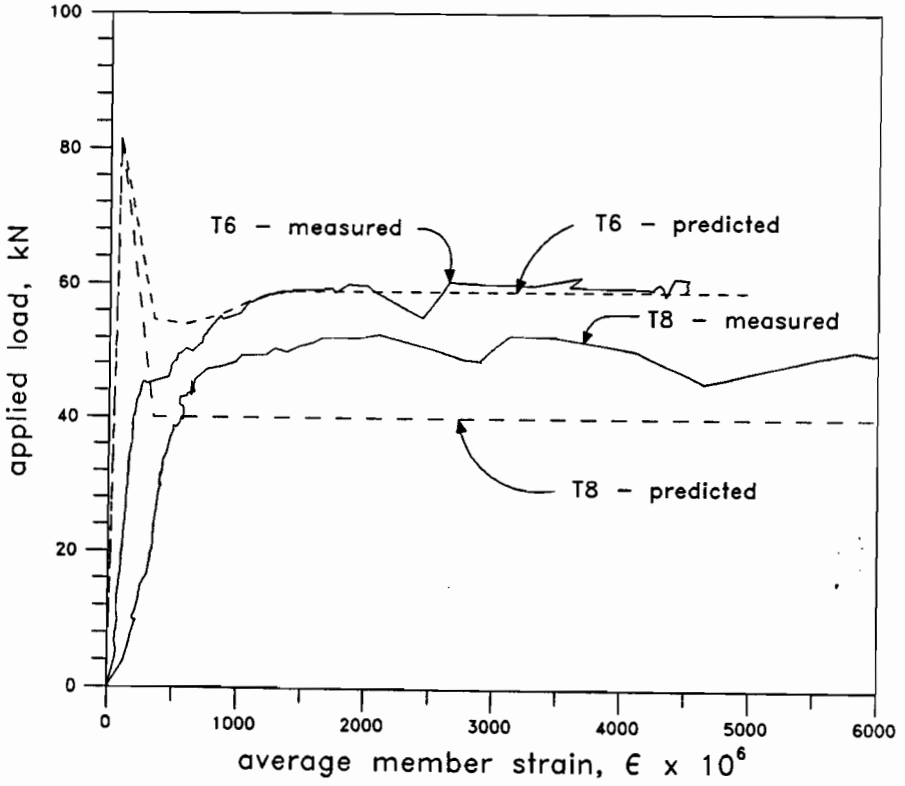

Figure 3-6 (b) Comparison of predicted and measured responses of Specimens T6 and T8

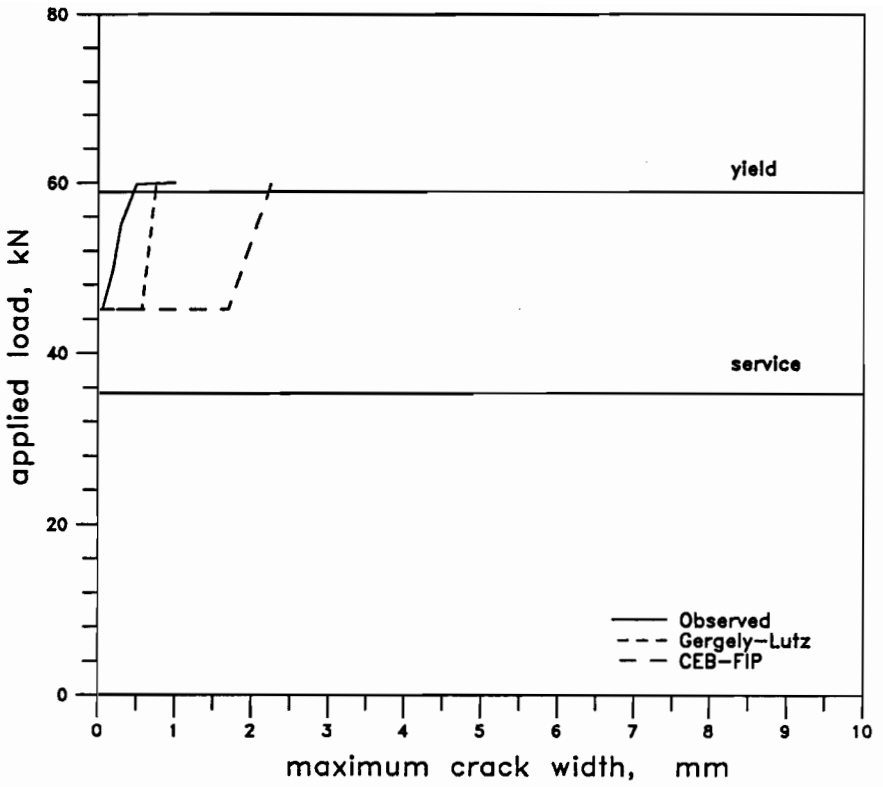

Figure 3-6 (c) Load versus maximum crack width for Specimen T6

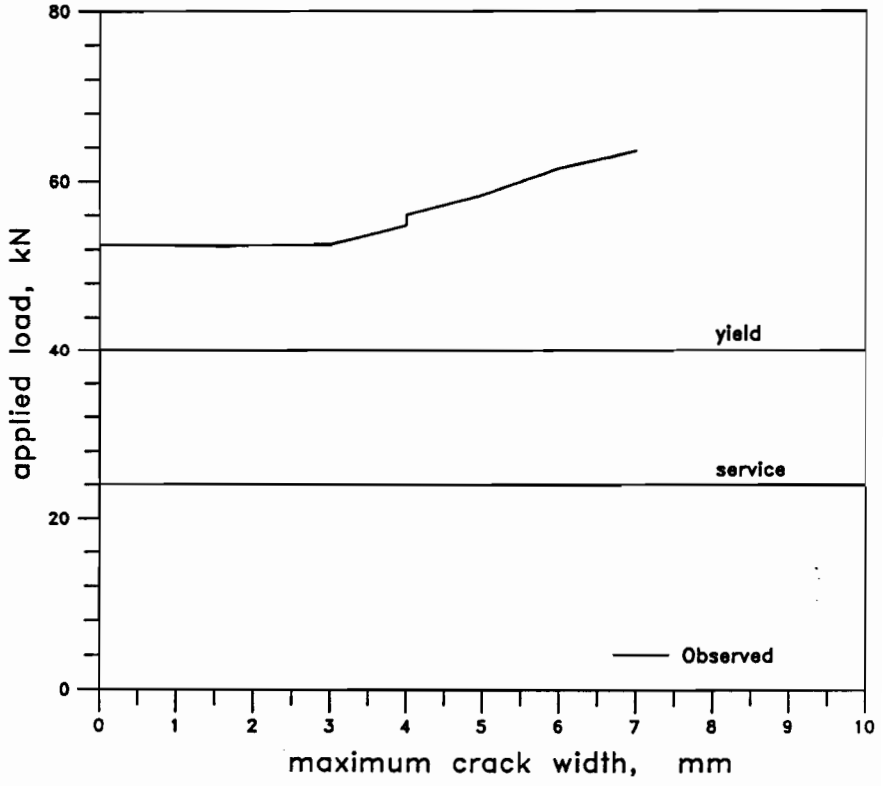

Figure 3-6 (d) Load versus maximum crack width for Specimen T8

3.3.3 Specimens T13 (f_y = 589 MPa) and T14 (f_y = 407 MPa)

These two specimens had a 75 mm square cross-section and were cast with 64 MPa concrete. Their reinforcement ratio was 1.78%. The load-strain relationships for these two specimens are shown in Fig. 3-7a. Specimen T13 failed outside of the gauge length at an average strain of 1.41% whereas Specimen T14 demonstrated a considerably more ductile response, rupturing at a peak strain of 13.7%.

Specimens T13 and T14 both cracked at a load of about 10 kN, which is very close to the predicted cracking load as can be seen in Fig. 3-7b. Since $f_{s,cr}$ was well below the yield stress of both steels, the two specimens were able to withstand much greater loads and therefore develop a large number of cracks. In fact, both specimens developed transverse cracks at all of the cross ties. The predicted responses are compared with the observed behaviour of both specimens in Fig. 3-7b, which shows that the predicted behaviour underestimates the actual response.

Figures 3-7c and 3-7d show the crack development for Specimens T13 and T14, respectively. For Specimen T13, the maximum crack width at service load was measured as 0.30 mm while Specimen T14 had a maximum crack width of 0.25 mm. Immediately following cracking, Specimens T13 and T14 had respective maximum cracks widths of 0.05 and 0.10 mm. The Gergely-Lutz equation underestimates the maximum measured crack widths while the CEB-FIP expression offers a conservative prediction. Specimen T13 was found to have an average crack spacing of 150 mm, while Specimen T14 had an average crack spacing of 81 mm. These two specimens cracked at all of the cross tie locations since the spacing of the transverse reinforcement (150 mm) was similar to the average crack spacing from Eq. 1-9, s_m = 142 mm.

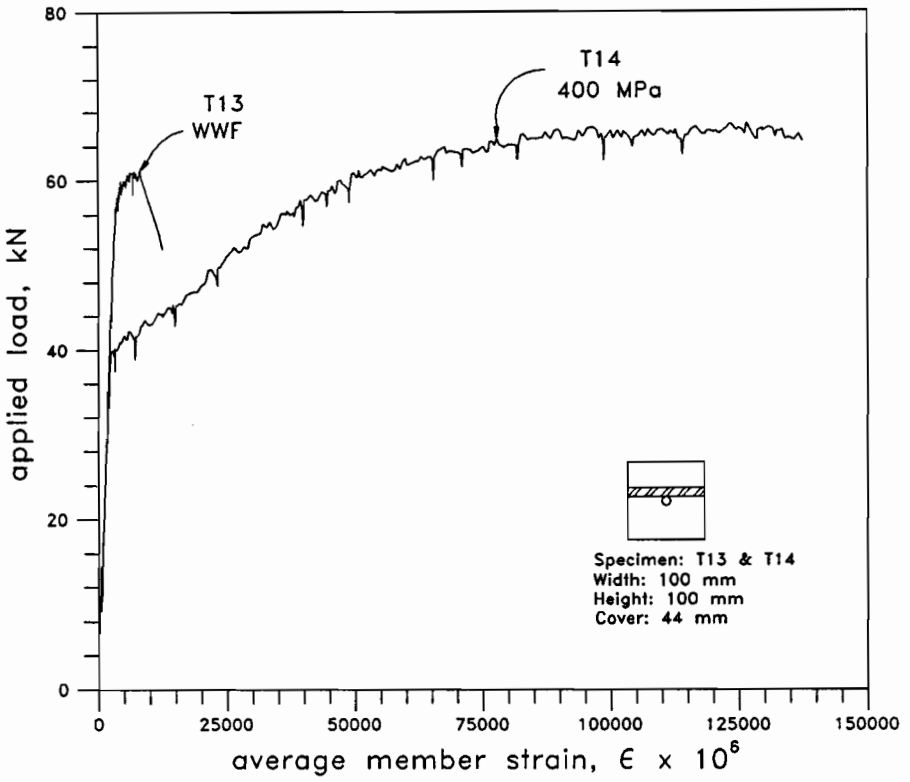

Figure 3-7 (a) Load versus average strain response of Specimens T13 and T14

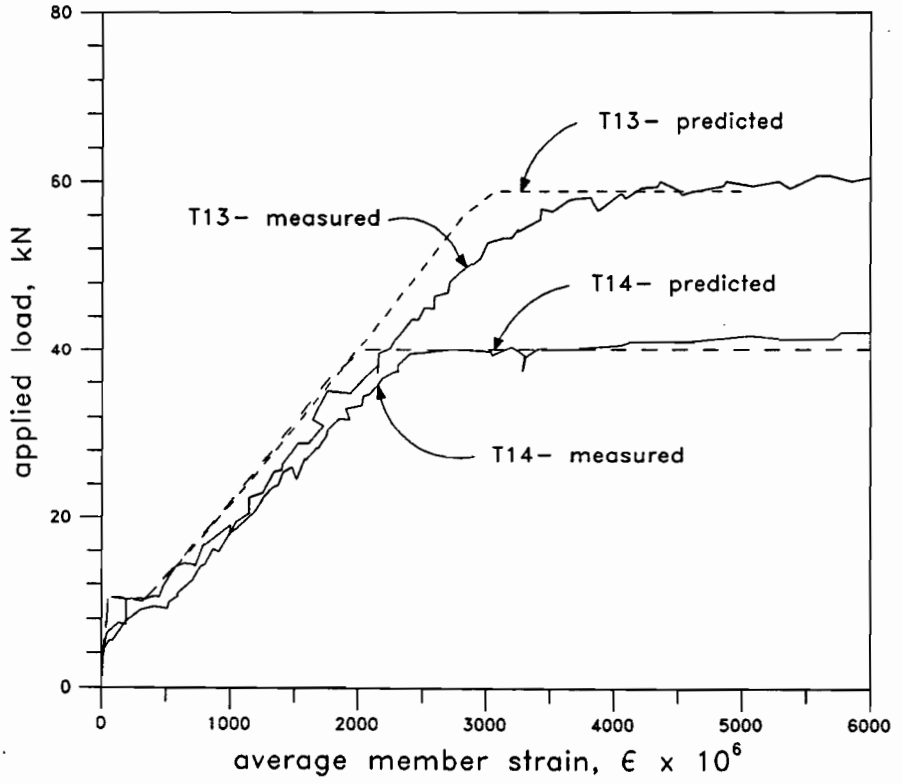

Figure 3-7 (b) Comparison of predicted and measured responses of Specimens T13 and T14

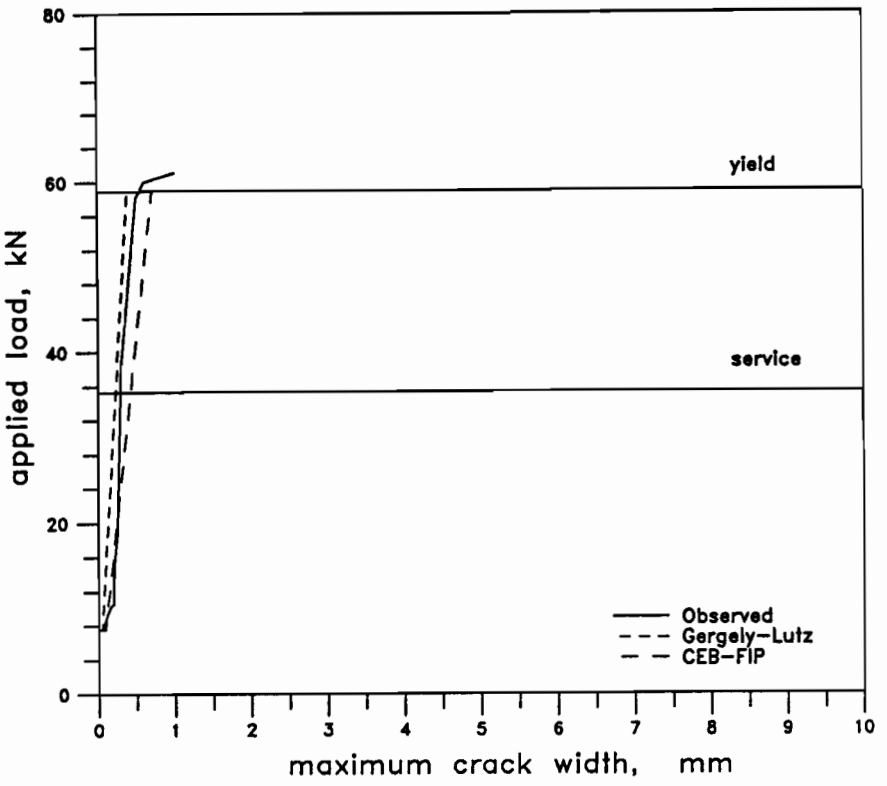

Figure 3-7 (c) Load versus maximum crack width for Specimen T13

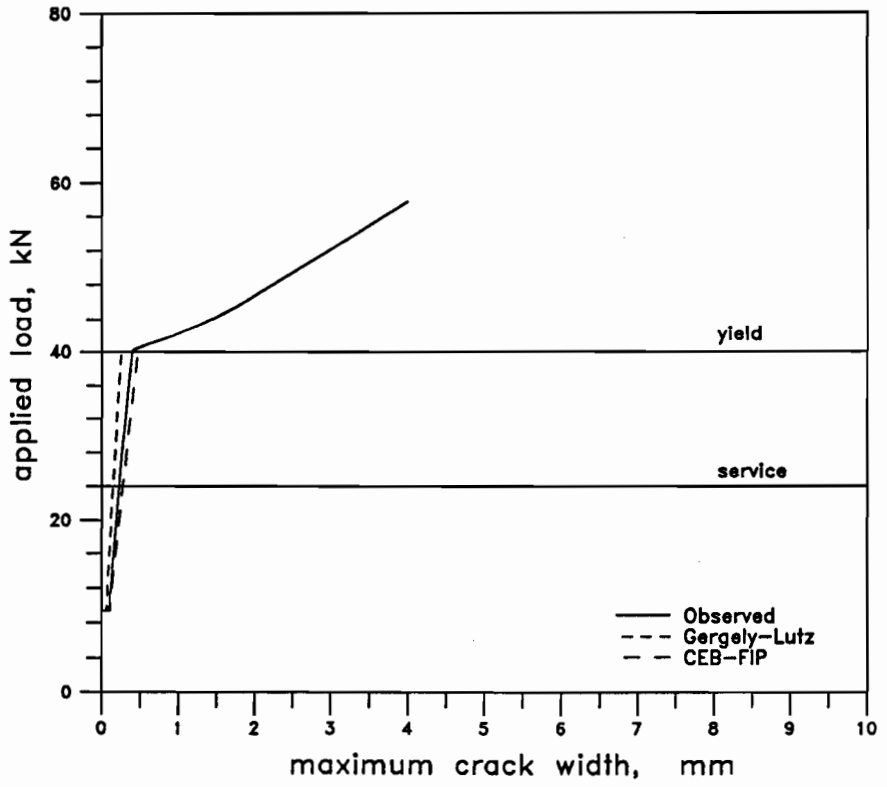

Figure 3-7 (d) Load versus maximum crack width for Specimen T14

3.3.4 Specimens T15 (f_y = 589 MPa) and T16 (f_y = 407 MPa)

Specimens T15 and T16 had a reinforcement ratio, ρ, of 1%, had cross-sectional dimensions of 100 by 100 mm and a concrete strength of 64.0 MPa. As can be seen in Fig. 3-8a, Specimen T15 reached an average ultimate strain of 0.84% prior to failing outside its gauge length, whereas T16, displaying a more ductile response, ruptured at an average strain of 11.4%.

The predicted and observed responses of both specimens are shown in Fig. 3-8b. The predicted cracking load matches the load of 24.4 kN at which cracking occurred. A large number of cracks formed in both specimens as the load was increased due to the low steel stress at initial cracking.

Figures 3-8c and 3-8d present the variation of maximum crack widths with increasing loading. At first cracking, Specimens T15 and T16 both had a maximum crack width of 0.25 mm. The CEB-FIP equations predict maximum crack widths that exceed the measured values while the Gergely-Lutz expression underestimates the maximum crack widths. The average crack spacings were 180 mm and 75 mm for Specimens T15 and T16, respectively.

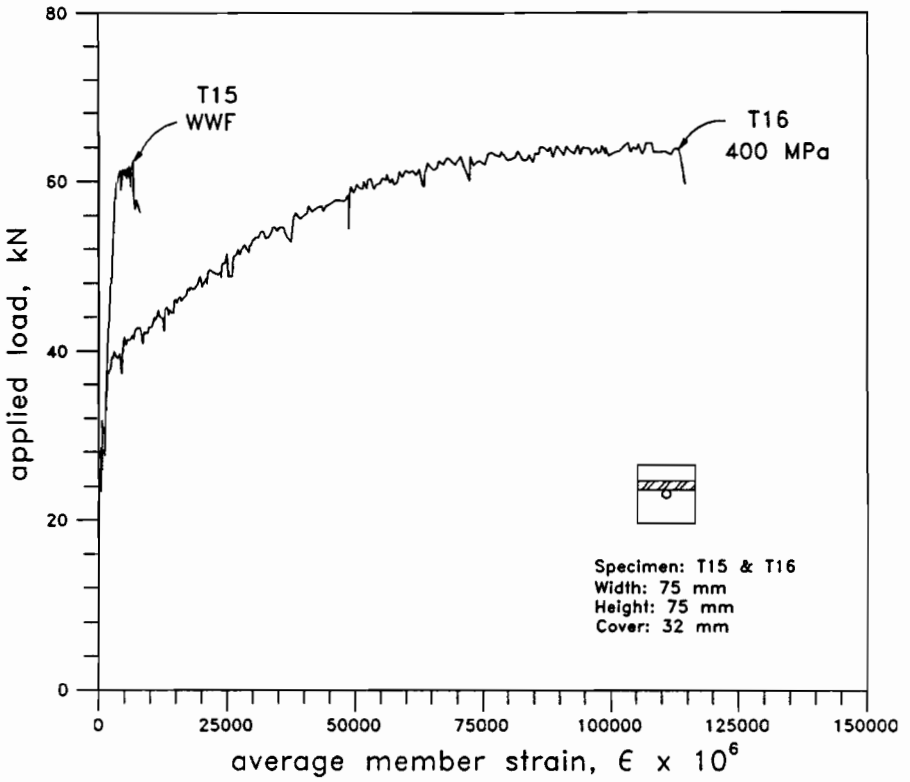

Figure 3-8 (a) Load versus average strain response of Specimens T15 and T16

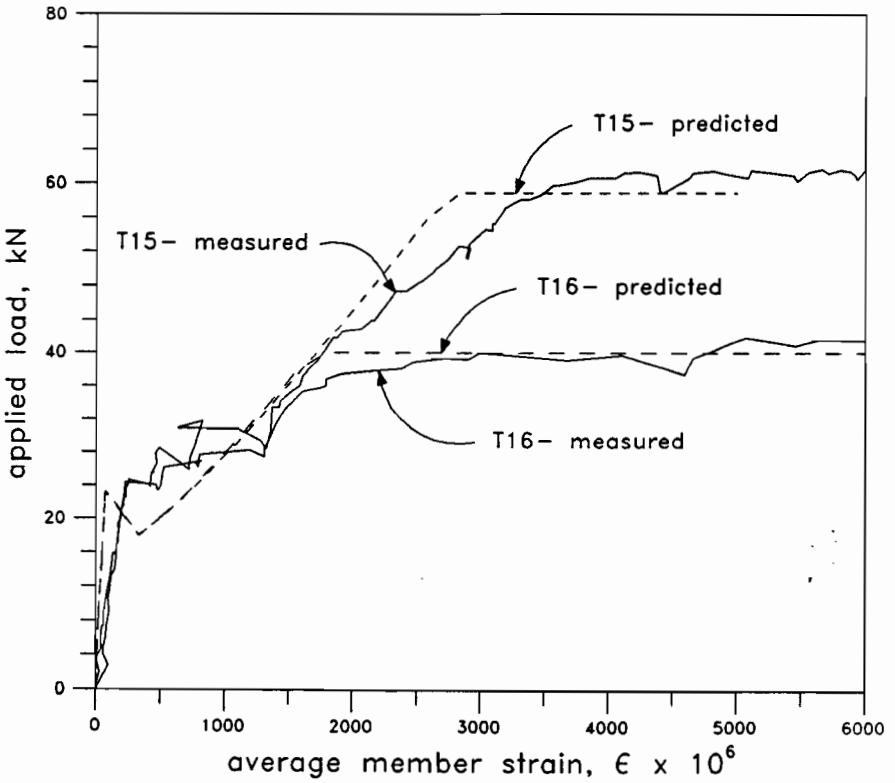

Figure 3-8 (b) Comparison of predicted and measured responses of Specimens T15 and T16

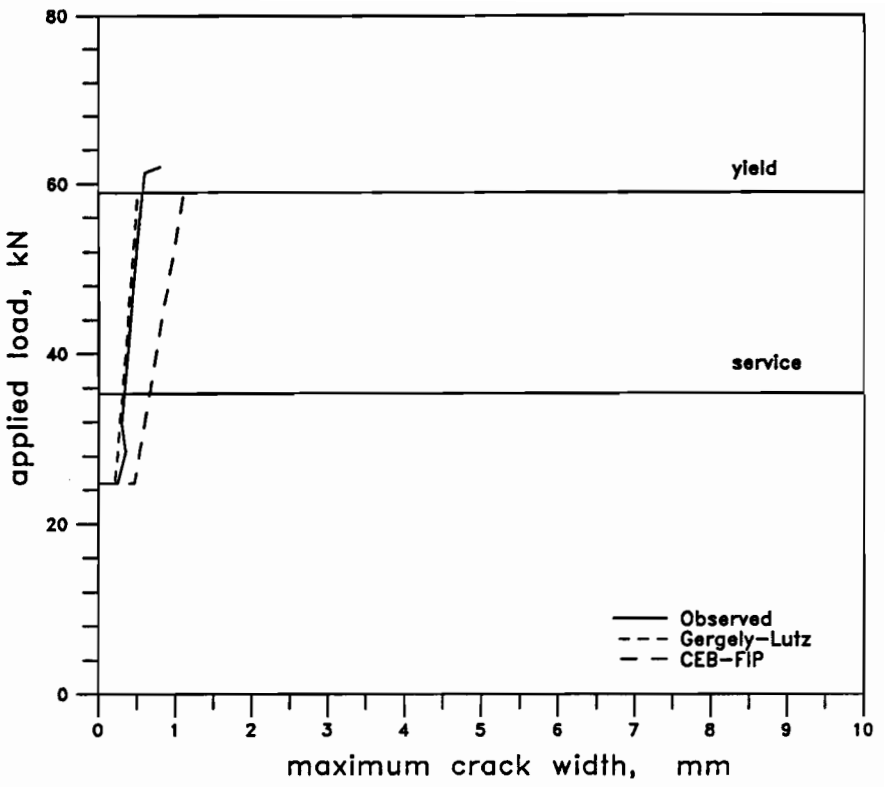

Figure 3-8 (c) Load versus maximum crack width for Specimen T15

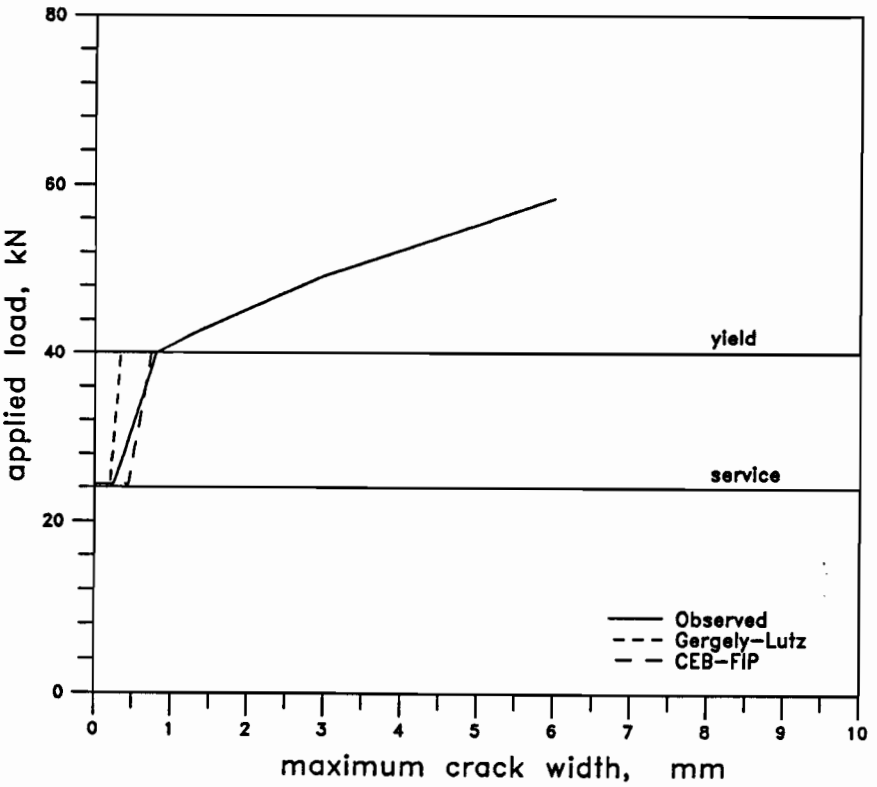

Figure 3-8 (d) Load versus maximum crack width for Specimen T16

3.4 Influence of Reinforcement Properties, Concrete Strength and Reinforcement Ratio on the Response

The influence of the reinforcement ratio on the steel stress at cracking is shown in Fig. 3-9. The steel stress at cracking, $f_{s,cr}$, is normalized with respect to the measured yield stress for both types of steel, and the reinforcement ratio is normalized by multiplying by $f_y/\sqrt{f'_c}$, to give a reinforcement index. The stress in the reinforcing steel obviously increases with decreasing reinforcing indices.

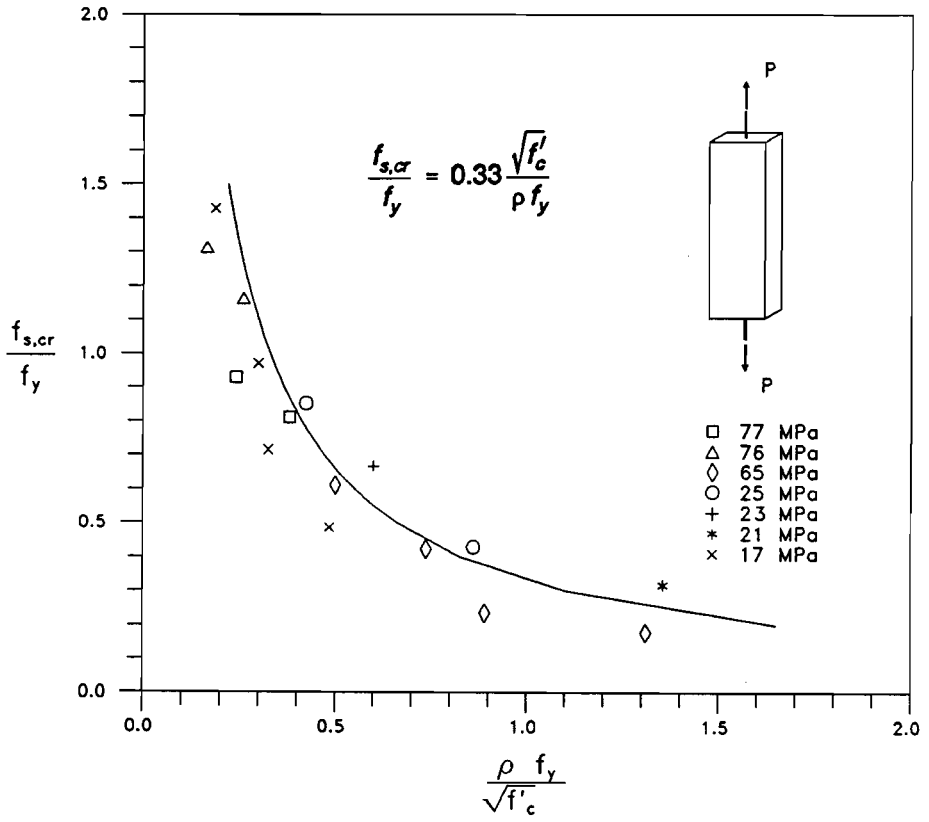

Figure 3-9 Steel stress at cracking as a function of the reinforcing index

The predicted variation of $f_{s,cr}/f_y$ for different reinforcing indices was obtained by rearranging Eq. (1-12) and (1-13) and taking the direct tensile strength of the concrete as $0.33\sqrt{f'_c}$

such that:

$$\frac{f_{s,cr}}{f_y} = 0.33\frac{\sqrt{f'_c}}{\rho f_y} \qquad (3\text{-}1)$$

This equation predicts $f_{s,cr}/f_y$ very well for the full range of specimens tested. The variations from the predictions are caused by the variability of the direct tensile strength of the concrete.

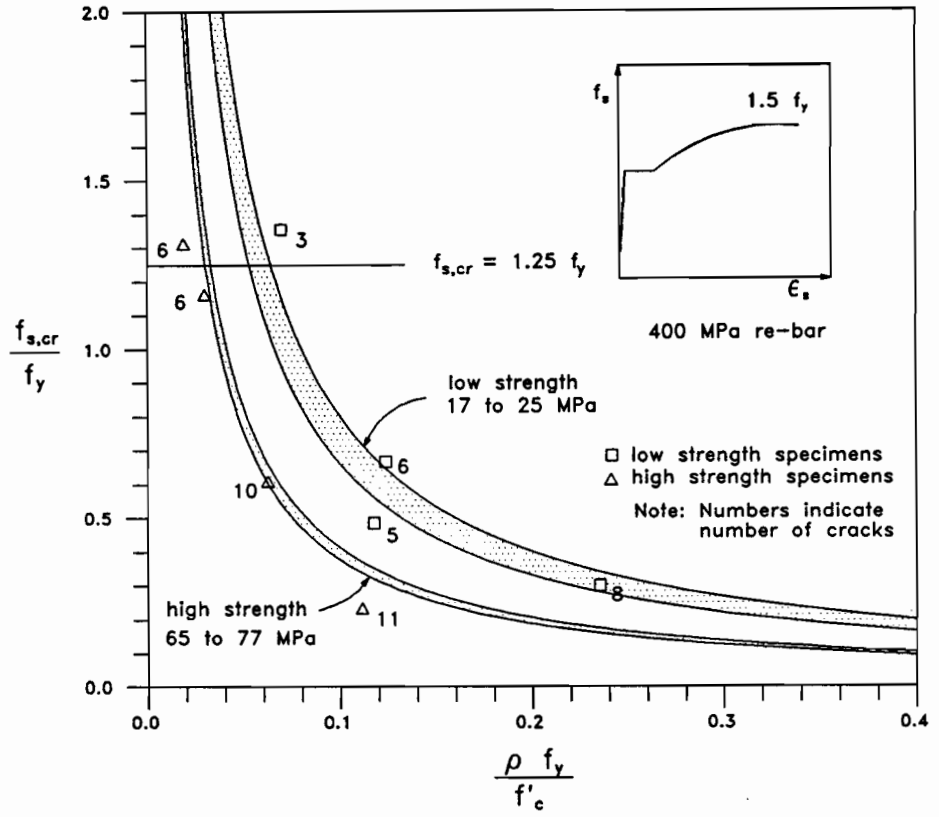

Figure 3-10 Steel stress at cracking as a function of the reinforcement ratio for specimens reinforced with Grade 400, hot-rolled steel

Figures 3-10 and 3-11 show the steel stress at cracking as a function of the reinforcement ratio multiplied by f_y/f'_c in order to differentiate between the high and low-strength concrete tests, for the specimens reinforced with Grade 400, hot-rolled reinforcement and for the specimens containing cold-rolled, deformed welded-wire fabric, respectively. For both types of reinforcement, an increased ductility was observed in specimens having increasing reinforcement ratios. Since

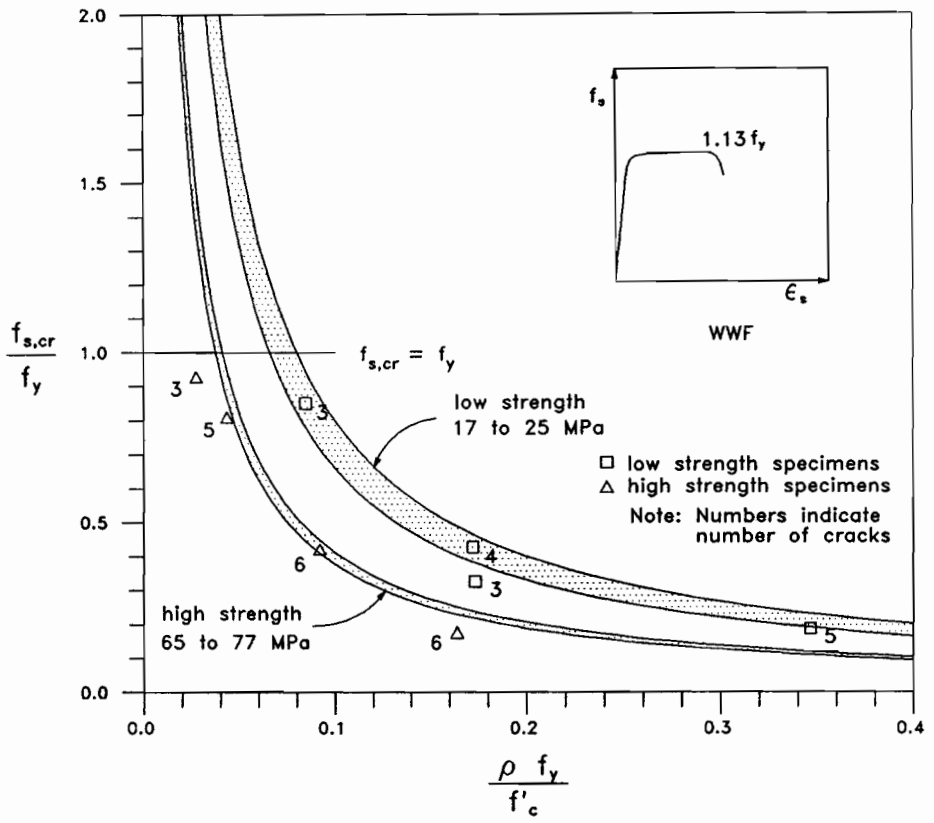

Figure 3-11 Steel stress at cracking as a function of the reinforcement ratio for specimens reinforced with Grade 500, cold-rolled welded-wire fabric

the cracking load, P_{cr}, for the specimens having high reinforcement ratios was less than the yield load, they were able to develop loads in excess of the cracking load and hence allowed more cracks to form prior to failure. The number of transverse cracks that developed in each specimen is shown in Figs. 3-10 and 3-11, next to each data point. Transverse cracks that crossed the longitudinal bar in the test specimens, which caused a strain in the bar were counted as a crack. If a crack did not penetrate through the thickness of the test specimen, it was not counted as a complete transverse crack.

The crack formation mechanism depended on the reinforcement ratio. In specimens having low reinforcement ratios, transverse cracks formed as a result of splitting cracks originating from high localized stresses at the ends of the specimens, which branched out at the cross-tie

locations. Photographs of the low and high strength concrete specimens having the lowest and highest reinforcement ratios are shown in Figs. 3-12 and 3-13, respectively.

The elongation at failure was in the order of 10% for specimens reinforced with the Grade 400, hot-rolled steel, while it only reached a maximum of 1.4% for the specimens containing Grade 500, cold-rolled, deformed welded-wire fabric. This difference reflects the differing ductilities of the two types of steel. The different cracking behaviour was caused by the different bond characteristics of the two steels. The welded-wire fabric had improved bond due to the presence of the welded cross-ties and the deformations on the deformed wire. The welded-wire fabric resulted in less bond slip at a crack location, and hence, smaller crack widths and overall elongations. A significant amount of bond slip occurred at the cracks in specimens reinforced with the hot-rolled reinforcement, resulting in larger crack widths. The exposed reinforcing bar at a crack would begin to strain harden and the specimen would develop a crack at another location, causing a redistribution of the cracking. The welded-wire fabric reinforcement did not exhibit significant strain hardening and therefore this redistribution was not as pronounced.

For the welded-wire fabric, the bare steel ruptured at a strain of 4.75%, while the reinforced concrete member ruptured at average strain values of 0.65% to 1.4%, excluding cases in which the steel ruptured outside of the gauge length. Because of the ductility and strain hardening, the specimens containing hot-rolled reinforcement developed average rupture strains from 7.3% to 13.7% The reinforced concrete members reinforced with hot-rolled, Grade 400 reinforcement therefore exhibited a more ductile response than those containing Grade 500, cold-rolled, welded-wire fabric.

The curves plotted in Figures 3-10 and 3-11 represent the expected variation of the steel stress at cracking with respect to the reinforcement ratio, for the low and high strength concrete specimens. The banded regions between the predicted curves represent the variation in the concrete strengths, with one bandwidth representing lower strength concrete (17 to 25 MPa) and the other representing higher strength concretes (65 to 77 MPa). For both types of reinforcement,

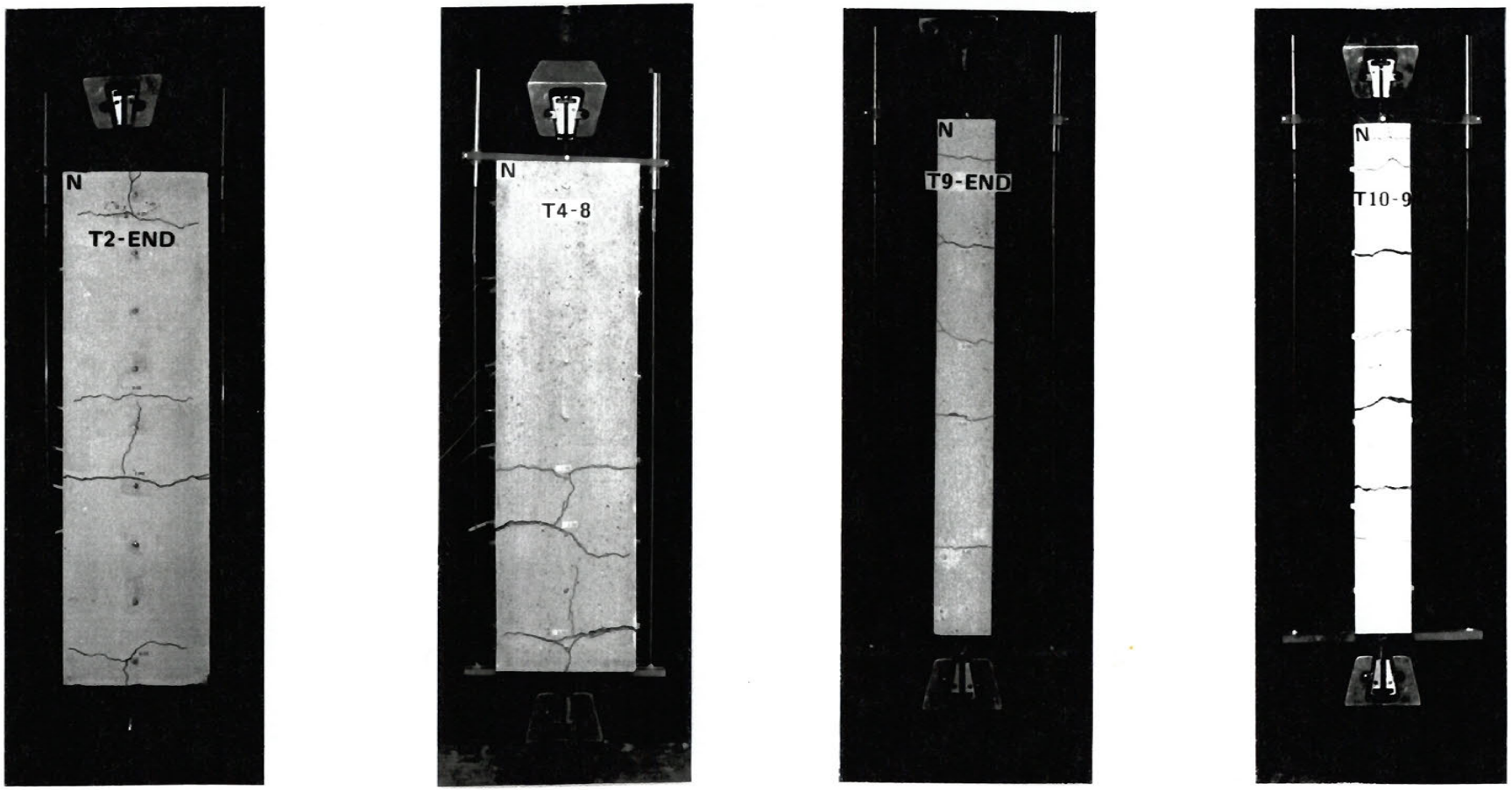

f_y = 589 MPa
f'_c = 25.0 MPa
ρ = 0.36%

f_y = 400 MPa
f'_c = 20.7 MPa
ρ = 0.36%

f_y = 589 MPa
f'_c = 17.0 MPa
ρ = 1.0%

f_y = 400 MPa
f'_c = 17.0 MPa
ρ = 1.0%

Figure 3-12 Cracking patterns of specimens having the lowest and highest reinforcement ratios in the low-strength concrete test series

the high strength concrete increased the number of cracks that formed for a given reinforcement ratio by as much as 50%, thus improving the performance of the specimens. The improved cracking behaviour obtained with the high strength concrete specimens resulted in a more ductile response.

3.5 Minimum Reinforcement for Crack Control

The purpose of minimum reinforcement is to prevent brittle failures and provide warning of failure. Hence, a specimen containing at least the minimum amount of reinforcement would not fail in a brittle manner at the formation of the first crack.

The variation of the steel stress at cracking, $f_{s,cr}$, as a function of the amount of reinforcement, expressed as $\rho f_y/f'_c$, is shown in Fig. 3-10 for the Grade 400, hot-rolled steel. This figure demonstrates that specimens having low reinforcement ratios can exhibit ductile failures even though $f_{s,cr}$ exceeds the yield stress. Therefore, the suggestion that $\rho_{min} = f_{cr}/f_y$ is conservative for hot-rolled reinforcing bars which have considerable strain hardening, and hence, can generate stresses much greater than f_y. The specimens tested demonstrated that for low amounts of reinforcement, more than one crack was developed even for cases where $f_{s,cr}$ exceeds $1.25\ f_y$. Thus, providing $\rho_{min} = f_{cr}/1.25\ f_y$ for hot-rolled reinforcement, satisfies the requirement for minimum reinforcement. Taking the cracking stress of the concrete as $0.33\sqrt{f'_c}$ gives:

$$\rho_{min} = \frac{f_{cr}}{1.25 f_y} = \frac{0.33\sqrt{f'_c}}{1.25 f_y} \qquad (3\text{-}2)$$

This limiting amount of reinforcement is shown in Fig. 3-10. The value of f_y used in Fig. 3-10 corresponds to the measured yield stress in the steel. It is noted that it may even be possible to develop more than one crack for values of $f_{s,cr}$ approaching $1.5\ f_y$, but a suitable reserve of strength after cracking would not be provided (i.e. $M_u/M_{cr} < 1.2$).

The specimens reinforced with cold-rolled, Grade 500, welded-wire fabric having the

lowest reinforcement ratios in this test series were capable of developing a minimum of 3 cracks prior to failure (see Fig. 3-11). Due to the small amount of strain hardening it is suggested that specimens reinforced with cold-rolled welded-wire fabric contain a minimum reinforcement ratio as follows:

$$\rho_{min} = \frac{f_{cr}}{f_y} = \frac{0.33\sqrt{f'_c}}{f_y} \qquad (3\text{-}3)$$

This limiting amount of reinforcement is shown in Fig. 3.11. The value of f_y used in Fig. 3-11 corresponds to the measured yield stress in the steel. The minimum reinforcement ratio as given by Eq. 3-3 would ensure that the welded-wire fabric would provide adequate crack control and the reinforced concrete section would exhibit a ductile response.

The above equations were developed using the measured yield stresses of the two types of reinforcement and the observed responses of the reinforced concrete specimens. For a case where f'_c = 30 MPa, the minimum reinforcement ratio required to provide crack control and a ductile response is ρ_{min} = 0.36% for both hot-rolled steel having f_y of 400 MPa and cold-rolled welded-wire fabric having f_y equal to 500 MPa. For a higher strength concrete having f'_c = 70 MPa, the values of ρ_{min} are 0.55% for both types of reinforcement.

Chapter 4

Observed Responses of Tee Beams

This chapter summarizes the observed responses of two full-scale beam specimens tested under simulated uniform loading. Details of the test specimens are given in Section 2.2.1. In order to obtain more information from each beam test the stirrup spacing differed in the west and east halves of the beams. The stirrups in the east half were more closely spaced than those in the west half. This enabled the influence of the stirrup spacing on the serviceability performance to be studied.

4.1 Tee Beam Subjected to High Shear (TH500)

Beam TH500 had a clear span of 3.8 m and a design load of 162.1 kN/m. During testing, the load stages were taken at 15 kN/m increments until the longitudinal steel yielded. Beyond yielding, deflection control was used during loading.

The load-deformation response of TH500 is shown in Fig. 4-1. This figure shows the flexural cracking load, the shear cracking load, the service load level, the loads causing first yielding of the west and east stirrups and flexural yielding, as well as the ultimate shear strength of the beam as predicted by the CSA Standard (Ref. 17). The first flexural crack appeared near midspan at an applied load of 20.0 kN/m which agrees well with the predicted flexural cracking load of 20.5 kN/m. The first inclined shear crack occurred at an applied load of 44.9 kN/m. Flexure-shear cracking was predicted to occur at a location d/2 from the support face at a load of 45.3 kN/m. As loading continued, more flexure-shear cracks developed with web-shear cracks

forming near the supports. Yielding of the stirrups in the west end of the beam occurred at a load of 123.0 kN/m and the more closely spaced east end stirrups yielded at 141.2 kN/m. The load was increased to a maximum value of 208.5 kN/m when concrete crushing was observed on the top surface of the flange and the test was stopped. TH500 reached a maximum midspan deflection of 78.6 mm.

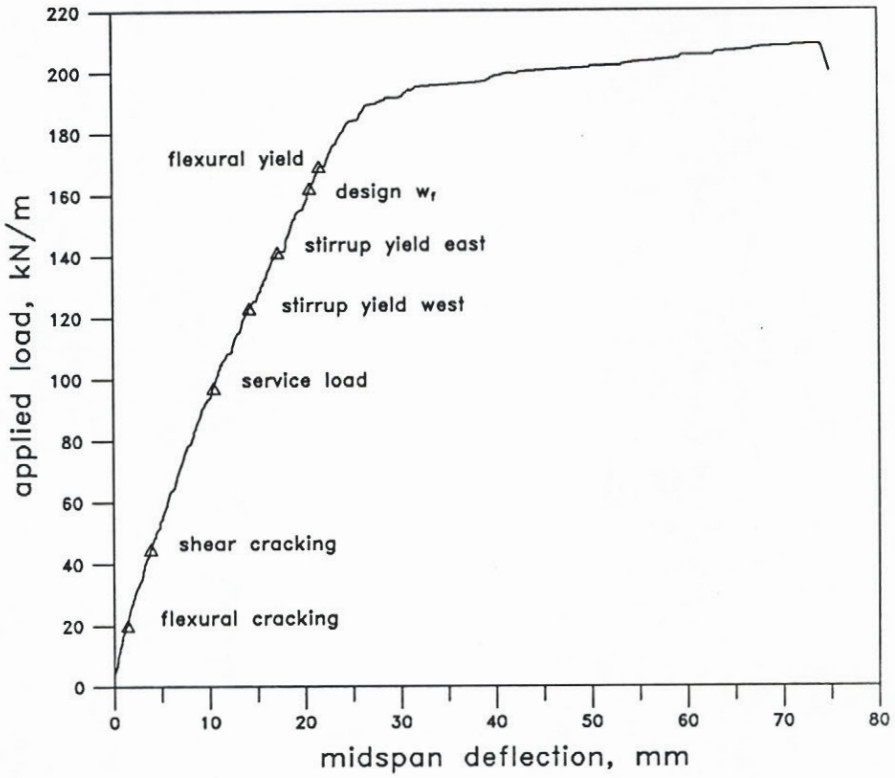

Figure 4-1 Load-deformation response of tee beam subjected to a high shear (TH500)

Figures 4-2 and 4-3 present photographs of TH500 at first cracking in shear, at service load, after first yielding of the stirrups and at the maximum load attained for both the west and east ends of the beam. These photographs show the development of both flexural and shear cracking throughout the test.

The stirrup strains measured in the top and bottom halves of the web are shown for every second load stage in Figs. 4-4 and 4-5, for the west and east ends of the beam, respectively. The maximum of the top and bottom stirrup strains and the average of the top and bottom stirrup

strains are given in Fig. 4-6 and Fig. 4-7 for the two ends of the beam. In Figs. 4-4 through 4-7, the yield strain that is shown corresponds to the measured "yield" stress, defined by G30.14-M83 (Ref. 3), divided by the modulus of the steel (i.e., a value of $562/192505 = 2.92 \times 10^{-3}$). A comparison of Fig. 4-6a and 4-7a reveals that on the west end of the beam, 7 stirrups yielded while only 6 stirrups reached yield in the east half of the beam. Although some stirrups yielded before others, there was considerable spreading of the yielding with continued loading. The east end stirrups were subjected to much lower strains than the west end stirrups due to the smaller stirrup spacing. The maximum stirrup strains at service load were 1.72×10^{-3} and 1.27×10^{-3} for the west and east ends, respectively. At the end of the test, the maximum stirrup strains in the west and east ends were 9.13×10^{-3} and 9.34×10^{-3}, respectively (see Fig. 4-6a and 4-7a). No sudden decrease was observed in the measured stirrup strains. This indicates that the anchorage provided by two 8 mm diameter wires welded at the top of the stirrups was sufficient to develop strains well beyond yield in the stirrups.

Figures 4-8 and 4-9 show the maximum shear crack widths measured in both stirrup band regions of the west and east ends of the beam. These figures show that TH500 developed shear cracks in the west end before they appeared in the east end. At service load, taken as 60% of the shear design load, the maximum crack width in the west and east ends were 0.10 mm and 0.05 mm, respectively. Throughout most of the response, the widths of the shear cracks were greater in region 1, closest to the support, than in stirrup band region 2 (see Figs. 4-8 and 4-9). By comparing the maximum shear crack widths from Figs. 4-8 and 4-9, it is apparent that the cracks in the east end were better controlled by the more closely spaced stirrups.

Fig. 4-10 shows the magnitudes and directions of the principal strains near the end of the test, measured in the rosettes centred about the top and bottom halves of every second stirrup (see Fig. 2-11). This figure shows the dominance of the moment near midspan, where the principal angle of compression, θ, is close to 90 degrees, while close to the support, shear dominates with the principal compressive strains inclined at an angle of about 30 degrees. In the

west end of the beam, the angle of principal compression was measured as 30 degrees near the support while it was steeper in the east end (θ = 34 degrees), due to the more closely spaced stirrups. The measured value of θ in the west end agrees with the minimum used in design (θ = 29.4 degrees). Photographs of TH500 shown in Figs. 4-2 and 4-3 demonstrate that the cracks which formed in the latter stages of the test were inclined at angles comparable to the principal angle of compression computed from the strain rosette data.

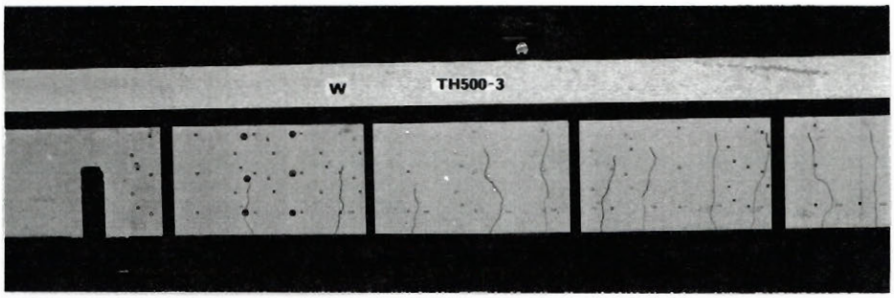

a) first shear cracking

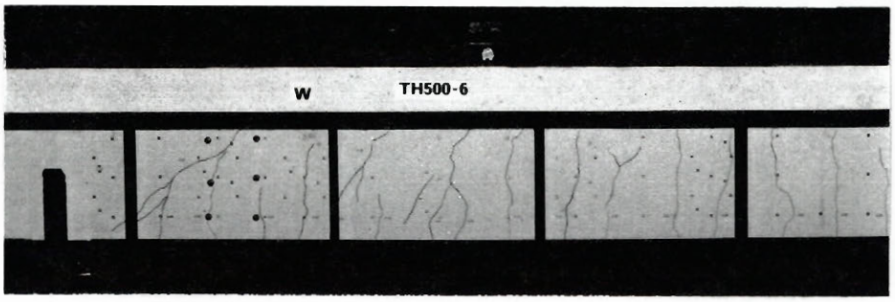

b) service load

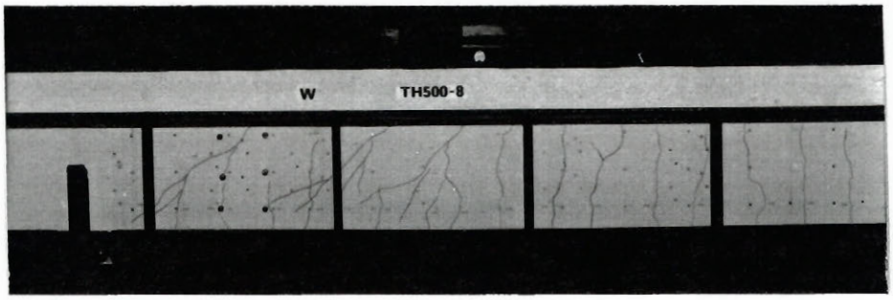

c) stirrup yield

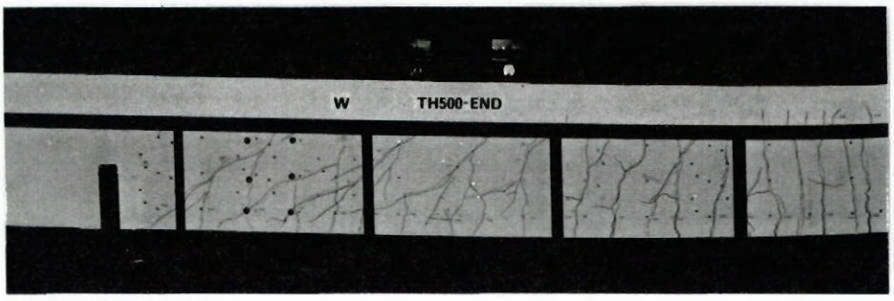

d) end of test

Figure 4-2 Crack patterns in west end of beam TH500

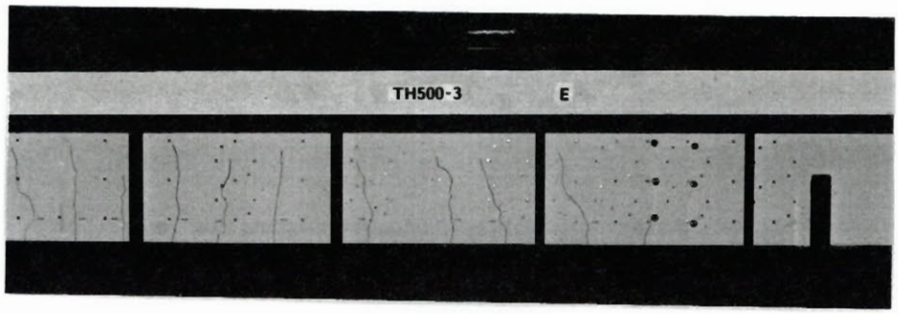

a) first shear cracking

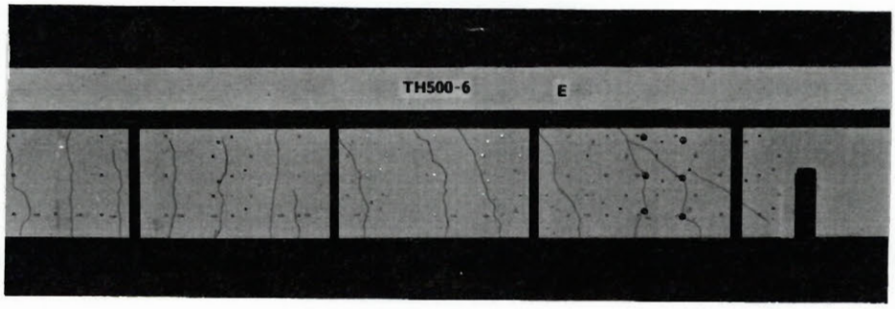

b) service load

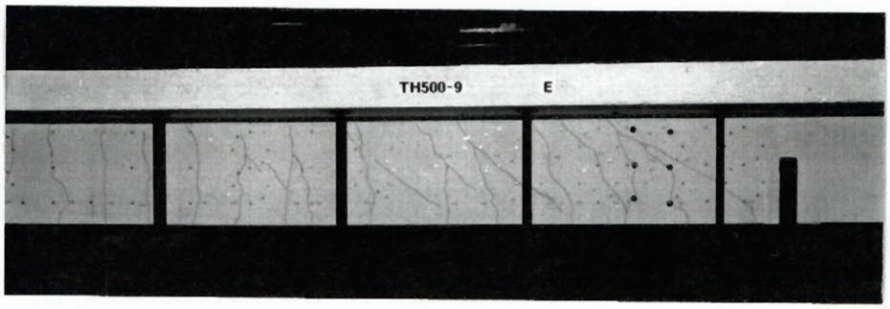

c) stirrup yield

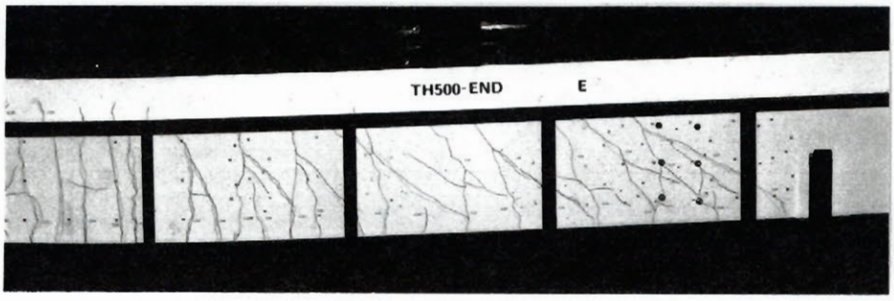

d) end of test

Figure 4-3 Crack patterns in east end of beam TH500

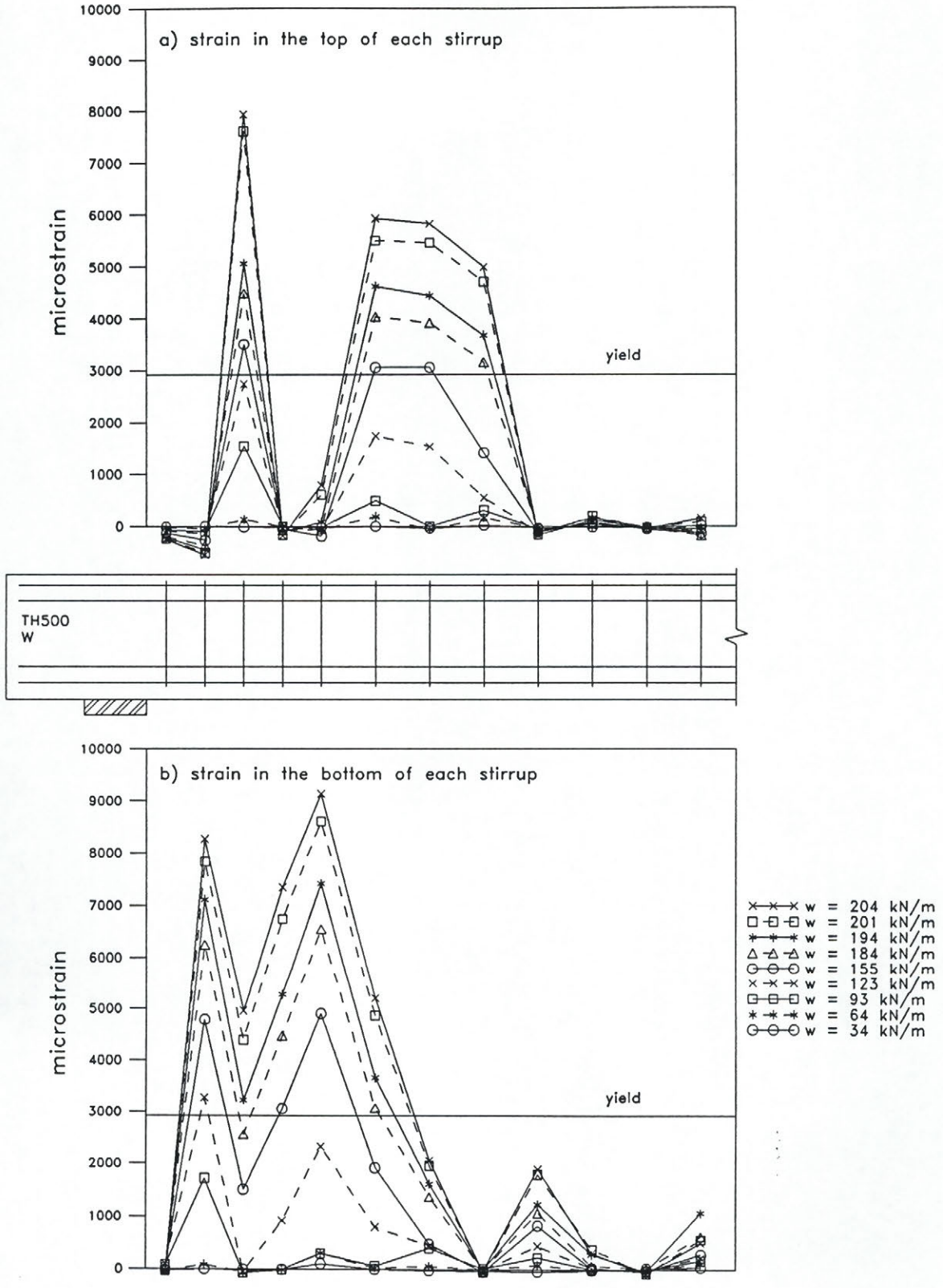

Figure 4-4 Stirrup strains measured in the top and bottom of each stirrup for west half of TH500

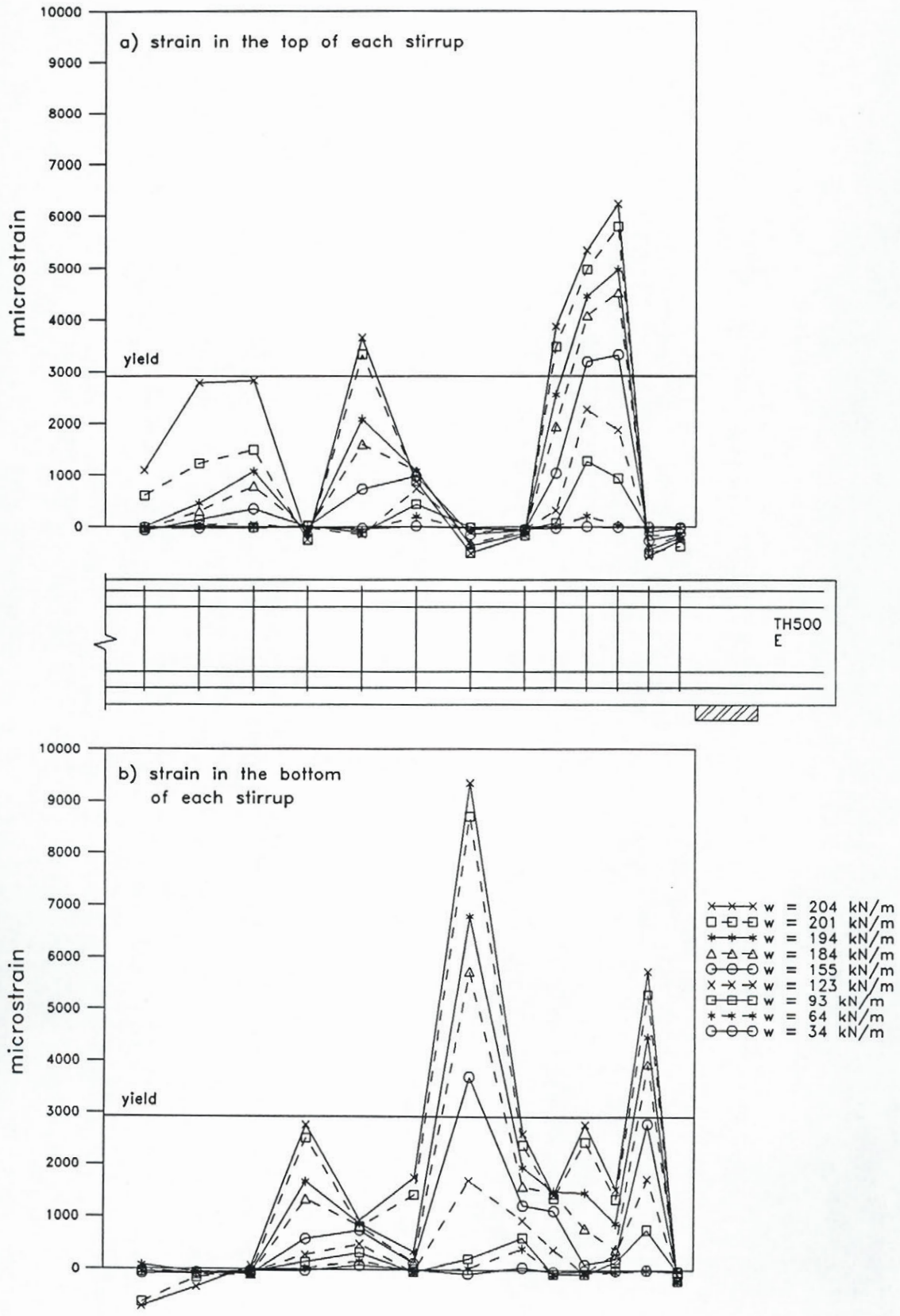

Figure 4-5 Stirrup strains measured in the top and bottom of each stirrup for east half of TH500

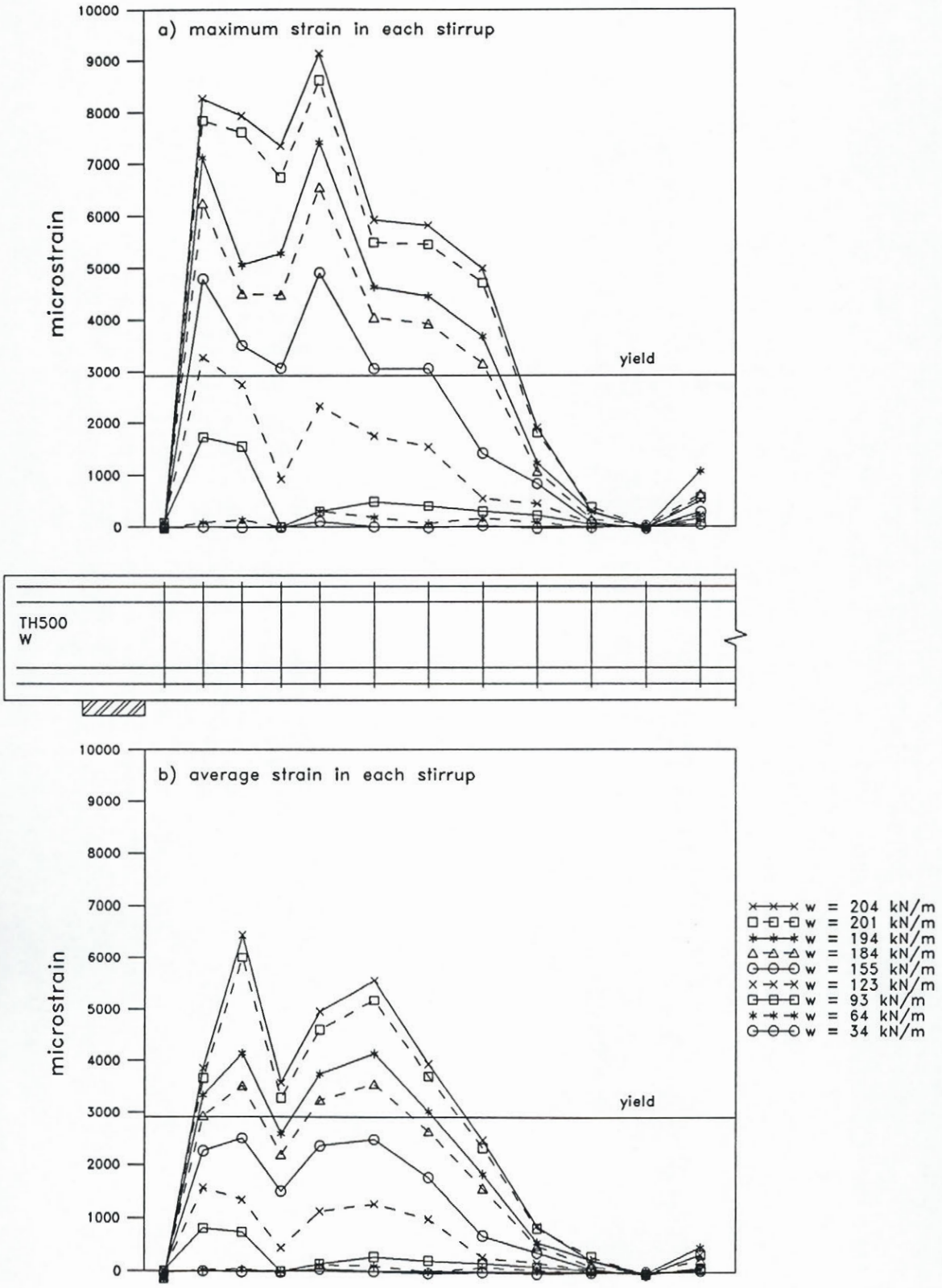

Figure 4-6 Maximum and average stirrup strains measured in each stirrup for west half of TH500

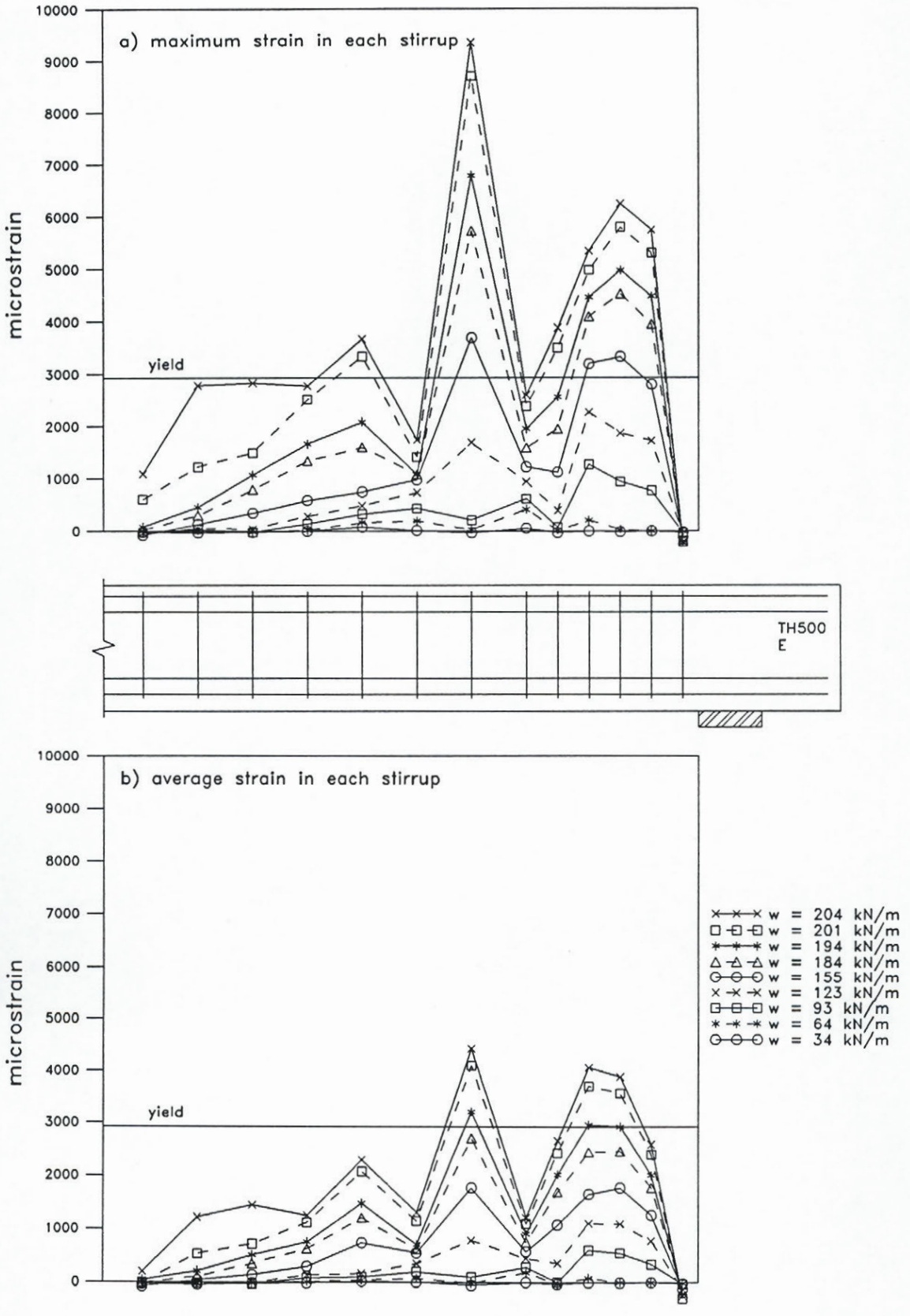

Figure 4-7 Maximum and average stirrup strains measured in each stirrup for east half of TH500

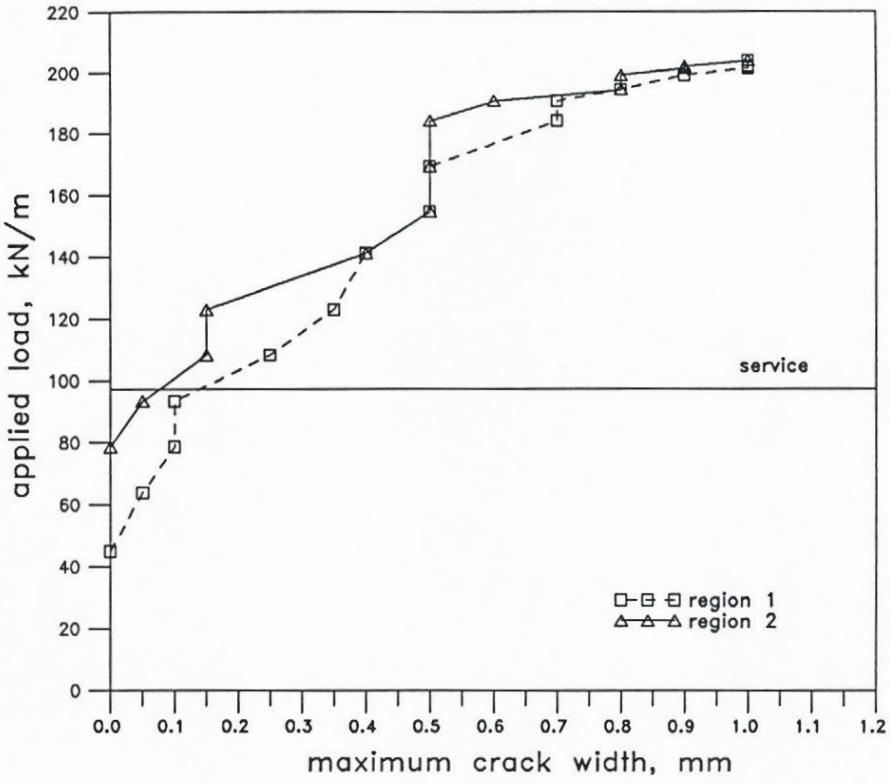

Figure 4-8 Load versus maximum shear crack width in west end of TH500

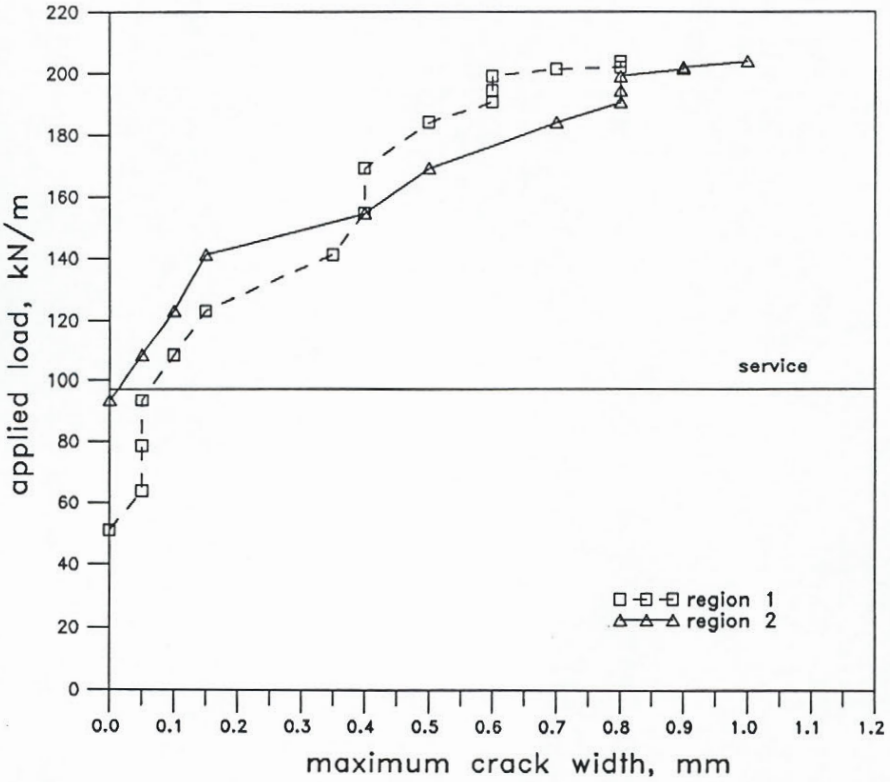

Figure 4-9 Load versus maximum shear crack width in east end of TH500

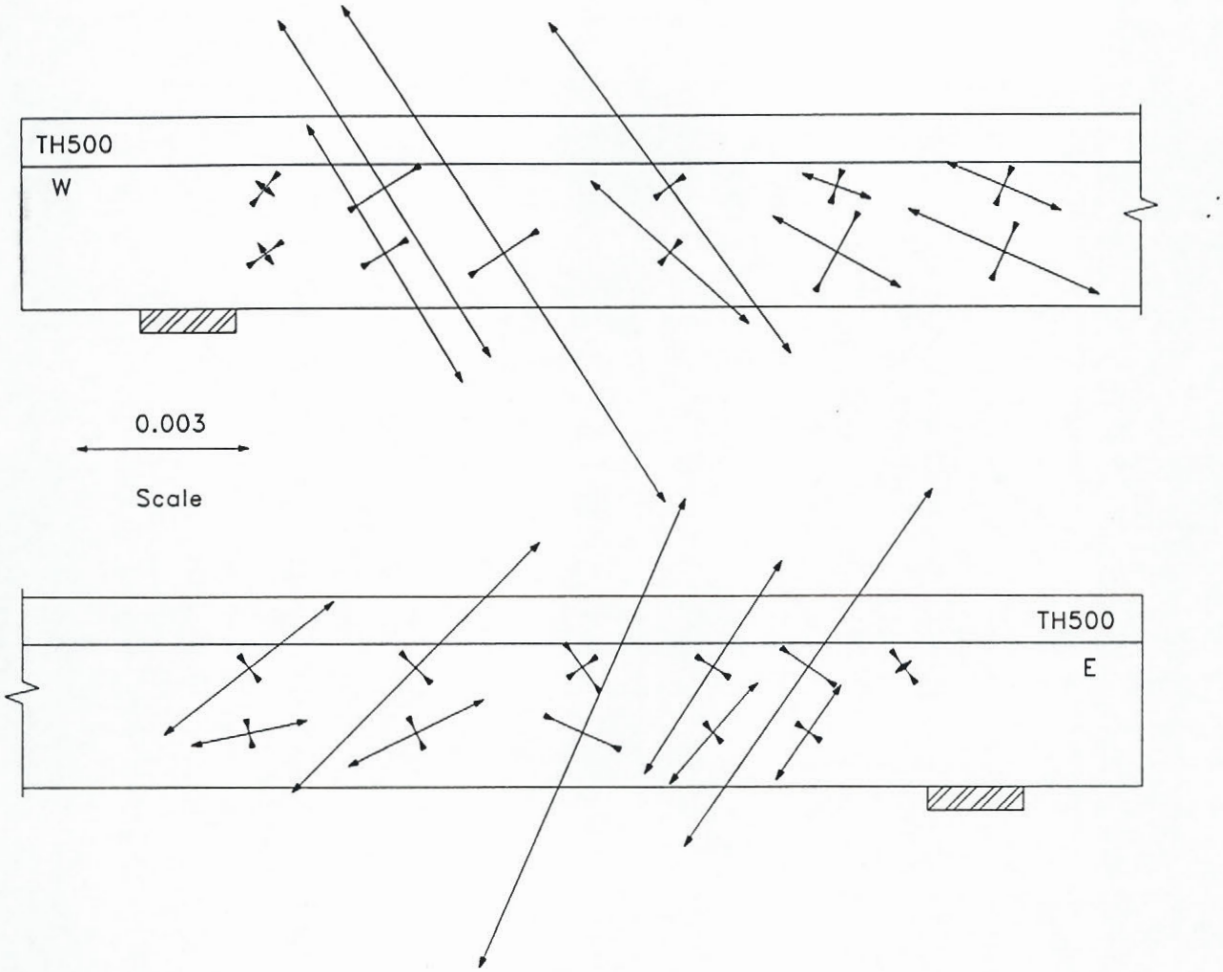

Figure 4-10 Magnitudes and directions of principal strains measured in TH500 near failure

4.2 Tee Beam Subjected to Moderate Shear (TM500)

Beam TM500 had a clear span of 4.6 m and had a design load of 100.6 kN/m. In the elastic range of the test, a load stage was taken at 10 kN/m increments and deflection control was used once the longitudinal steel yielded.

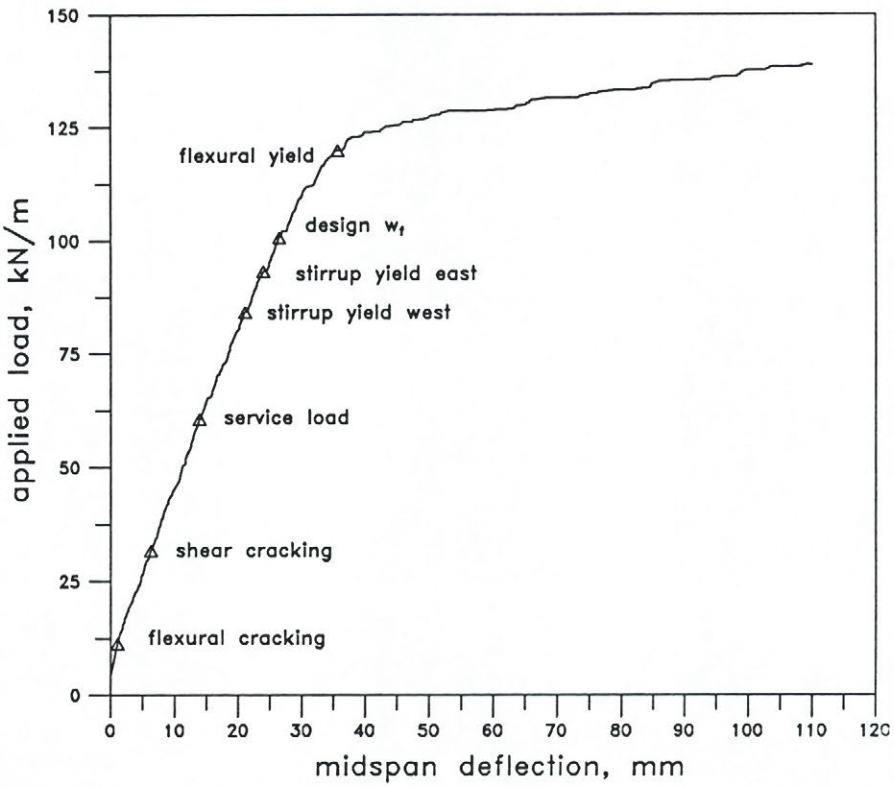

Figure 4-11 Load-deformation response of tee beam subjected to a moderate shear (TM500)

The load-deflection response of TM500 is shown in Fig. 4-11 and includes the following key points: the flexural cracking load, the shear cracking load, the service load level, the flexural yield load, the load that caused first yielding in the stirrups at the west and east ends of the beam and the ultimate capacity of the beam based on the shear design performed according to the CSA Standard (Ref. 17). Flexural cracking was first observed at a load of 11.3 kN/m which is close to the predicted value of 13.0 kN/m. The first inclined shear cracks appeared at a load of 32.1 kN/m which compares well with the predicted flexure-shear cracking load of 32.9 kN/m.

Additional flexure-shear cracks occurred with increased loading and web-shear cracks formed near the supports. The stirrups in the west end of the beam "yielded" at a load of 84.1 kN/m while the more closely spaced stirrups in the east end of the beam "yielded" at a higher load of 93.1 kN/m. The load was increased until crushing of the concrete was observed on the top surface of the flange, at a load of 139.0 kN/m. The testing was ended at this point, with TM500 having reached a maximum midspan deflection of 110.0 mm.

Photographs of TM500 at first cracking, service load, just after yielding of the stirrups and at the end of the test are shown for the west and east ends of the beam, in Figs. 4-12 and 4-13, respectively. These photographs show the cracking sequence as the test progressed.

The stirrup strains, measured in the top and bottom halves of each stirrup, are shown for every second load stage, in Figs. 4-14 and 4-15, for the west and east ends of the beam, respectively. The maximum and average of the top and bottom stirrup strains are given in Figs. 4-16 and 4-17 for each end of TM500. At service load levels, the maximum strain in a stirrup in the west half of the beam was 0.40×10^{-3}, while it was slightly lower in the east half of the beam ($\epsilon = 0.39 \times 10^{-3}$). In the west half of the beam, 6 stirrups reached yield (see Fig. 4-16a) while 8 stirrups yielded in the east half of the beam as shown in Fig. 4-17a. The maximum stirrup strains, measured in the west and east halves of the beam, were 11.73×10^{-3} and 6.12×10^{-3}, respectively. The smaller stirrup spacing in the east end significantly improved the behaviour, since a much more uniform strain distribution with lower peak strains resulted (see Fig. 4-16a and 4-17a). Since no sudden drop was observed in the measured stirrup strains, adequate anchorage was provided by the two cross-wires, welded at the top of the stirrup cage.

The variations of maximum shear crack widths with increasing loads are shown in Fig. 4-18, for the west end of the beam, and Fig. 4-19, for the east end of the beam. The maximum shear crack widths at service load were 0.13 mm and 0.08 mm, respectively, in the west and east ends of the beam. Throughout most of the response, the widths of the inclined shear cracks were greater in region 1, closest to the support, than in the design region closer to midspan (region

2). Greater crack widths were observed in the west half of the beam than in the east half, throughout the entire test. The smaller stirrup spacing in the east end was therefore successful at reducing the crack widths and improving the response (see Figs. 4-18 and 4-19).

Figure 4-20 shows the magnitudes of the principal strains, ϵ_1 and ϵ_2, and the variation of the principal angle of compression, θ, along the span. These values are shown for a load stage near the end of the test and were calculated from readings from the rosettes shown in Fig. 2-11. Near midspan, the principal angle of compression, θ, is close to 90 degrees due to the moment effects, while θ is close to 26 degrees near the support, where shear effects dominate. The principal angle of compression was steeper in the east end of the beam due to the smaller stirrup spacing that was provided, than in the west end of the beam. A value of θ of 26 degrees was determined in the region closest to the support in the west end of the beam. This is similar to the value of θ_{min} of 27 degrees used in determining the stirrup spacings. The angles of the inclined cracks that formed in the latter stages of the test agreed well with the angles of principal compression computed from the strain rosette data.

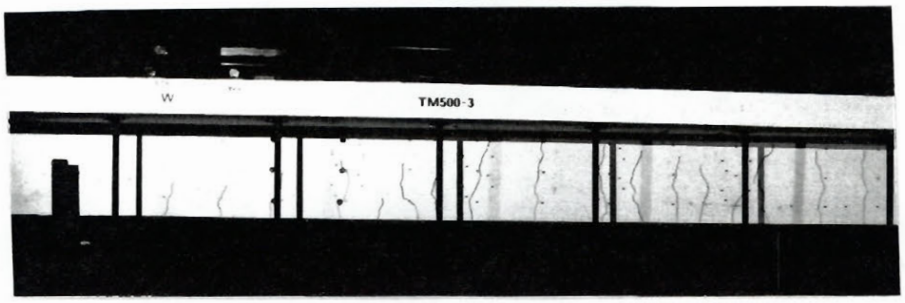

a) first shear cracking

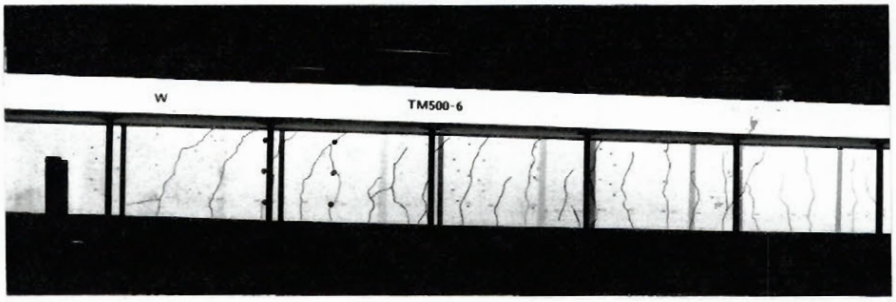

b) service load

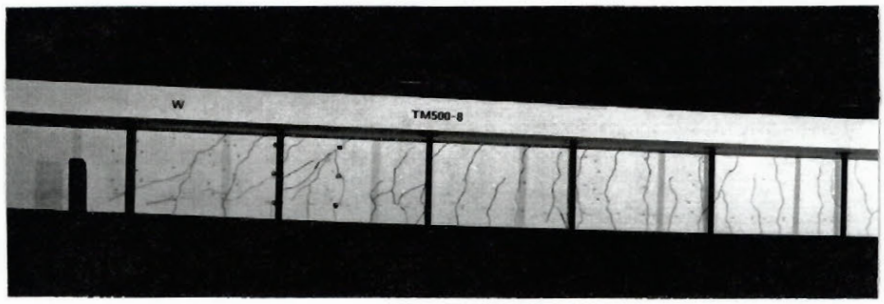

c) stirrup yield

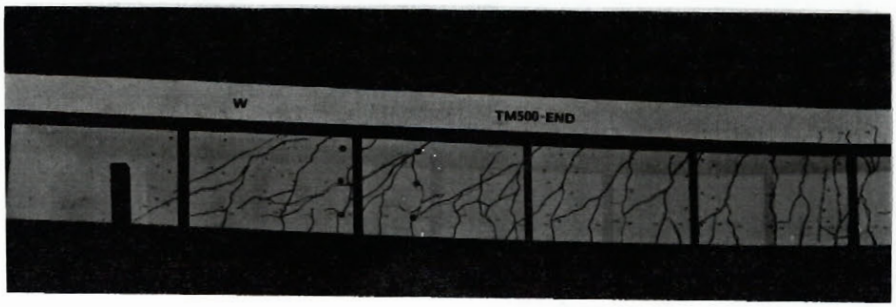

d) end of test

Figure 4-12 Crack patterns in west end of beam TM500

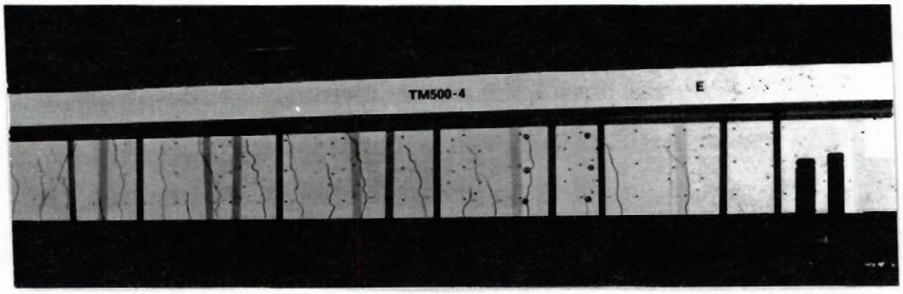

a) first shear cracking

b) service load

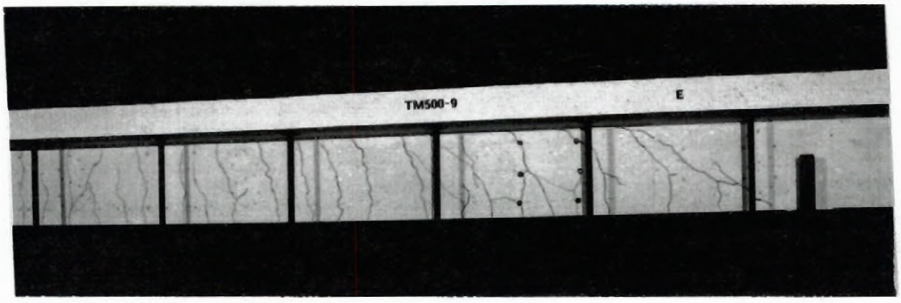

c) stirrup yield

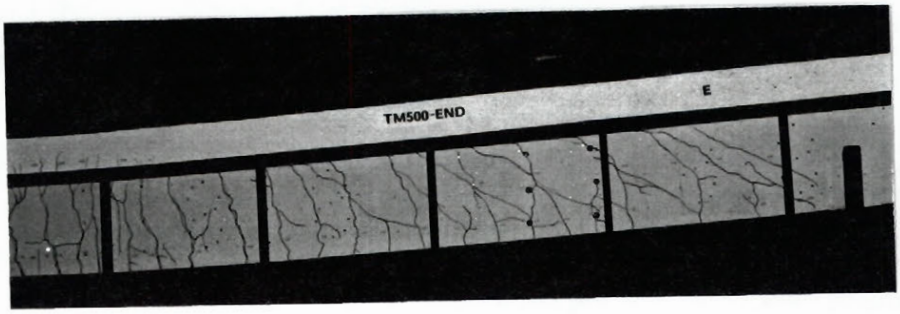

d) end of test

Figure 4-13 Crack patterns in east end of beam TM500

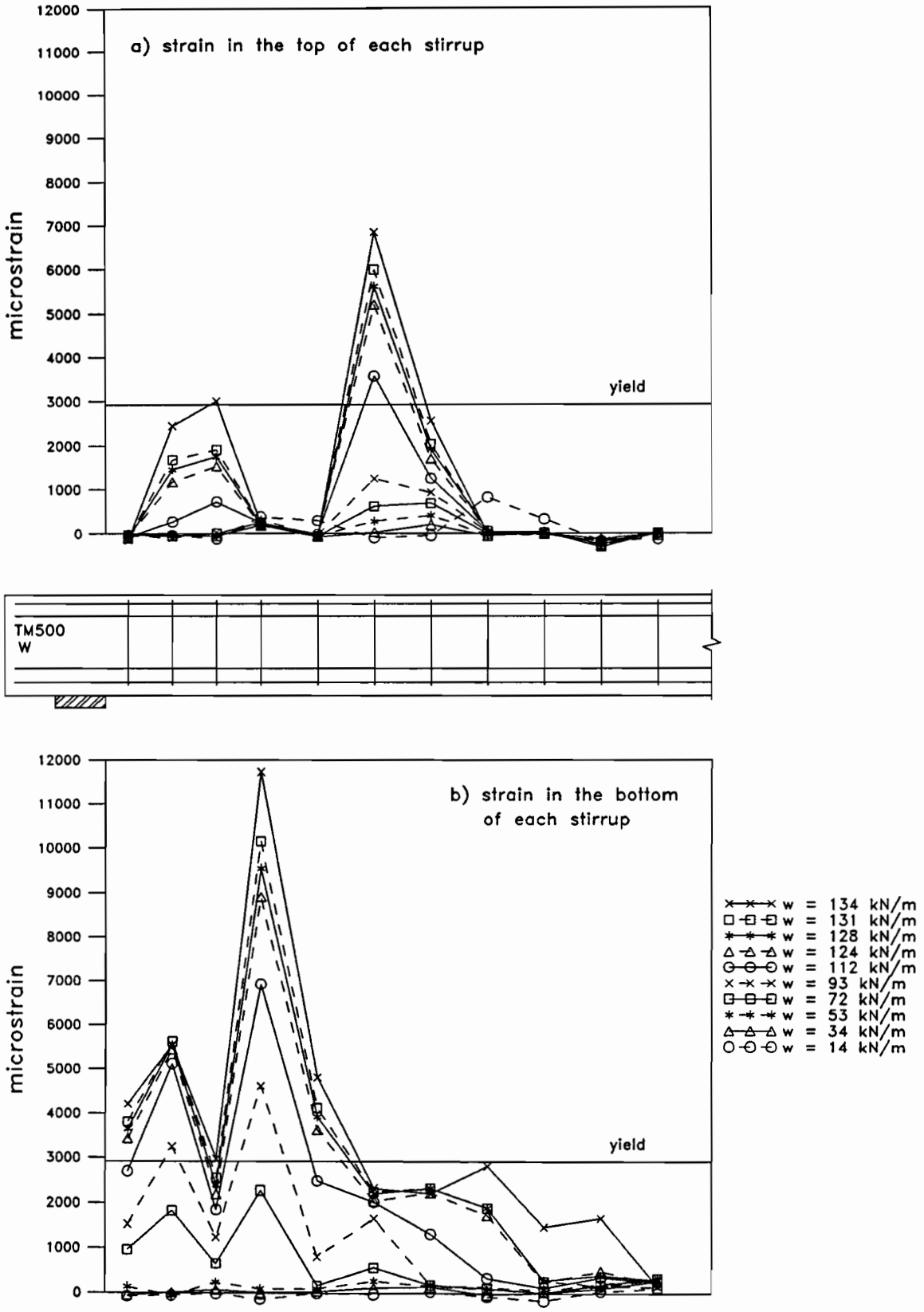

Figure 4-14 Stirrup strains measured in the top and bottom of each stirrup for west half of TM500

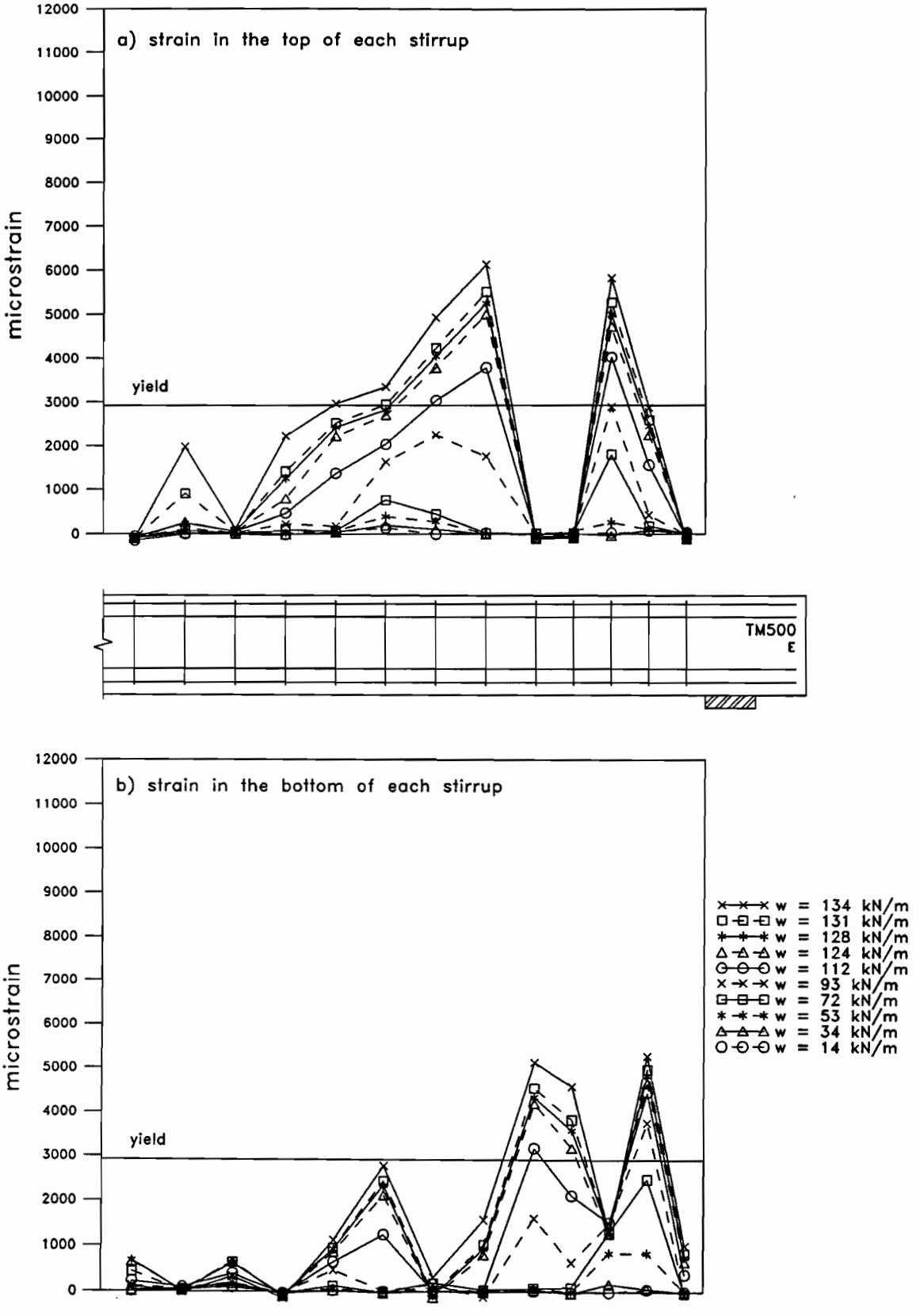

Figure 4-15 Stirrup strains measured in the top and bottom of each stirrup for east half of TM500

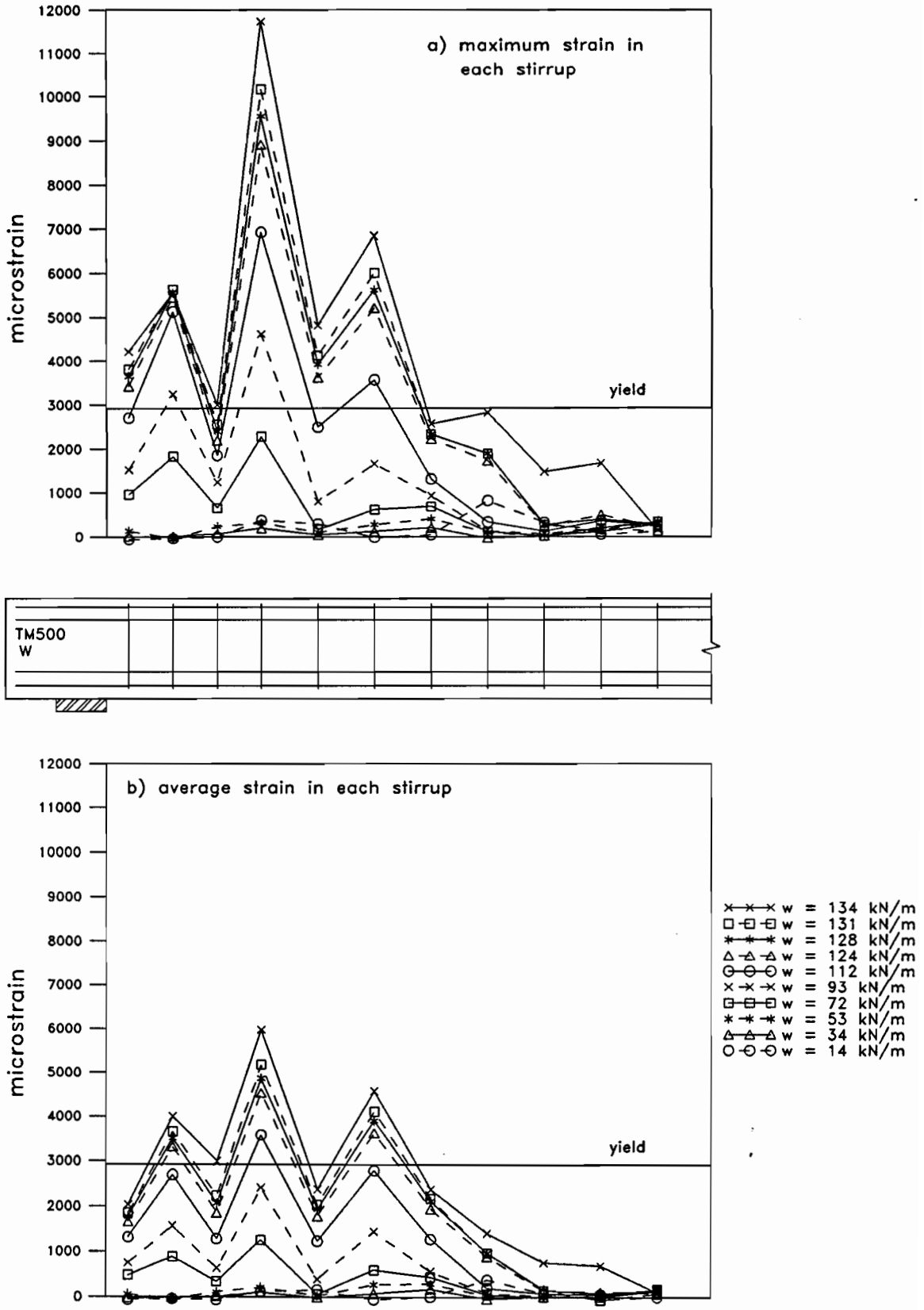

Figure 4-16 Maximum and average stirrup strains measured in each stirrup for west half of TM500

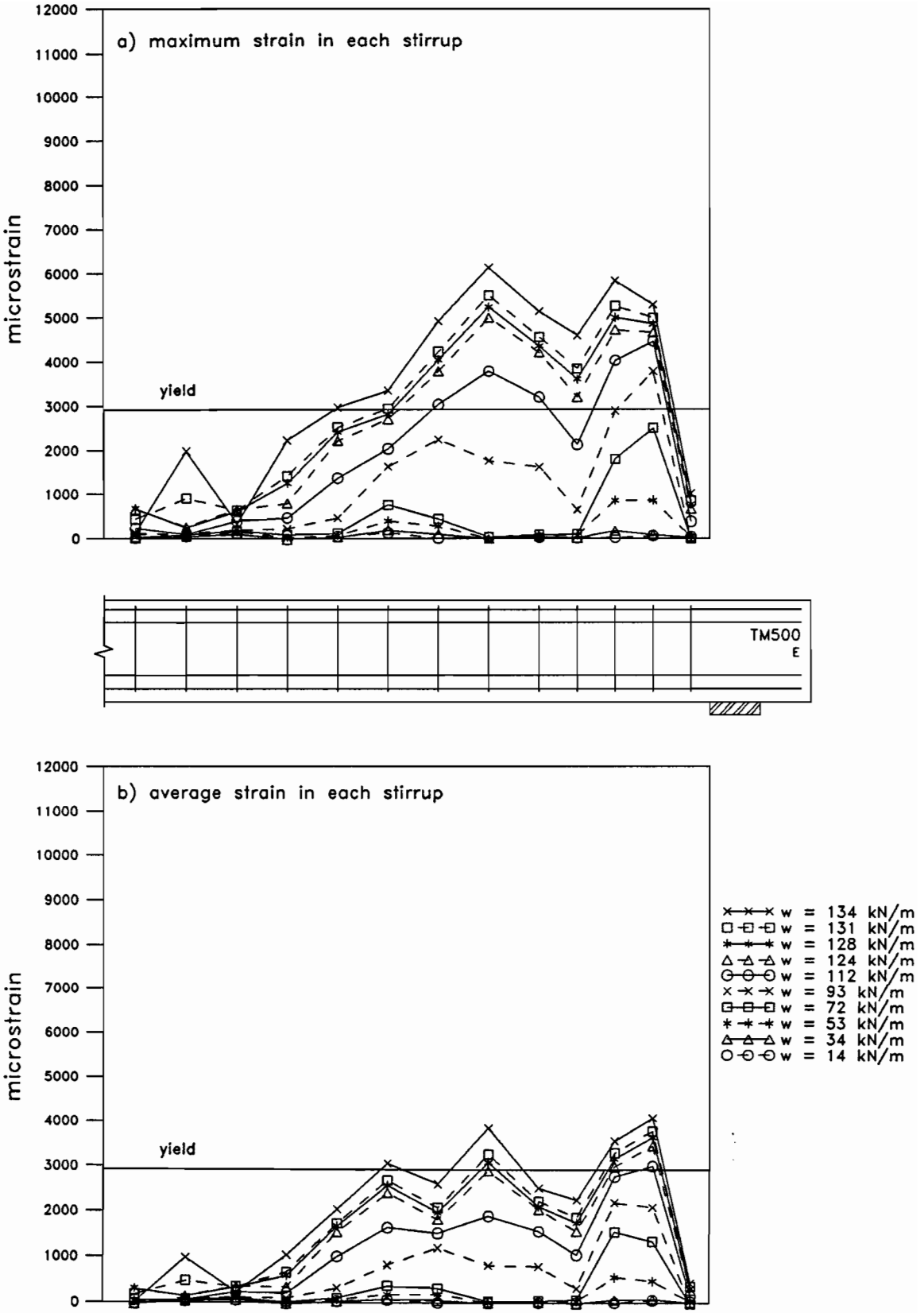

Figure 4-17 Maximum and average stirrup strains measured in each stirrup for east half of TM500

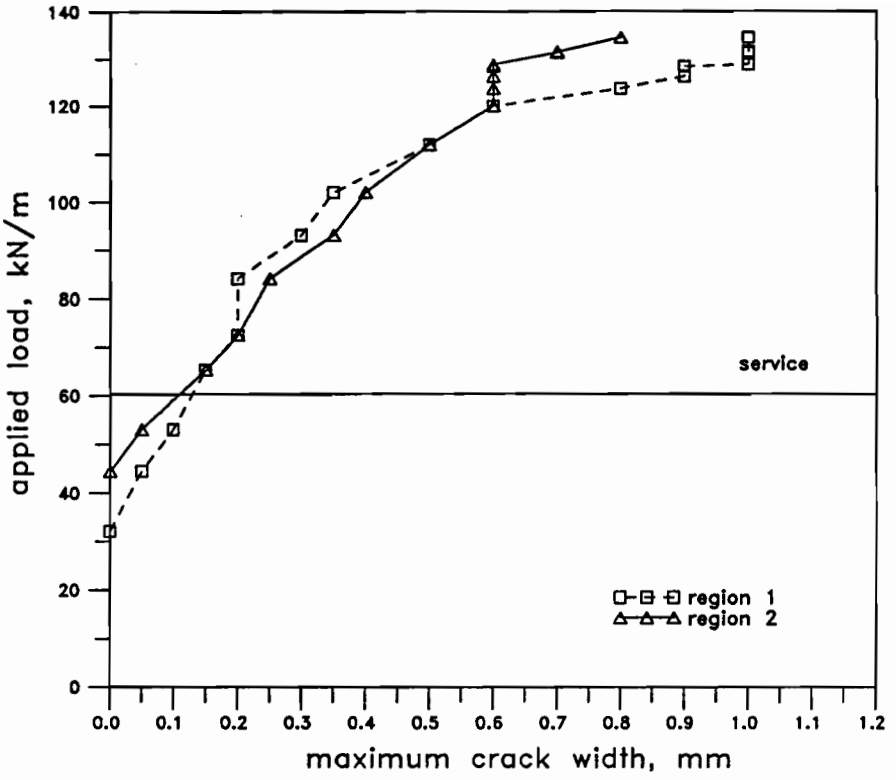

Figure 4-18 Load versus maximum shear crack width in west end of TM500

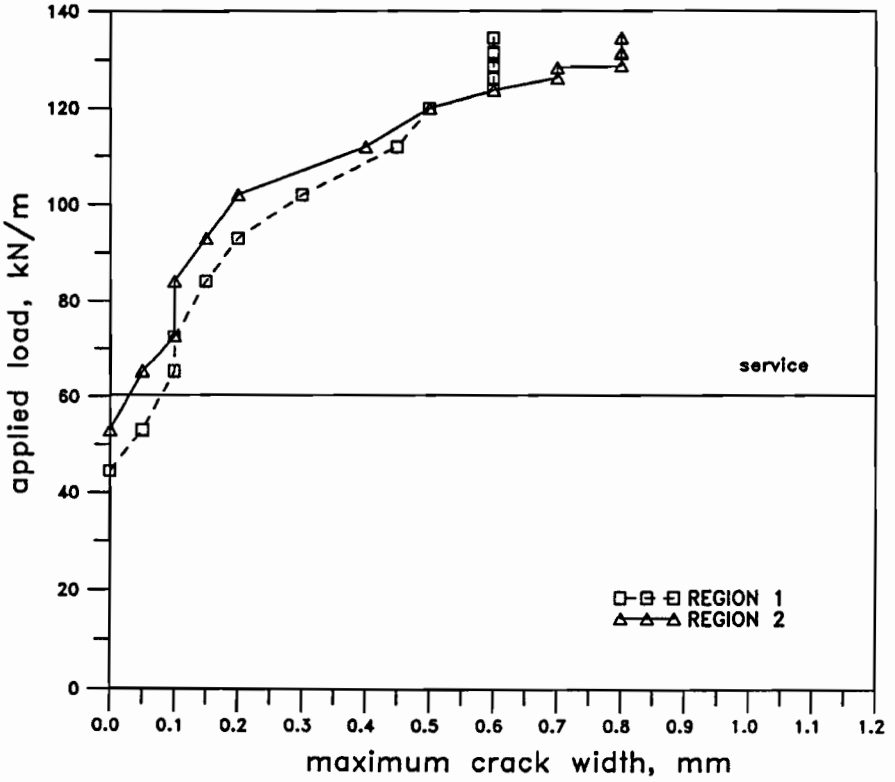

Figure 4-19 Load versus maximum shear crack width in east end of TM500

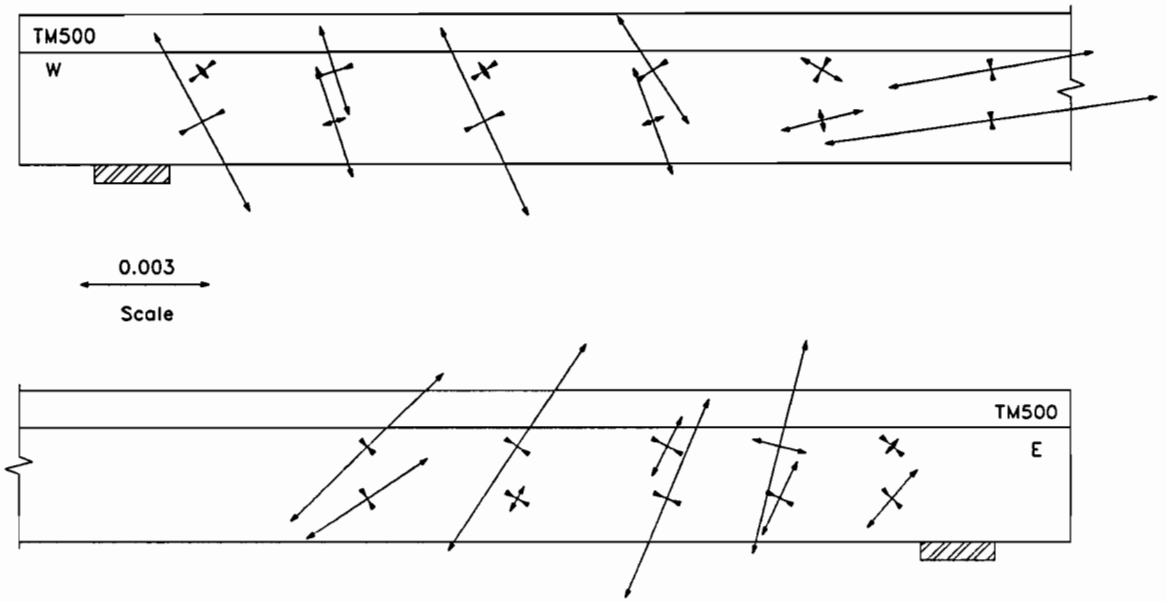

Figure 4-20 Magnitudes and directions of principal strains measured in TM500 near failure

4.3 Comparison of Responses of Beams TH500 and TM500

Table 4-1 compares some of the response characteristics, observed in the west halves of Beam TH500 (high shear) and Beam TM500 (moderate shear). Both beams contained the same amount of flexural reinforcement and hence have the same flexural capacities. Since Beam TH500 is shorter than Beam TM500, the moment-to-shear ratio is smaller than that in Beam TM500. This lower moment-to-shear ratio results in a smaller cracking shear, V_{cr}. Beam TH500 has a smaller stirrup spacing and a larger cracking shear than Beam TM500. This results in smaller shear cracks at service load (see Table 4-1). Due to the more closely spaced stirrups and lower moment-to-shear ratio, Beam TH500 has a higher shear capacity than Beam TM500.

Beam	Stirrup Spacing s_1 mm	V_{cr} kN	w_{max} @ service mm	V_{max} kN
TH500	125	78.4	0.10	396
TM500	175	72.1	0.13	334

Table 4-1 Comparison of shear response characteristics in west halves of TH500 and TM500

Photographs of Beams TH500 and TM500, in their final deflected positions, at the end of testing, are shown in Fig. 4-21. Figure 4-22 shows the beams after unloading and after removal of the loading apparatus. The steeper inclination of the shear cracks that formed in Beam TH500 can be seen in Fig. 4-22.

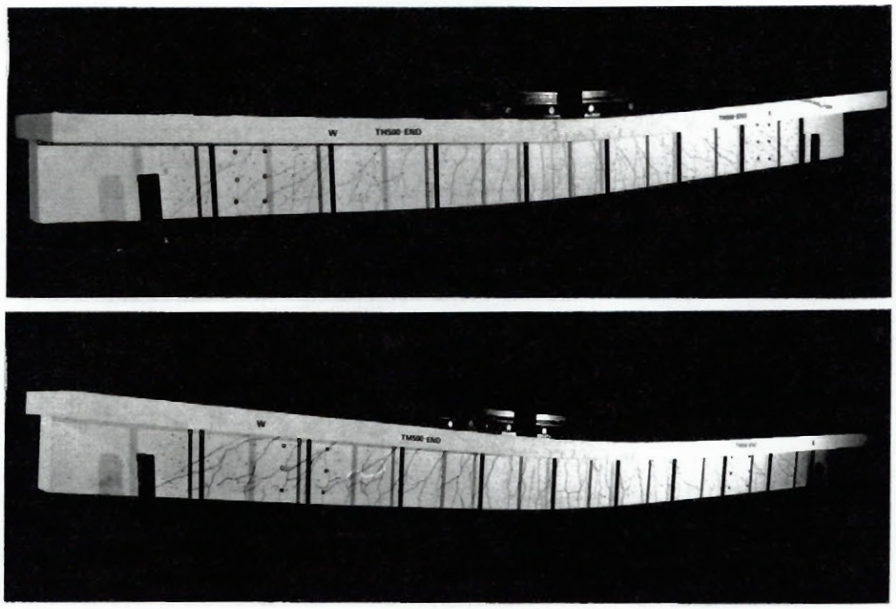

Figure 4-21 Beams TH500 (top) and TM500 (bottom) at respective ultimate loads

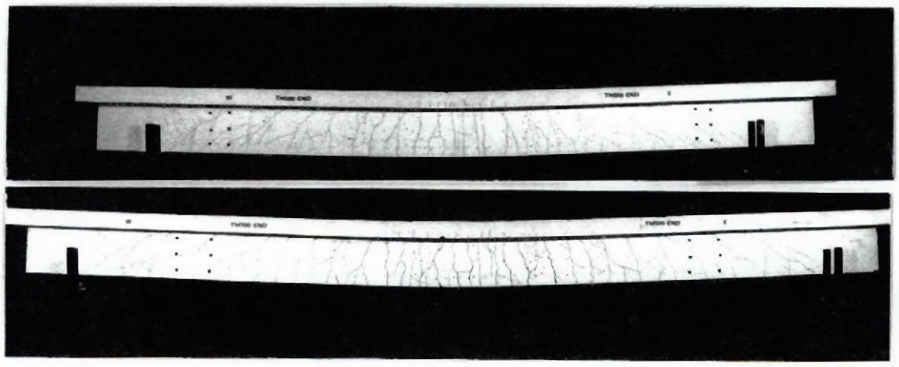

Figure 4-22 Beams TH500 (top) and TM500 (bottom) after removal of loading apparatus

Chapter 5

Predicted Responses of Tee Beams

In this chapter, the predicted behaviour of the two beams, TH500 and TM500, will be compared with their observed responses. The current CSA Standard's General Method for shear design (§11.4, Ref 17), will be used to determine the shear design capacities of the beams. In addition, the ultimate capacities of the beams will be predicted using the computer program RESPONSE (Refs. 10 and 29), which incorporates the modified compression field theory. For all calculations involved in determining the ultimate strengths of the beams, the material reduction factors, ϕ_c and ϕ_s, were taken as 1.0 and measured values of material properties were used.

5.1 Analysis Using CSA Standard's Equations

The General Method for shear design is based on the compression field theory which was described Section 1.4.2. Clause 11.4.2.6 of the CSA Standard states that the angle of principal compression, θ, must lie between 15 and 75 degrees. The longitudinal strain at mid-depth of the member, ϵ_x was taken as 0.002 as permitted by §11.4.2.5. Equation 1-20 offers an approximation of the limiting value of θ_{min}. Choosing a value of θ less than the maximum angle of principal compression from Eq. 1-21 ensures that the stirrups yield prior to the concrete crushing. The staggering concept for shear design was used to design the stirrups for TH500 and TM500 since they were subjected to uniform loading patterns.

An iterative procedure must be used to determine θ_{min} which involves assuming an

applied uniformly distributed load, w, in kN/m, determining the shear at the support face, computing θ_{min} using Eq. 1-20 and calculating the shear capacity of the stirrup band from Eq. 1-29. The shear capacity of the section is then compared to the applied shear at the end of the first design region, that is, at a distance $d_v / \tan\theta$ from the support face. This procedure is repeated until the shear forces agree. At this point, one must verify that the diagonal compressive stress, f_2, given by Eq. 1-15 is less than the diagonal crushing strength of the concrete, f_{2max} from Eq. 1-22.

Since the stirrup spacing was larger in the west end of the beam than in the east end, the stirrup spacing in the west end of the beam governed the shear strength. The ultimate capacities of the two beams, determined using the measured material properties and performing the iterations as described above, are shown in Table 5-1.

Beam	General Method of shear design			Measured	
	w_f kN/m	V_{supp} kN	θ_{min} degrees	w_u kN/m	V_{supp} kN
TH500	162.1	308	29.4	208.5	396
TM500	100.6	241	26.4	139.0	334

Table 5-1 Strength predictions using the Compression Field Theory

5.2 Computer Analysis Using Program "RESPONSE"

The computer program, RESPONSE (Refs. 10 and 29), is capable of analysing a reinforced concrete member subjected to any combination of shear, moment and an axial load. This program was used to determine the sectional responses of the two tee beams. The iterative analysis procedure links a plane sections analysis for flexure and axial load with the Modified Compression Field Theory for shear and axial load.

RESPONSE can perform shear analyses using either the Compression Field Theory (Ref.

19) or the Modified Compression Field Theory (Ref. 12 and 22). The Modified Compression Field Theory offers a better prediction of the behaviour than does the Compression Field Theory, since it accounts for the contribution of tensile stresses in the concrete between the cracks.

A parabolic stress-strain relationship was assumed for the concrete and a tri-linear relationship was used for the reinforcing steel. An equivalent yield stress of 588 MPa was used for the welded-wire fabric stirrups. The discretization of the beam cross-section and the assumed material stress-strain relationships are shown in Fig. 5-1 and the input data files are included in Appendix A.

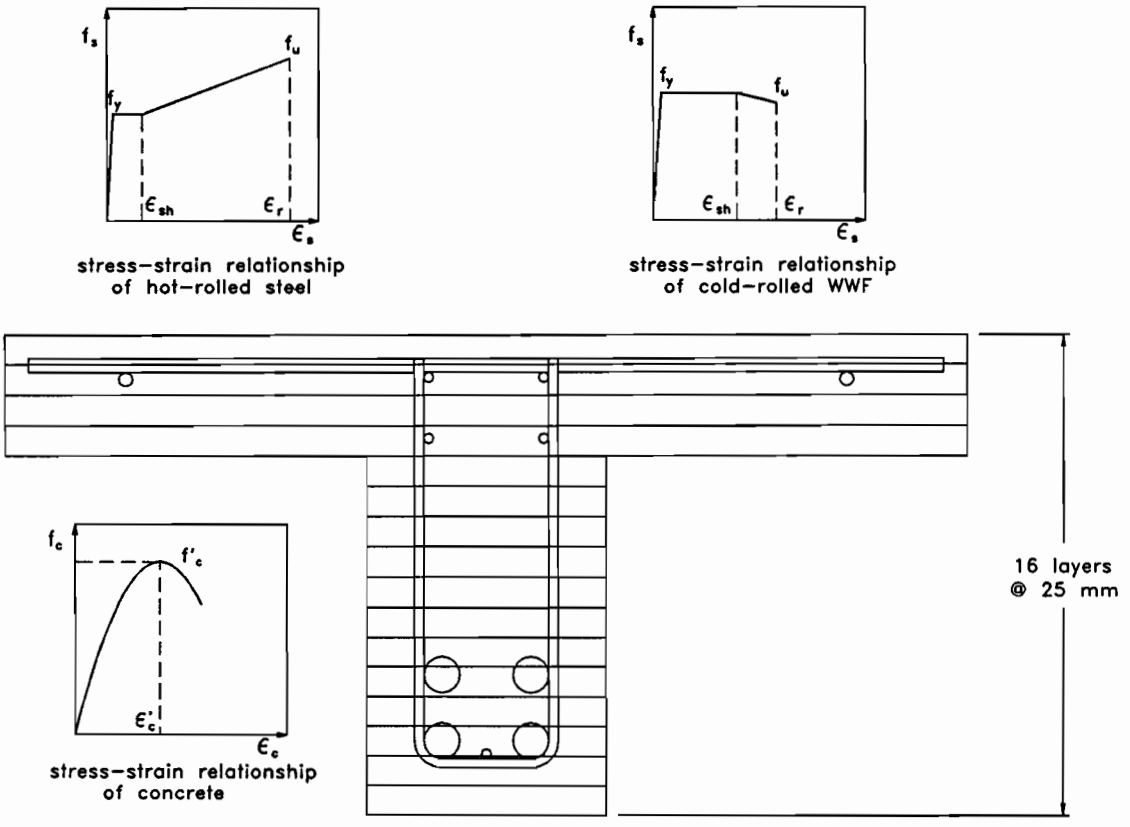

Figure 5-1 Discretization of beam cross-section and material stress-strain relationships used in RESPONSE predictions

An analysis was carried out using the Modified Compression Field Theory, accounting for the influence of moment shear interaction at a given section. Figures 5-2 and 5-3 show the

results of the computer analyses for Beams TH500 and TM500, respectively. The shear and moment capacities were determined at the end of each design region (d_v/ tanθ) and the staggering concept was used in developing the shear and moment diagrams. In regions close to midspan, where flexure dominates, the program RESPONSE did not converge. Therefore, analyses were carried out using the flexure and an axial load option of RESPONSE, with a tensile load of N_v, due to shear effects (see Eq. 1-16). From Fig. 5-2 it is predicted that TH500 will fail in flexure, under an applied load of 199.1 kN/m while the predicted shear capacity of this beam, close to the support is 207.4 kN/m. It is also predicted that TM500 will fail in flexure under a load of 123.0 kN/m since it has a predicted shear capacity of 127.6 kN/m (see Fig. 5-3). The predicted ultimate shear and moment resistances of the two beams and the resulting applied loads are summarized in Table 5-2.

Beam	Predicted Shear Capacity			Predicted Moment Capacity		Predicted Failure Mode	Measured		
	w_r kN/m	V_{supp} kN	θ_{min} degrees	w_r kN/m	M_r kN-m		w_u kN/m	V_{supp} kN	M_u kN-m
TH500	207.4	394	26.9	199.1	369	flexural	208.5	396	386
TM500	127.6	306	24.1	123.0	362	flexural	139.0	334	409

Table 5-2 Predicted failure loads from combined shear and moment analyses using RESPONSE with Modified Compression Field Model for shear

5.3 Comparison of Strength Predictions with Test Results

Table 5-3 shows the comparison of the measured failure loads and the predicted capacities of the two beams, determined using the CSA Standard's General Method for shear design and the Modified Compression Field Theory.

The predictions offered by the CSA Standard assume that the critical section of the beam will occur in the first d_v/ tanθ region, close to the support. As can be seen from Figs. 5-2 and 5-3, the predictions using program RESPONSE indicate that in both cases, the beams will fail in

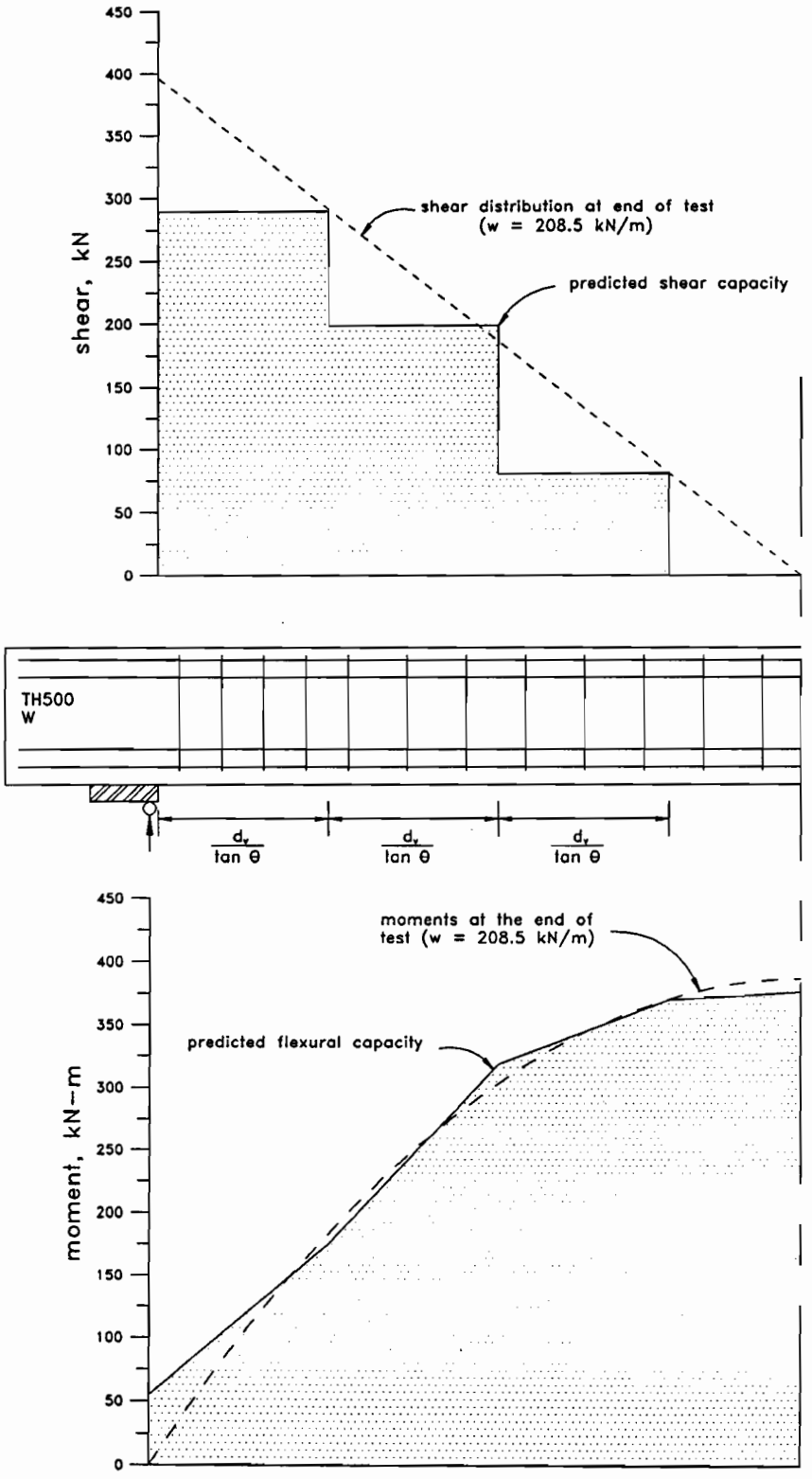

Figure 5-2 Comparison of predicted and experimental shear and moment diagrams at failure for TH500

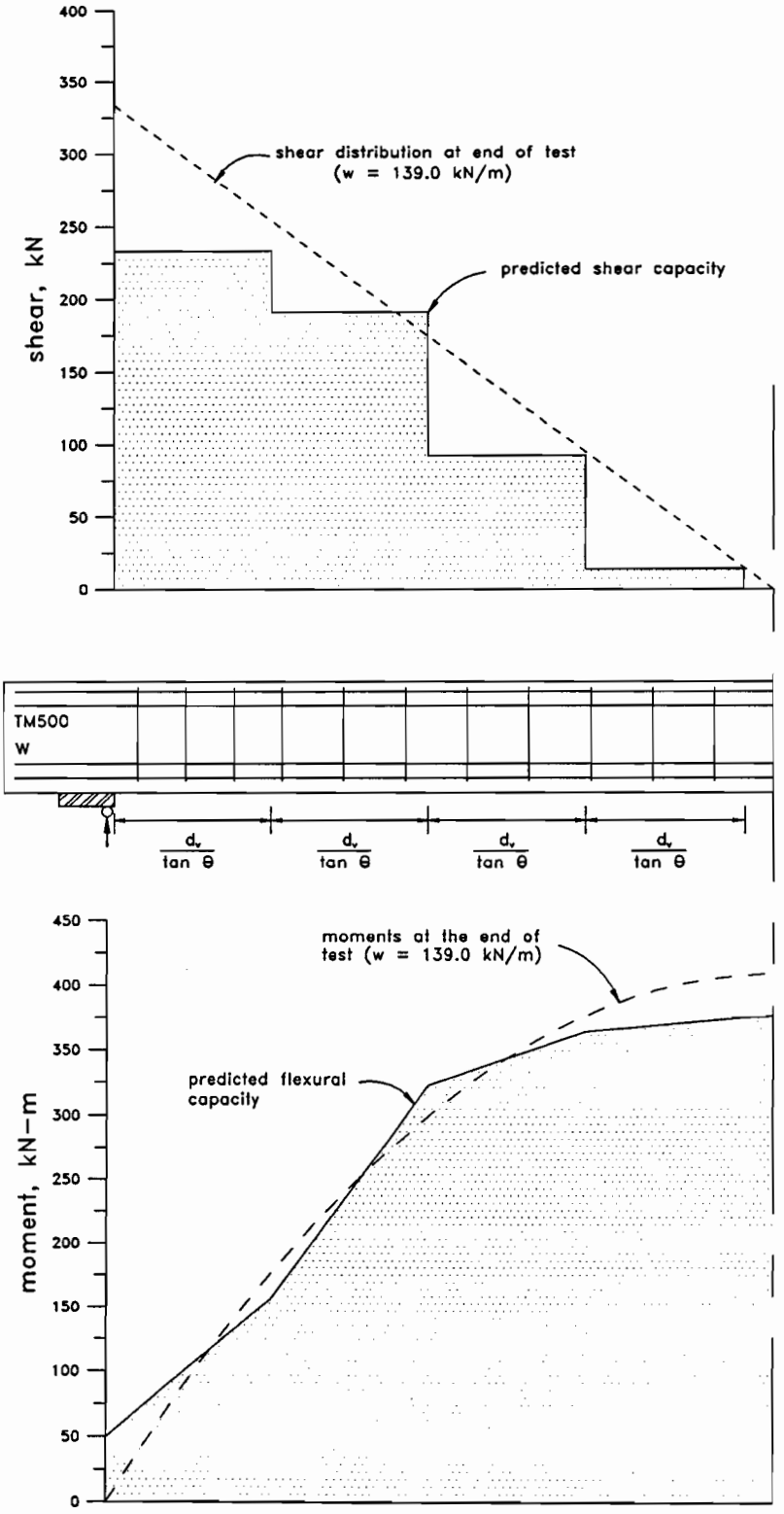

Figure 5-3 Comparison of predicted and experimental shear and moment diagrams at failure for TM500

flexure, with regions of high stirrup strains existing near the supports.

Beam	Measured	Strength Predictions			
		CSA Standard		RESPONSE	
	V_{max} kN	V_r kN	*measured / predicted*	V_r kN	*measured / predicted*
TH500	396	308	1.29	394	1.01
TM500	334	241	1.38	306	1.09

Table 5-3 Comparison of test results and shear strength predictions

The ratios of the measured maximum shears to the predicted shears at failure are also shown in Table 5-3. It can be seen from these ratios that the CSA Standard, which predicts shear failures in both beams, offers conservative estimates of the shear capacities. Neglecting the contribution of the concrete in tension results in predicted shear capacities that are approximately 30% less than the shears corresponding to the measured failure loads. In contrast, the shear strength predictions using the Modified Compression Field Theory, which accounts for the contribution of concrete in tension, offers a more accurate prediction of the shear capacities. As can be seen in Table 5-3, the Modified Compression Field Theory predicts shear capacities very close to the measured maximum shears. Although both beams failed in flexure rather than shear, extremely large strains (about 4 times yield) were measured in the stirrups and very large shear crack widths (greater than 1 mm) were observed. These observations indicate that both beams were very close to their shear capacities and hence the Modified Compression Field Theory predictions are accurate and slightly conservative.

The predicted flexural capacities of the two beams determined using both the CSA Standard approach and computer program RESPONSE were 4 and 11% below the observed moments at failure.

The 1984 CSA Standard states that the control of diagonal cracking must be investigated at service load if the shear due to specified loads, V_{se}, exceeds the cracking shear resistance, V_{cr},

of the beam. This serviceability requirement was included in the Standard to prevent excessively wide shear cracks. As can be seen in Table 5-4, both beams have calculated strains at service load which exceed the maximum specified strains for interior and exterior exposure, which are 0.001 and 0.0008, respectively. The stirrup spacings would therefore have to be reduced in both beams, in order to satisfy the serviceability requirements of the Standard. This would provide the beams with a greater shear strength than the shear capacity shown in Table 5-3. The maximum stirrup strains, measured in the region closest to the support, for TH500 and TM500 are also shown in Table 5-4. This table demonstrates that the CSA Standard overestimates the stirrup strains at service load levels.

			West End Region 1			East End Region 1		
Beam	V_{cr} kN	V_{se} kN	ϵ_{se}	ϵ_{meas}	w_{max} @service mm	ϵ_{se}	ϵ_{meas}	w_{max} @service mm
TH500	79	136	0.0024	0.0017	0.10	0.0019	0.0013	0.05
TM500	79	110	0.0022	0.0004	0.13	0.0019	0.0004	0.08

Table 5-4 Predicted and measured strains at service load levels

The CSA Standard limits the yield stress to be used in shear design calculations to 400 MPa (§11.2.2.5, Ref. 17). This limitation helps to control shear crack widths at service loads and is aimed at reducing the possibility of brittle fracture at the bends in stirrup anchorages. Table 5-5 displays two shear capacities for the beams containing welded-wire fabric stirrups, calculated using the CSA Standard approach.

The two capacities shown in this table correspond to the nominal yield stress of 500 MPa and to the limiting Standard yield stress of 400 MPa. Limiting the yield stress of the welded-wire fabric to 400 MPa gives overly conservative predicted shear capacities for both beams. Furthermore, the welded-wire fabric controlled the crack widths at service load to reasonable

widths and the stirrups were capable of developing strains of about 4 times their yield strain without brittle failures.

Beam	Nominal Yield = 500 MPa			CSA Yield Limit = 400 MPa		
	w_r kN/m	V_{supp} kN	θ_{min} degrees	w_r kN/m	V_{supp} kN	θ_{min} degrees
TH500	151.8	288	28.5	133.7	254	26.9
TM500	93.7	225	25.6	81.5	196	24.2

Table 5-5 Strength predictions using nominal yield and maximum yield stress permitted by the CSA Standard

Chapter 6

Effectiveness of Welded-Wire Fabric as Shear Reinforcement

In this chapter, the behaviour of the two tee beams, TH500 and TM500, having deformed welded-wire fabric stirrup cages will be compared to the response of two companion beams tested by Mailhot (Ref. 27), which had hot-rolled Grade 400, stirrups. The details of the reinforcement for these four beams are shown in Figs. 2-5 and 2-7.

Table 6-1 summarizes the important features of the four beams that were tested. Beam TH500 and Beam A, were both subjected to a high level of shear and were designed for the same service and factored loads. The only significant difference between these companion specimens was the type of shear reinforcement. As can be seen from Table 6-1, Beam TH500 was reinforced with Grade 500 cold-rolled, deformed welded-wire fabric stirrups while its companion, Beam A, was reinforced with Grade 400, hot-rolled stirrups.

The second set of beams, TM500 and Beam B, was designed for a moderate shear load level of about 101 kN/m. These two beams were almost identical (see Table 6-1), but contained different types of stirrup reinforcement. The stirrups provided in Beam TM500 consisted of bent-up, cold-rolled, Grade 500, welded-wire fabric while those provided in Beam B were hot-rolled, Grade 400, U-stirrups.

The beams investigated in this experimental programme, TH500 and TM500, were designed to have the same yield force ($A_v f_y/s$) in each design region, as the companion beams tested by Mailhot (see Table 6-1). Due to the higher yield of the welded-wire fabric stirrups, the

Beam	Design Service Load w_{se} kN/m	Design Load w_f kN/m	Clear Span ℓ_n m	Type of Stirrups	West End Stirrups Closest to Support	$\frac{A_v f_y}{s}$	Flexural Steel
TH500 f'_c=41	97.3	162.1	3.8	Grade 500 WWF Cold-rolled	MD50 @ 125 mm f_y=562 MPa	450	4-No. 30 f_y=467 MPa
A f'_c=39	98.1	163.5	3.8	Grade 400 Hot-rolled	9.5mm dia. @120 mm f_y=407 MPa	482	4-No. 30 f_y=430 MPa
TM500 f'_c=41	60.4	100.6	4.8	Grade 500 WWF Cold-rolled	MD50 @ 175 mm f_y=562 MPa	321	4-No. 30 f_y=467 MPa
B f'_c=39	61.0	101.6	4.8	Grade 400 Hot-rolled	9.5mm dia. @170 mm f_y=407 MPa	340	4-No. 30 f_y=430 MPa

Table 6-1 Design parameters and reinforcement details of the four tee beams

stirrups in beams TH500 and TM500 had a smaller diameter (8 mm) than those used in Beams A and B. For all four beams, the stirrups were more closely spaced in the east halves than they were in the west halves. This different amount of stirrup reinforcement enabled a comparison of the serviceability performance of the two halves of each beam. Using the measured yield stresses of the steels, f_y = 562 MPa for the welded-wire fabric and f_y = 407 MPa for the hot-rolled reinforcement, resulted in 28% less stirrup steel (A_v) in beams TH500 and TM500 than in their respective companions, Beams A and B.

The loading apparatus (see Fig. 2-8) and test procedures were identical for the four beam tests, in all aspects other than the support conditions. Beams A and B were supported on steel bearing pads, resting on steel stands, whereas Beams TH500 and TM500 were supported on a fixed roller at one end and a free roller at the other.

6.1 Measured Responses

A summary of the important load stages is shown in Table 6-2 for the two pairs of beams. Beams TH500 and TM500 developed flexural cracks and inclined shear cracks at slightly lower loads than their companion beams, even though f'_c was slightly higher. This may be due to the variability of the tensile strength of concrete and to the longitudinal restraint caused by the support conditions of Beams A and B.

Beam	M_{cr} kN-m	w @ M_{cr} kN/m	V_{cr} kN	w @ V_{cr} kN/m	1st stirrup yield west w, kN/m	1st stirrup yield east w, kN/m	V_{supp} kN	w_u kN/m
TH500	37	20.0	78.4	44.9	123.0	141.2	396	208.5
A	45	25.2	82.3	47.1	128.4	167.4	398	209.4
TM500	33	11.3	72.1	32.1	84.1	93.1	334	139.0
B	40	14.0	81.3	36.2	110.6	126.4	311	129.7

Table 6-2 Comparison of the measured responses of the beams with WWF stirrups and the beams with hot-rolled stirrups

The stirrups in the two beams containing welded-wire fabric stirrups yielded at a lower shear load than those in the beams using Grade 400 stirrups. This "early yielding" of the stirrups in the beams reinforced with welded-wire fabric was expected, since the yield force provided in these beams was slightly lower (see Table 6-1). In all beams, the stirrups in the west ends reached yield before those in the east ends, due to the smaller stirrup spacing in the east ends of the beams.

6.1.1 Load-Deflection Response

The applied load as a function of the midspan deflection is shown in Figs. 6-1 and 6-2 for the beams subjected to a high shear loading and those subjected to a moderate shear loading, respectively. The effect of the longitudinal restraint caused by the support conditions in Mailhot's

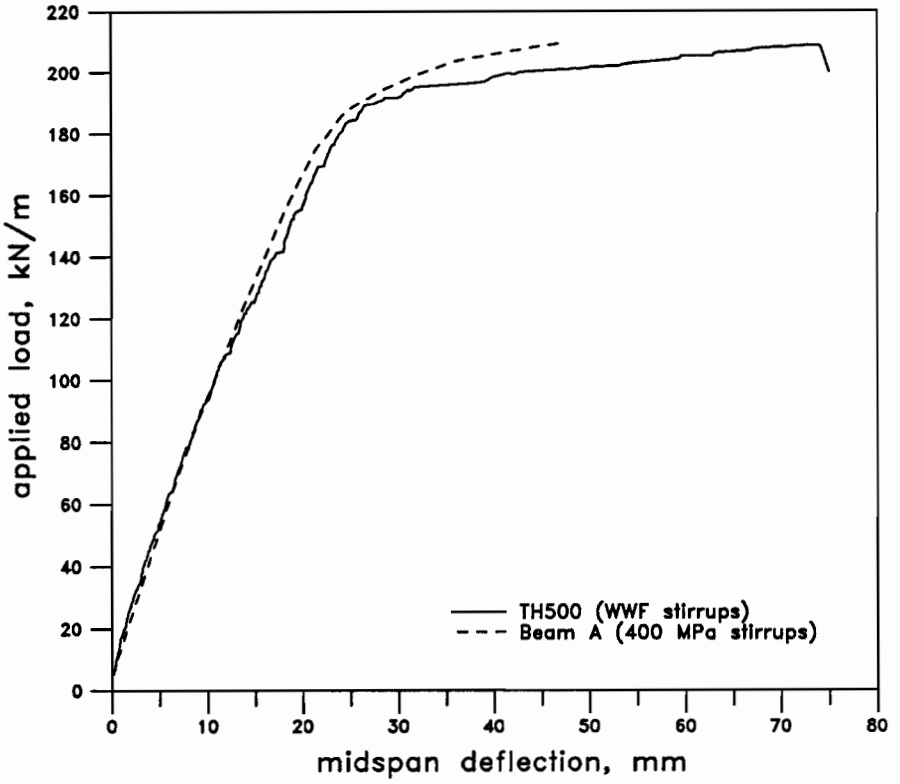

Figure 6-1 Load deformation responses of beams subjected to a high shear

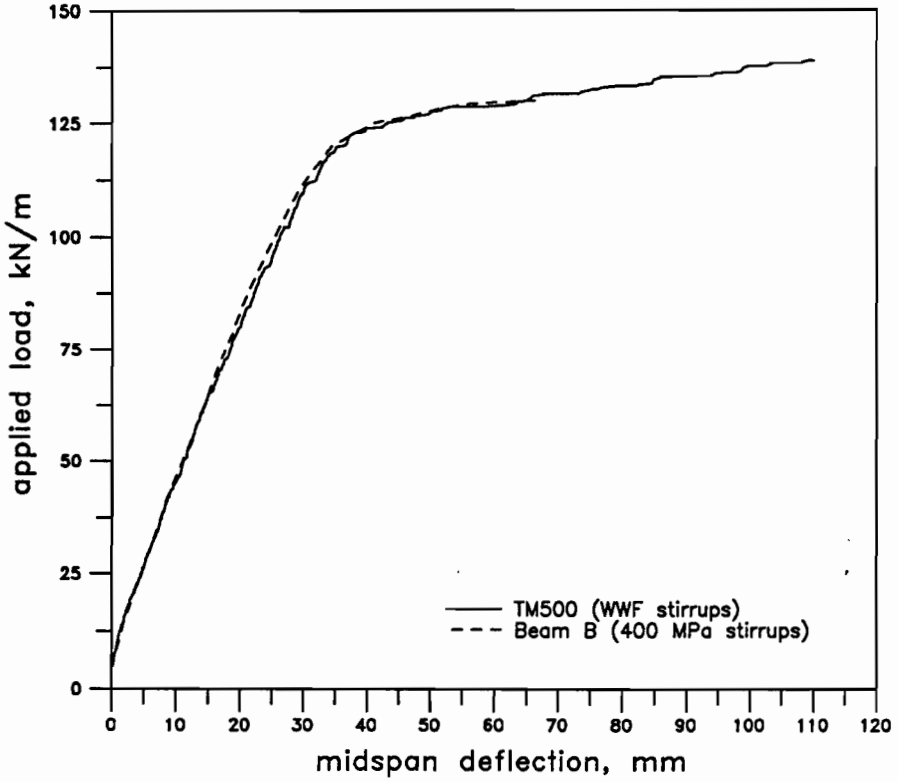

Figure 6-2 Load deformation responses of beams subjected to a moderate shear

tests can be seen in these figures. Both Beams A and B exhibited a slightly stiffer loading response than Beams TH500 and TM500, indicating a very small restraint effect. As can be seen in Table 6-2, TH500 and Beam A reached almost the same ultimate loads, while TM500 reached a slightly higher ultimate load than Beam B.

6.1.2 Stirrup Strains

The maximum stirrup strains measured in each stirrup are compared for the companion specimens in Figs. 6-3 and 6-4. These strains are shown at service load levels and at the maximum deflection measured in Mailhot's tests, since Beams TH500 and TM500 were both tested to significantly greater deflections (almost 40% greater) than their companions. These figures demonstrate that the strains in the stirrups are larger for the Grade 500 steel, both at service and ultimate load levels. These larger strains in the welded-wire fabric are due to the smaller area of stirrup reinforcement that is provided in Beams TH500 and TM500.

6.1.3 Shear Crack Widths

The same concrete cover was provided in both the beams reinforced with Grade 500, welded-wire fabric and the beams containing Grade 400, hot-rolled U-stirrups. Although the companion specimens had stirrups with nearly the same yield force, the stirrup spacings were almost identical because smaller diameter stirrups were provided in the welded-wire fabric. These similarities enable a comparison of the crack control characteristics of Beams TH500 and TM500 with their respective companions, Beams A and B.

The load versus maximum shear crack widths for the east and west halves of the beams are shown in Figs. 6-5, 6-6, 6-7 and 6-8. Smaller crack widths were observed in the east ends of the beams due to the larger amounts of shear reinforcement provided. These figures show that, at service load levels, smaller shear cracks formed in the beams reinforced with welded-wire fabric stirrups than in the beams reinforced with hot-rolled stirrups. The smaller crack widths for

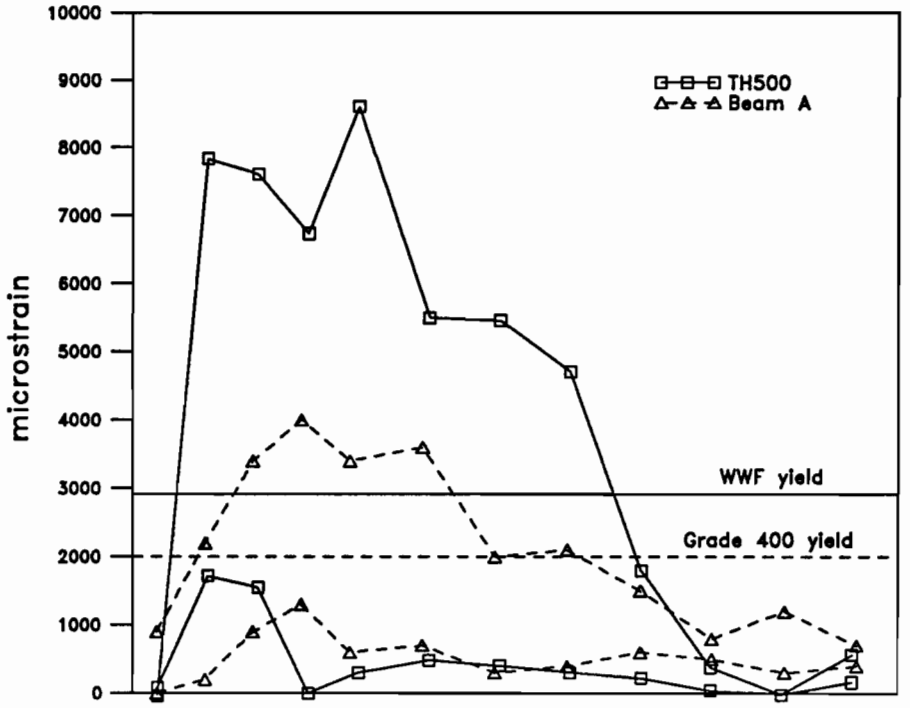

Figure 6-3 (a) Maximum strains measured in the stirrups at service and ultimate load levels in the west half of the beams subjected to a high shear

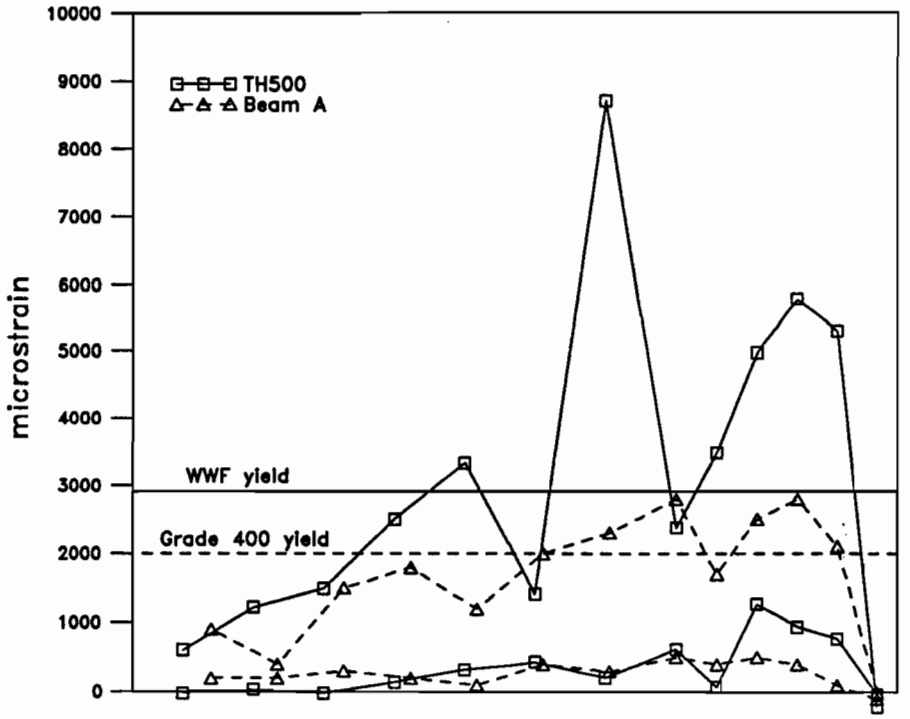

Figure 6-3 (b) Maximum strains measured in the stirrups at service and ultimate load levels in the east half of the beams subjected to a high shear

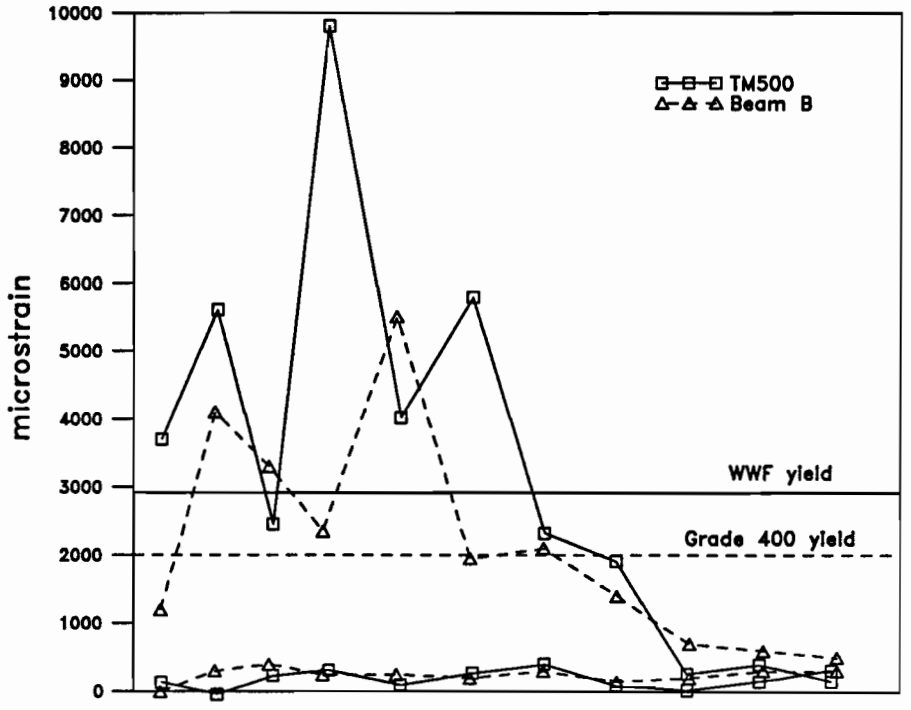

Figure 6-4 (a) Maximum strains measured in the stirrups at service and ultimate load levels in the west half of the beams subjected to a moderate shear

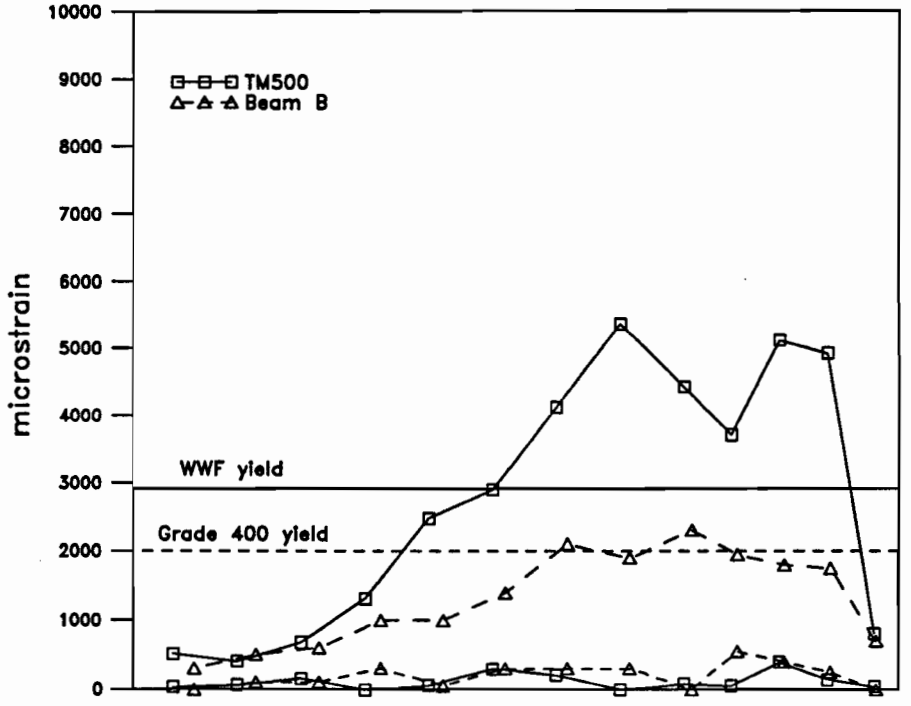

Figure 6-4 (b) Maximum strains measured in the stirrups at service and ultimate load levels in the east half of the beams subjected to a moderate shear

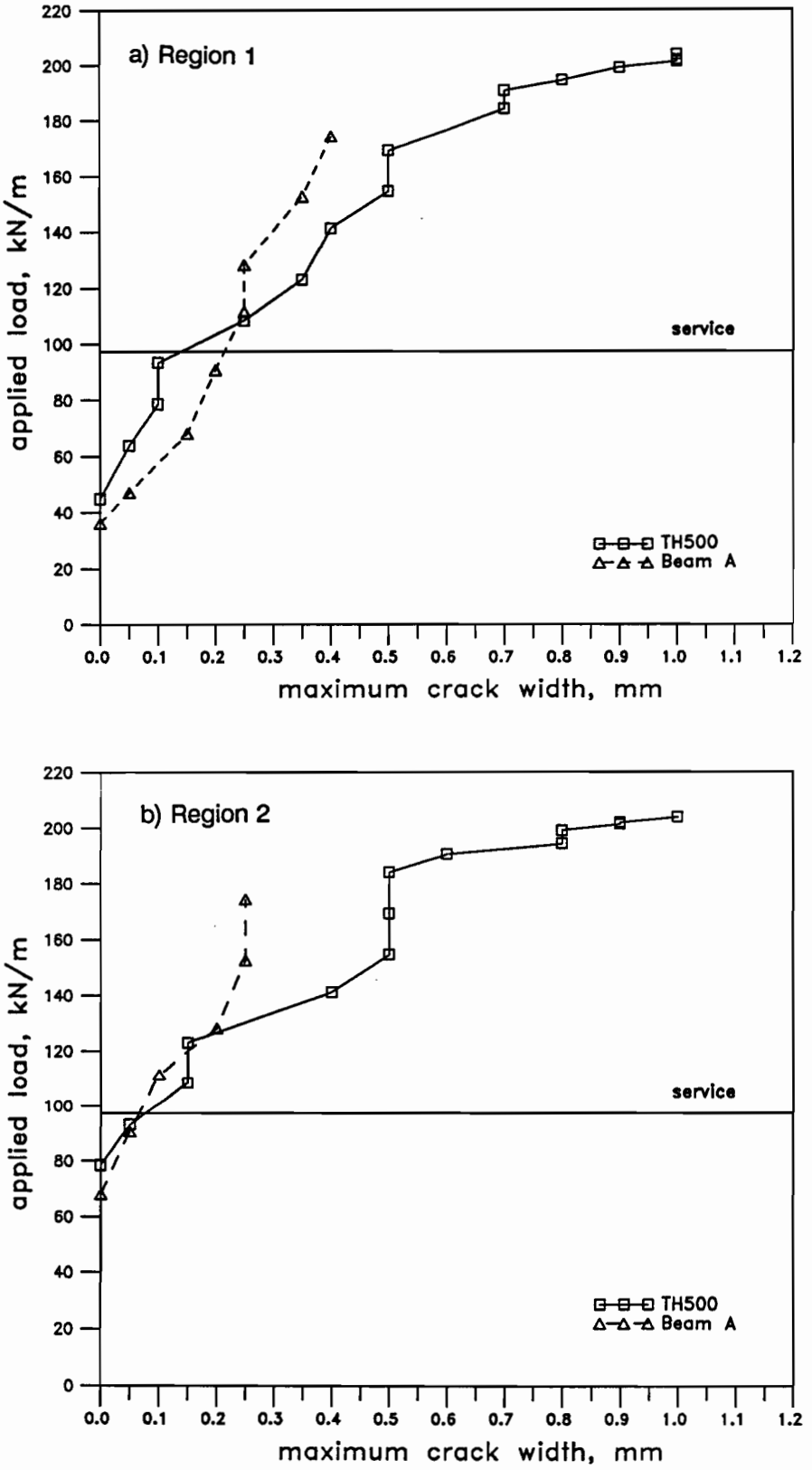

Figure 6-5 Maximum shear crack widths in west end of beams subjected to a high shear

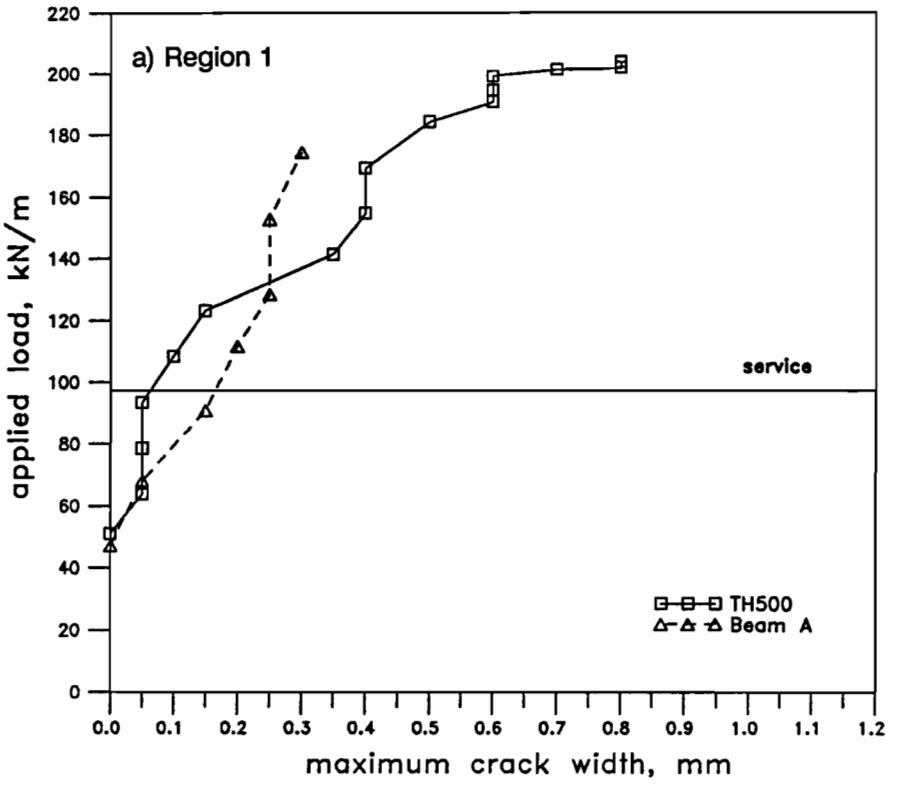

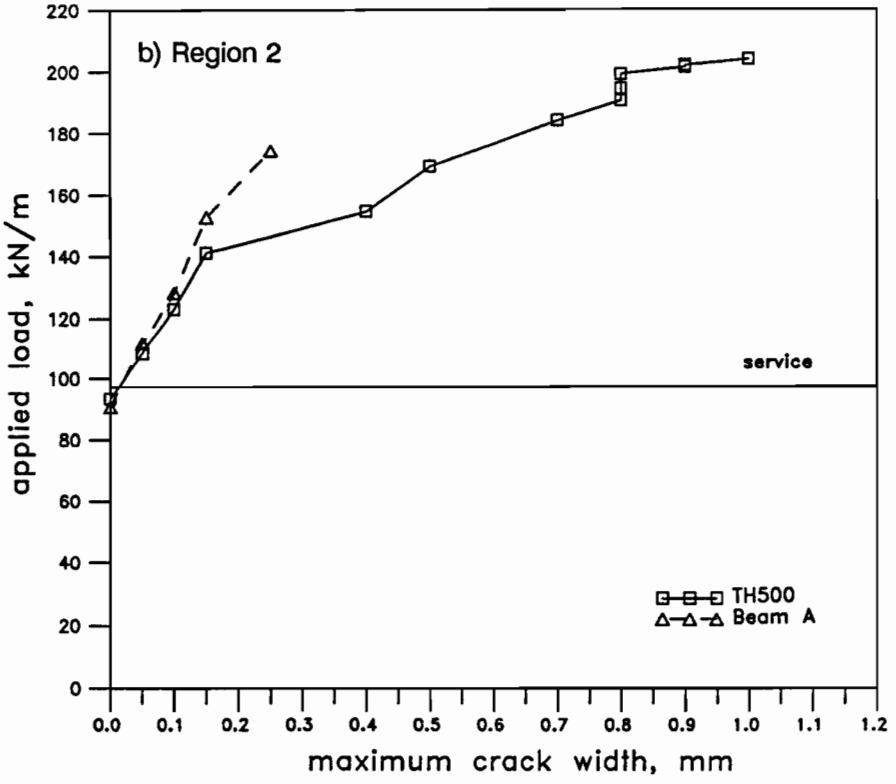

Figure 6-6 Maximum shear crack widths in east end of beams subjected to a high shear

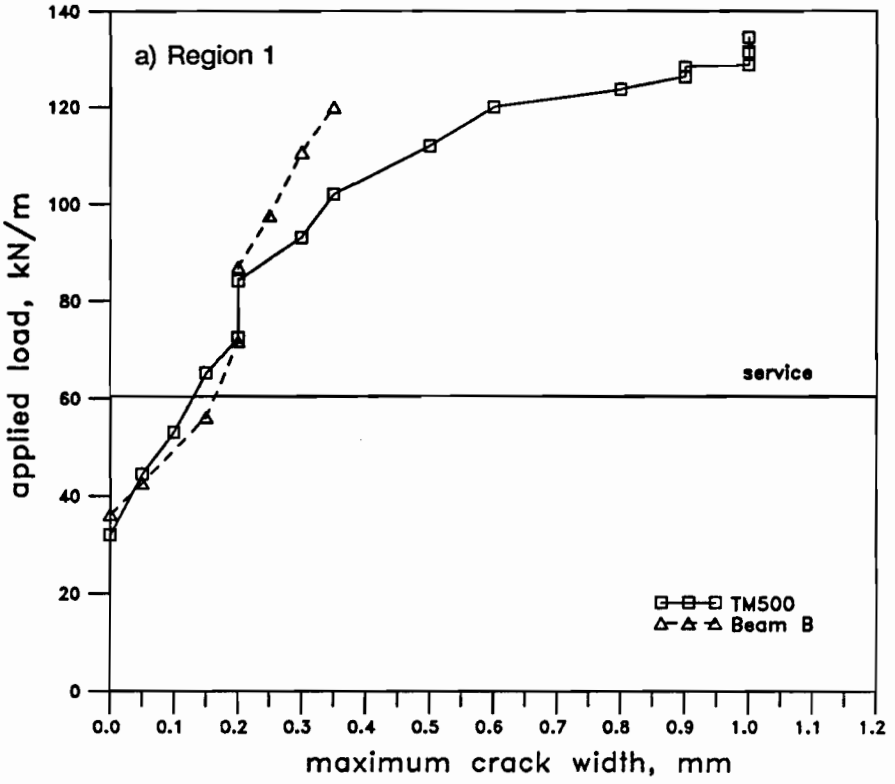

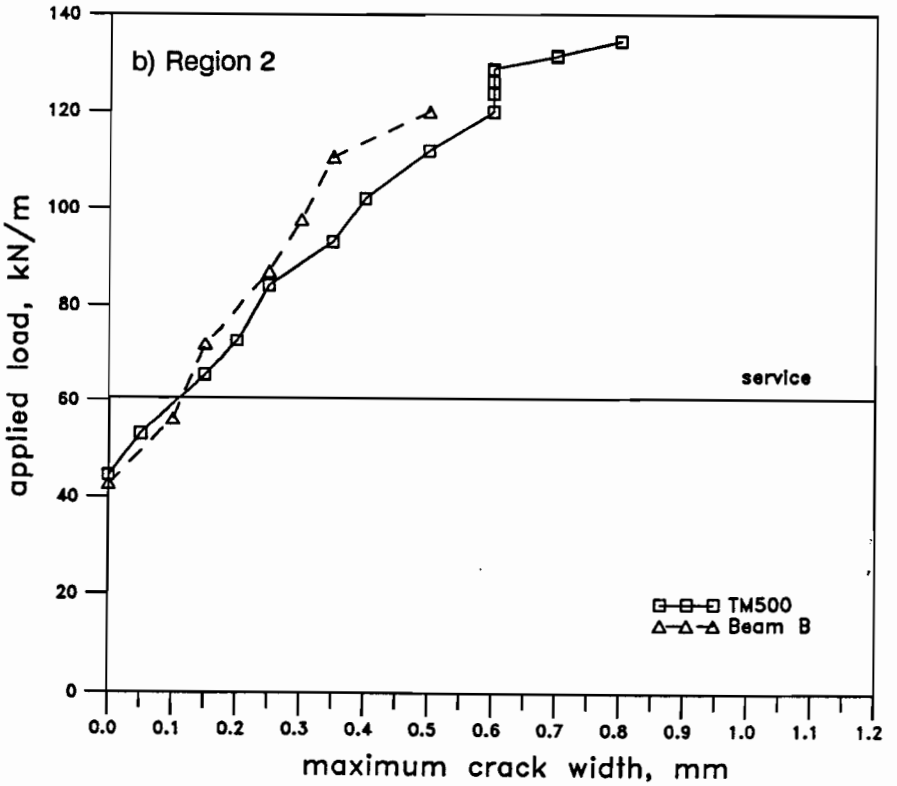

Figure 6-7 Maximum shear crack widths in west end of beams subjected to a moderate shear

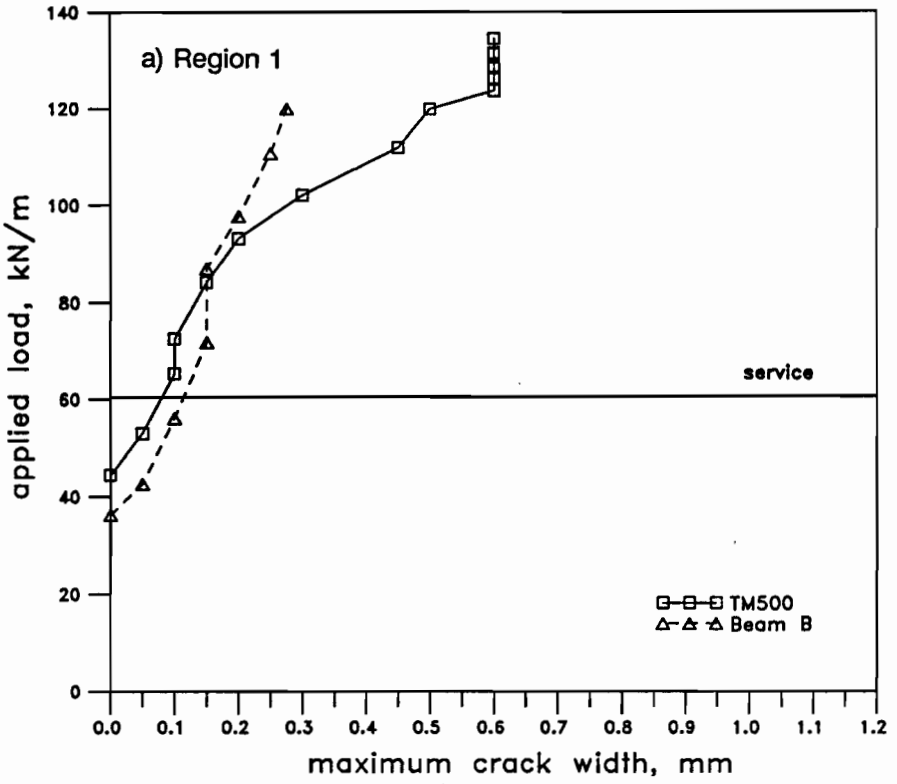

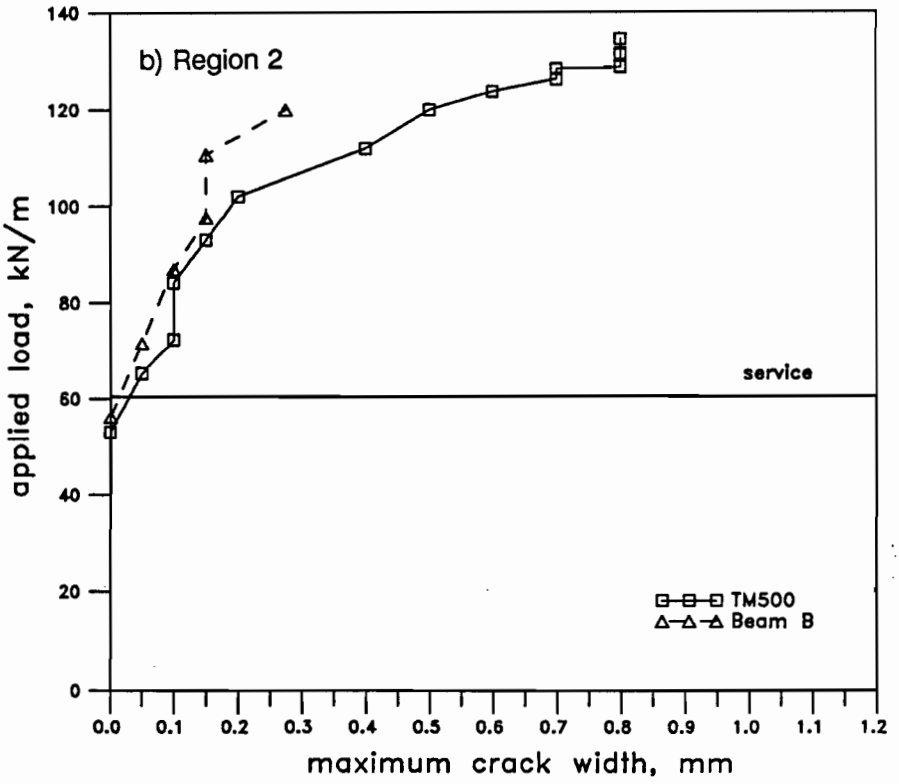

Figure 6-8 Maximum shear crack widths in east end of beams subjected to a moderate shear

the beams reinforced with welded-wire fabric indicates the improved bond performance of the smaller diameter deformed welded-wire fabric. However, at loads beyond service load level, the beams with welded-wire fabric stirrups eventually developed larger cracks than their companion beams. This is due to the smaller area of reinforcement which must develop larger strains at higher load levels. These tests demonstrate that the Grade 500, welded-wire fabric used as a direct replacement for Grade 400, hot-rolled stirrups, provides slightly better crack control at service load levels. In addition, the same shear capacity was attained for these two types of reinforcement.

6.2 Predicted Responses

The predicted capacities of the four beams, computed according to the CSA Standard and using the measured material properties, are shown in Table 6-3. Since the stirrups were more closely spaced in the east end of the beams, the west ends governed their design capacities. This table shows that TH500 and Beam A, and TM500 and Beam B, had almost the same design capacities. The CSA Standard predicted that the four beams would all fail in shear.

Beam	General Method of shear design			Measured	
	w_r kN/m	V_{supp} kN	θ_{min} degrees	w_r kN/m	V_{supp} kN
TH500	162.1	308	29.4	208.5	396
A	163.5	311	30.4	209.4	398
TM500	100.6	241	26.4	139.0	334
B	101.6	244	27.1	129.7	311

Table 6-3 Strength predictions using the Compression Field Theory

The computer program RESPONSE (Refs. 10 and 29) was used to predict the ultimate capacities of Beams A and B. The analysis that was carried out used the same material stress-

strain relationships and the same beam discretization shown in Fig. 5-1. A copy of the input data files are included in Appendix A. The beams capacities were determined, using the Modified Compression Field Theory, at increments of $d_v / \tan\theta$ away from the support face. These predictions accounted for the shear-moment interaction at a given section. The results of the computer analyses of Beams A and B are shown in Figs. 6-9 and 6-10, respectively. It can be seen from these figures that both Beams A and B are predicted to fail in flexure at loads of 190.5 kN/m and 119.4 kN/m, respectively. The predicted shear capacities are shown in Table 6-4.

Beam	Predicted Shear Capacity			Predicted Moment Capacity		Predicted Failure Mode	Measured		
	V_{supp} kN	w_r kN/m	θ_{min} degrees	M_r kN-m	w_r kN/m		w_u kN/m	V_{supp} kN	M_u kN-m
TH500	394	207.4	26.9	369	199.1	flexural	208.5	396	386
A	376	198.0	27.4	344	190.5	flexural	209.4	398	378
TM500	306	127.6	24.1	362	123.0	flexural	139.0	334	409
B	305	127.1	24.4	344	119.4	flexural	129.7	311	374

Table 6-4 Predicted failure loads from combined shear and moment analyses using RESPONSE with Modified Compression Field Model for shear

Table 6-5 compares the predicted shear capacities of the beams with the maximum measured shear. Once again, it can be seen that the CSA Standard significantly underestimates the actual shear capacity of the beams, whereas the Modified Compression Field Theory offers a more accurate and slightly conservative prediction.

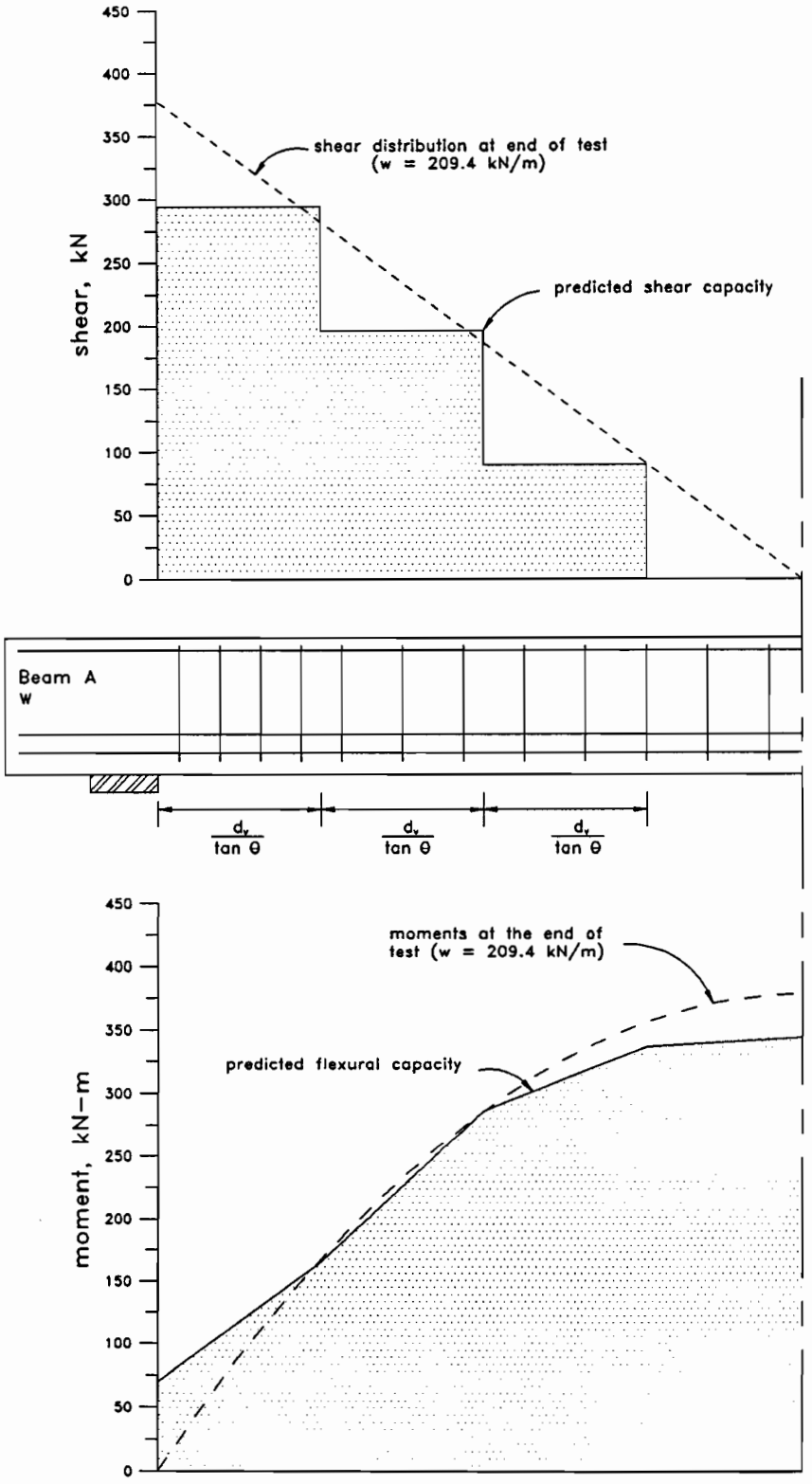

Figure 6-9 Comparison of predicted and experimental shear and moment diagrams at failure for Beam A

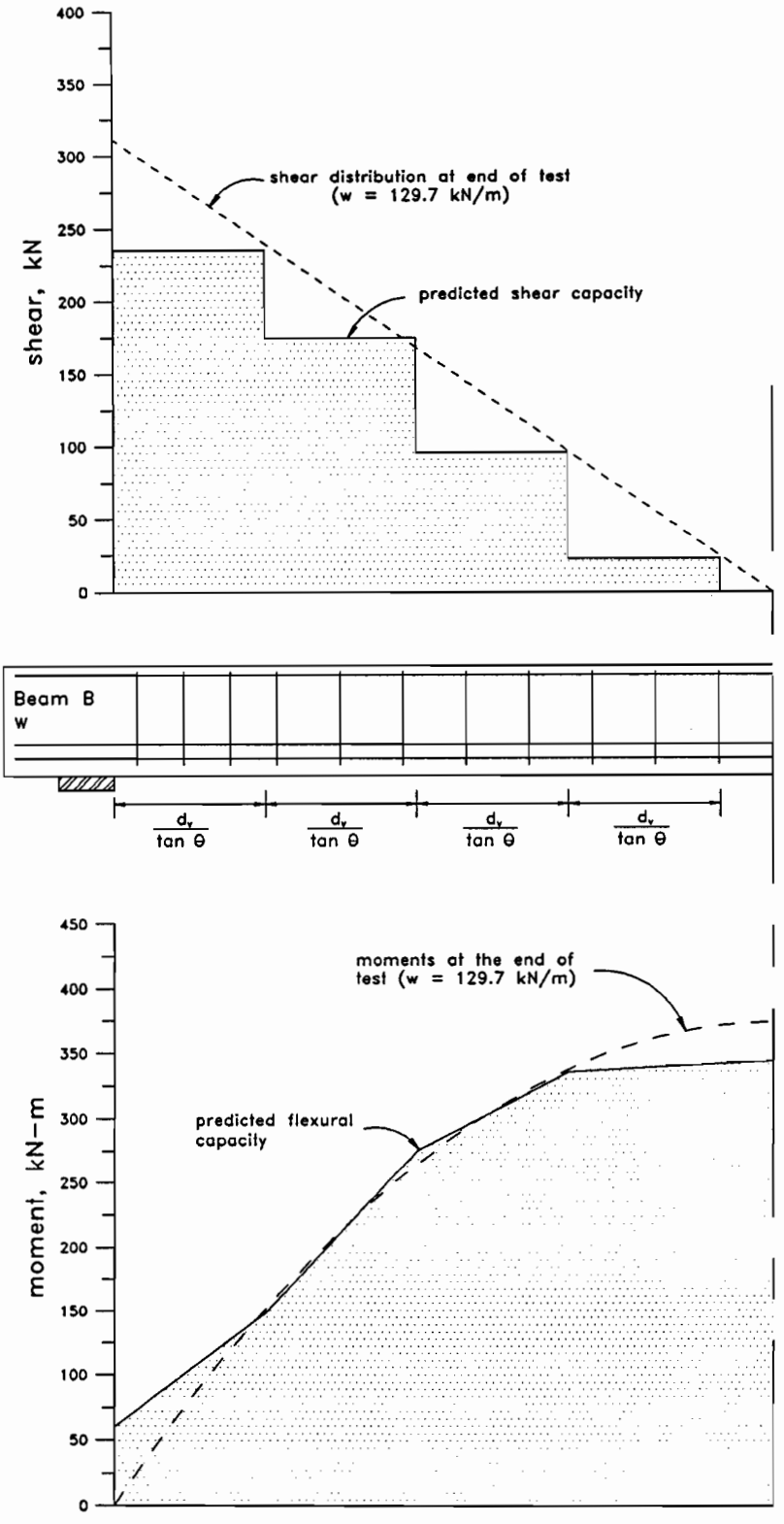

Figure 6-10 Comparison of predicted and experimental shear and moment diagrams at failure for Beam B

Beam	Measured	Strength Predictions			
		CSA Standard		RESPONSE	
	V_{max} kN	V_r kN	*measured / predicted*	V_r kN	*measured / predicted*
TH500	396	308	1.29	394	1.01
A	398	311	1.28	376	1.06
TM500	334	241	1.38	306	1.09
B	311	244	1.28	305	1.02

Table 6-5 Comparison of test results and shear strength predictions

Chapter 7

Conclusions

7.1 Conclusions

This research programme consisted of two distinct experimental studies to assess the behaviour of deformed welded-wire fabric as reinforcement. The first test series consisted of 16 tension specimens while the second test series consisted of two full-scale tee beams subjected to simulated uniform loading. The conclusions are discussed below.

The tension tests enabled a direct comparison of specimens reinforced with Grade 500, cold-rolled, deformed welded-wire fabric and companion specimens containing Grade 400, hot-rolled reinforcement. These tests led to the following conclusions:

1. The deformed welded-wire fabric improves the crack control over the hot-rolled reinforcement at service load levels. The welded cross-wires improve the bond characteristics of the welded-wire fabric and hence reduce the crack widths.

2. The members reinforced with welded-wire fabric undergo less elongation prior to failure than the members reinforced with the Grade 400, hot-rolled reinforcement. This loss of "ductility" is due to the cold-rolling process, which results in an increased yield stress, but reduces the rupture strain.

3. The tension members were able to develop more than one crack prior to failure as long as a minimum area of reinforcement was provided. The minimum reinforcement ratios that must be provided in order to provide adequate crack control and to ensure a ductile failure are:

For Grade 400, hot-rolled reinforcement:

$$\rho_{min} = \frac{f_{cr}}{1.25 f_y} = \frac{0.33\sqrt{f'_c}}{1.25 f_y}$$

For Grade 500, welded-wire fabric:

$$\rho_{min} = \frac{f_{cr}}{f_y} = \frac{0.33\sqrt{f'_c}}{f_y}$$

These two expressions account for both the concrete tensile strength, assumed to be $0.33\sqrt{f'_c}$, and the shape of the stress-strain relationship of the steel. It is interesting to note that both of these types of steel require the same minimum area of reinforcement for a given concrete strength, since f_y for the Grade 500 steel is 1.25 times f_y for the Grade 400 steel.

4. High strength concrete improves the cracking behaviour of reinforced concrete members subjected to axial tension. Specimens cast with high strength concrete developed a greater number of cracks and a more uniform crack pattern than did specimens cast with lower strength concrete, having the same reinforcement ratio (ρ). This improved performance is due to the better bond and the increased tensile strength of the high strength concrete.

The tests of the full-scale beams showed that welded-wire fabric U-stirrups performed adequately as shear reinforcement in beams designed according to the General Method for Shear Design and subjected to moderate and high shear loading. These tests led to the following conclusions:

1. The deformed welded-wire fabric offers better crack control than an equivalent amount (i.e., having the same $A_v f_y/s$) of hot-rolled, Grade 400 reinforcement up to and slightly above service load levels.

2. The two deformed cross wires, welded at the top of the stirrup cage, provided

sufficient anchorage to develop significant strains in the stirrups.

3. The cold-rolled deformed welded-wire fabric stirrups exhibited sufficient ductility to redistribute the stresses in the stirrups to avoid a sudden, brittle shear failure.

4. The Modified Compression Field Theory offers a more accurate prediction of the behaviour of beams in shear than does the Compression Field Theory, since it accounts for the contribution of tensile stresses in the concrete between the cracks.

5. The maximum yield stress to be used in shear design calculations as specified in the CSA Standard is f_y = 400 MPa. This limit results in overly conservative estimates of the shear strength of beams designed according to the General Method and reinforced with welded-wire fabric. Since the welded-wire fabric is able to develop significant strains and exhibits sufficient ductility to redistribute the strains to avoid brittle shear failures, its nominal yield stress of f_y = 500 MPa could be used in design calculations.

7.2 Future Research

Since very little research has been carried out to determine the behaviour of deformed welded-wire fabric as reinforcement, a suggestion of future research is given below:

1. The effects of the cold-rolling process on the mechanical properties of the deformed, Grade 500 welded-wire fabric should be investigated. The loss of ductility that accompanies the increase in yield strength is caused by the amount of cold working required to shape the reinforcing steel. The welded-wire fabric used in this research programme consisted of bars drawn from a wire having an initial diameter of 13.5 mm. The cold-drawn bar underwent a reduction of area of 30%. Research needs to be done to investigate the likely improved ductility that would result if a smaller reduction of area were used in the rolling process.

2. A series of tests should be performed to determine the influence of the mechanical anchorage provided by the welded cross-ties.

3. A series of tests should be performed to determine the effect of high performance

concrete on the behaviour of beams having cold-rolled, Grade 500 welded-wire fabric as stirrups.

4. A series of tests should be carried out to determine whether welded-wire fabric stirrups are able to provide sufficient ductility for fatigue type loading and seismic type loading.

REFERENCES

1 Herkommer, F., Hütten, P., and Brodmeier, J., "Modern Building with Steel Fabric Reinforcement", Translation of an article published in "*beton*", Vol. 33, No. 11, 1983, pp. 405-412.

2 Wire Reinforcement Institute, "Bending Welded Wire Fabric for Concrete Reinforcement", McLean, Virginia, 1974.

3 Canadian Standards Association, "Deformed Steel Wire for Concrete Reinforcement", CSA G30.14-M83, Rexdale, Ontario, 1983.

4 Dove, A.B., "Some Observations on the Physical Properties of Wire for Plain and Deformed Welded Wire Fabric", *ACI Journal*, Sept-October 1983, pp. 424-430.

5 Canadian Standards Association, "Welded Deformed Steel Wire Fabric for Concrete Reinforcement", G30.15-M83, Rexdale, Ontario, 1983.

6 "A Metallurgical Investigation of Cold-Rolled Rebar", McGill University Internal Report, 1991, 13 pp.

7 Nilson, A.H., "High Strength Concrete - An Overview of Cornell Research", *Proceedings of the Symposium Utilization of High Strength Concrete*", Stavanger, Norway, June 1987, Tapir, Trondheim, pp. 127-133.

8 Carrasquillo, R.L., Nilson, A.H., and Slate, F.O., "Properties of High Strength Concrete Subject to Short-Term Loads", *ACI Journal*, Vol. 78, No. 3, May-June 1981, pp. 171-178.

9 Strategic Highway Research Program, "High Performance Concretes, A State-of-the-Art Report", National Research Council, Washington, D.C., 1991.

10 Collins, M. P., and Mitchell, D., *Prestressed Concrete Structures*, Prentice Hall, Englewood Cliffs, New Jersey, 1991, 766 pp.

11 Goto, Y., "Cracks Formed in Concrete around Deformed Tension Bars", *ACI Journal*, Vol. 68, No. 4, Apr. 1971, pp. 224-251.

12 Vecchio, F.J., and Collins, M.P., "The Modified Compression Field Theory for Reinforced Concrete Elements Subjected to Shear", *ACI Journal*, Vol. 83, No. 2, Mar-Apr. 1986, pp. 219-231.

13 CEB-FIP, *Model Code for Concrete Structures: CEB-FIP International Recommendations*, 3rd ed., Comité Euro-International du Béton, Paris, 1978, 348 pp.

14 Gergely, P., and Lutz, L.A., "Maximum Crack Width in Reinforced Concrete Flexural Members", *Causes, Mechanisms, and Control of Cracking in Concrete*, SP-20, American Concrete Institute, Detroit, 1968, pp. 87-117.

15 Rizkalla, S.H., Hwang, L.S. and El Shahawi, M., "Transverse Reinforcement Effect on Cracking Behaviour of R.C. Specimens", *Canadian Journal of Civil Engineering*, Vol. 10, No. 4, Dec. 1983, pp. 566-581.

REFERENCES *(cont'd)*

16 Williams, A., "Tests on Large Reinforced Concrete Elements Subjected to Direct Tension", Technical Report No. 562, Cement and Concrete Association, Wexham Springs, UK, Apr. 1986, 56 pp.

17 Canadian Standards Association, "Design of Concrete Structures for Buildings", CSA CAN3-A23.3-M84, Rexdale, Ontario, 1984.

18 Mansur, M.A., Lee, C.K., and Lee, S.L., "Anchorage of Welded Wire Fabric Used as Shear Reinforcement in Beams", *Magazine of Concrete Research*, Vol. 38, No. 134, March 1986, pp. 36-46.

19 Collins, M.P., and Mitchell, D., "Shear and Torsion Design of Prestressed and Non-Prestressed Concrete Beams", *PCI Journal*, Vol. 25, No. 5, Sept-Oct 1980, pp. 32-100.

20 Vecchio, F., and Collins, M.P., "The Response of Reinforced Concrete to In-Plane Shear and Normal Stresses", Publication No. 82-03, Department of Civil Engineering, University of Toronto, Mar. 1982, 332 pp.

21 Collins, M.P., and Mitchell, D., *Prestressed Concrete Basics*, CPCI, Ottawa, Canada, 1986, 614 pp.

22 Collins, M.P., Vecchio, F.J., Adebar, P., and Mitchell, D., "A Consistent Shear Design Model", Proceedings, Vol. 62, IABSE Colloquium, Stuttgart, 1991, pp. 457-462.

23 Leonhardt, F., and Walther, R., "Welded Wire Mesh as Stirrup Reinforcement. Shear Tests on T-Beams and Anchorage Tests", (Translation by W. Dilger of the article in *Die Bautechnik*, Vol. 42, Oct. 1965).

24 Taylor, M.A., and El-Hammasi, S., "Web Cracking Behavior of Beams Using Welded Wire Fabric as Shear Reinforcement", *ACI Journal*, Vol. 77, No. 1, Jan-Feb 1980, pp. 12-17.

25 Mansur, M.A., Lee, C.K., and Lee, S.L., "Deformed Wire Fabric as Shear Reinforcement in Concrete Beams", *ACI Structural Journal*, Vol. 84, No. 5, Sept-Oct 1987, pp. 392-399.

26 Pincheira, J.A., Rizkalla, S.H., and Attiogbe, E., "Welded Wire Fabric as Shear Reinforcement under Cyclic Loading", *Proceedings, 1988 CSCE Annual Conference*, May 1988, pp.643-663.

27 Mailhot, G., "Experiments on the Staggering Concept for Shear Design", Project Report No. G84-5, Department of Civil Engineering and Applied Mechanics, McGill University, Mar. 1985, 96 pp.

28 *1988 Annual Book of ASTM Standards*, Section 4, Vol. 4.02, American Society for Testing and Materials, 1988.

29 Felber, A.J., "RESPONSE: A Program to Determine the Load-Deformation Response of Reinforced Concrete Sections", M.A.Sc. thesis, Department of Civil Engineering, University of Toronto, 1990, 148 pp.

Appendix A

"RESPONSE" Input Files

A1. "RESPONSE" Data File for TH500 - Region 1

```
Response Version 1 Data-File
Copyright 1990 A. Felber
Name of Section:                    TH500-WEST
Units M/U 'Metric/U.S.Customary':          M
Number of Concrete Types (1-5):            1
   Type          f'c        ec'        fcr      Tension Stiffening
   Number       [Mpa]  [Milli-Strain] [Mpa]    Factor
        1     41.40     -1.950      2.57       1.00
Number of Rebar Types  (1-5):              3
   Type  Elastic Modulus    fy         esh       esrupt       fu
   Number     [Mpa]          [Mpa]      [---Milli-Strain--]  [Mpa]
        1    200000        467     72.300    150.000        711
        2    200000        602     31.800     44.000        515
        3    198050        588     33.200     42.000        515
Number of Tendon Types  (1-5):             0
Height of Section:                         400      mm
Distance to Moment Axis:                   264      mm
Shear Y/N 'Yes/No':                          Y
   Web width  (bw)  :                      200      mm
   Shear depth (jd) :                      284      mm
   Distance to web strain ex :              93      mm
   Distance to center of web :             235      mm
   Longitudinal crack spacing:             327      mm
   Maximum Aggregate size    :              20      mm
Stirrups Y/N 'Yes/No':                       Y
   Transverse crack spacing  :             329      mm
   Area of Stirrups (Av)     :             100      mm^2
   Stirrup Spacing  (s)      :             125      mm
   Stirrup (Rebar) Type      :               3
Number of Concrete Layers (1-20):          16
   Layer      y       bottom width  top width   height      Type
   Number     [mm]        [mm]        [mm]        [mm]      Number
        1       0        200         200          25         1
        2      25        200         200          25         1
        3      50        200         200          25         1
        4      75        200         200          25         1
        5     100        200         200          25         1
        6     125        200         200          25         1
        7     150        200         200          25         1
        8     175        200         200          25         1
        9     200        200         200          25         1
       10     225        200         200          25         1
       11     250        200         200          25         1
       12     275        200         200          25         1
       13     300        800         800          25         1
       14     325        800         800          25         1
       15     350        800         800          25         1
       16     375        800         800          25         1
Number of Rebar Layers  (0-10) :           5
   Layer       y          Area       Type
   Number      [mm]       [mm^2]     Number
        1      374        200        2
        2      365        100        3
        3      315        100        3
        4      123       1400        1
        5       63       1400        1
Consider displaced Concrete Y/N:             N
Thermal & Shrinkage Strains Y/N :            N
Initial Strains             Y/N :            N
```

A2. "RESPONSE" Data File for TH500 - Region 2

```
Response Version 1 Data-File
Copyright 1990 A. Felber
Name of Section:                    TH500-WEST
Units M/U 'Metric/U.S.Customary':          M
Number of Concrete Types (1-5):            1
   Type          f'c        ec'        fcr     Tension Stiffening
   Number       [Mpa]  [Milli-Strain] [Mpa]    Factor
       1     41.40    -1.950      2.57      1.00
Number of Rebar Types  (1-5):              3
   Type  Elastic Modulus   fy        esh      esrupt      fu
   Number    [Mpa]         [Mpa]     [---Milli-Strain--]  [Mpa]
       1    200000       467    72.300   150.000       711
       2    200000       602    31.800    44.000       515
       3    198050       588    33.200    42.000       515
Number of Tendon Types  (1-5):             0
Height of Section:                         400     mm
Distance to Moment Axis:                   264     mm
Shear Y/N 'Yes/No':                          Y
   Web width  (bw)  :                      200     mm
   Shear depth (jd) :                      284     mm
   Distance to web strain ex :              93     mm
   Distance to center of web :             235     mm
   Longitudinal crack spacing:             327     mm
   Maximum Aggregate size    :              20     mm
Stirrups Y/N 'Yes/No':                       Y
   Transverse crack spacing  :             419     mm
   Area of Stirrups (Av)     :             100     mm^2
   Stirrup Spacing  (s)      :             175     mm
   Stirrup (Rebar) Type      :             3
Number of Concrete Layers (1-20):          16
   Layer      y       bottom width  top width   height      Type
   Number     [mm]        [mm]        [mm]       [mm]       Number
       1        0        200         200         25         1
       2       25        200         200         25         1
       3       50        200         200         25         1
       4       75        200         200         25         1
       5      100        200         200         25         1
       6      125        200         200         25         1
       7      150        200         200         25         1
       8      175        200         200         25         1
       9      200        200         200         25         1
      10      225        200         200         25         1
      11      250        200         200         25         1
      12      275        200         200         25         1
      13      300        800         800         25         1
      14      325        800         800         25         1
      15      350        800         800         25         1
      16      375        800         800         25         1
Number of Rebar Layers  (0-10) :           5
   Layer       y          Area       Type
   Number      [mm]       [mm^2]     Number
       1       374        200        2
       2       365        100        3
       3       315        100        3
       4       123       1400        1
       5        63       1400        1
Consider displaced Concrete Y/N:             N
Thermal & Shrinkage Strains Y/N :            N
Initial Strains             Y/N :            N
```

A3. "RESPONSE" Data File for TM500 - Region 1

```
Response Version 1 Data-File
Copyright 1990 A. Felber
Name of Section:                    TM500-WEST
Units M/U 'Metric/U.S.Customary':          M
Number of Concrete Types (1-5):            1
   Type          f'c        ec'        fcr      Tension Stiffening
   Number       [Mpa]  [Milli-Strain] [Mpa]    Factor
        1     41.20     -1.990       2.33        1.00
Number of Rebar Types  (1-5):              3
   Type  Elastic Modulus    fy         esh       esrupt       fu
   Number     [Mpa]          [Mpa]      [---Milli-Strain--]  [Mpa]
        1     200000        467     72.300    150.000        711
        2     200000        602     31.800     44.000        515
        3     198050        588     33.200     42.000        515
Number of Tendon Types  (1-5):             0
Height of Section:                         400      mm
Distance to Moment Axis:                   264      mm
Shear Y/N 'Yes/No':                          Y
   Web width  (bw)  :                      200      mm
   Shear depth (jd) :                      284      mm
   Distance to web strain ex :              93      mm
   Distance to center of web :             235      mm
   Longitudinal crack spacing:             327      mm
   Maximum Aggregate size    :              20      mm
Stirrups Y/N 'Yes/No':                       Y
   Transverse crack spacing  :             509      mm
   Area of Stirrups (Av)     :             100      mm^2
   Stirrup Spacing  (s)      :             175      mm
   Stirrup (Rebar) Type      :             3
Number of Concrete Layers (1-20):          16
   Layer      y       bottom width  top width   height      Type
   Number     [mm]        [mm]        [mm]        [mm]      Number
        1       0        200         200          25         1
        2      25        200         200          25         1
        3      50        200         200          25         1
        4      75        200         200          25         1
        5     100        200         200          25         1
        6     125        200         200          25         1
        7     150        200         200          25         1
        8     175        200         200          25         1
        9     200        200         200          25         1
       10     225        200         200          25         1
       11     250        200         200          25         1
       12     275        200         200          25         1
       13     300        800         800          25         1
       14     325        800         800          25         1
       15     350        800         800          25         1
       16     375        800         800          25         1
Number of Rebar Layers  (0-10) :           5
   Layer       y          Area       Type
   Number      [mm]       [mm^2]     Number
        1      374        200        2
        2      365        100        3
        3      315        100        3
        4      123       1400        1
        5       63       1400        1
Consider displaced Concrete Y/N:             N
Thermal & Shrinkage Strains Y/N :            N
Initial Strains              Y/N :           N
```

A4. "RESPONSE" Data File for TM500 - Region 2

```
Response Version 1 Data-File
Copyright 1990 A. Felber
Name of Section:                    TM500-WEST
Units M/U 'Metric/U.S.Customary':            M
Number of Concrete Types (1-5):              1
   Type          f'c        ec'        fcr     Tension Stiffening
   Number       [Mpa]  [Milli-Strain] [Mpa]    Factor
       1     41.20     -1.990       2.33       1.00
Number of Rebar Types  (1-5):                3
   Type  Elastic Modulus    fy         esh       esrupt       fu
   Number     [Mpa]          [Mpa]      [---Milli-Strain--]  [Mpa]
       1     200000        467     72.300    150.000        711
       2     200000        602     31.800     44.000        515
       3     198050        588     33.200     42.000        515
Number of Tendon Types  (1-5):               0
Height of Section:                         400      mm
Distance to Moment Axis:                   264      mm
Shear Y/N 'Yes/No':                          Y
   Web width  (bw)  :                      200      mm
   Shear depth (jd) :                      284      mm
   Distance to web strain ex :              93      mm
   Distance to center of web :             235      mm
   Longitudinal crack spacing:             327      mm
   Maximum Aggregate size    :              20      mm
Stirrups Y/N 'Yes/No':                       Y
   Transverse crack spacing  :             509      mm
   Area of Stirrups (Av)     :             100      mm^2
   Stirrup Spacing  (s)      :             175      mm
   Stirrup (Rebar) Type      :               3
Number of Concrete Layers (1-20):           16
   Layer      y       bottom width  top width   height      Type
   Number    [mm]        [mm]         [mm]        [mm]       Number
       1        0        200          200          25         1
       2       25        200          200          25         1
       3       50        200          200          25         1
       4       75        200          200          25         1
       5      100        200          200          25         1
       6      125        200          200          25         1
       7      150        200          200          25         1
       8      175        200          200          25         1
       9      200        200          200          25         1
      10      225        200          200          25         1
      11      250        200          200          25         1
      12      275        200          200          25         1
      13      300        800          800          25         1
      14      325        800          800          25         1
      15      350        800          800          25         1
      16      375        800          800          25         1
Number of Rebar Layers  (0-10) :             5
   Layer       y          Area       Type
   Number     [mm]        [mm^2]     Number
       1      374         200        2
       2      365         100        3
       3      315         100        3
       4      123        1400        1
       5       63        1400        1
Consider displaced Concrete Y/N:             N
Thermal & Shrinkage Strains Y/N :            N
Initial Strains             Y/N :            N
```

A5. "RESPONSE" Data File for Beam A - Region 1

```
Response Version 1 Data-File
Copyright 1990 A. Felber
Name of Section:                          A-WEST
Units M/U 'Metric/U.S.Customary':            M
Number of Concrete Types (1-5):              1
   Type          f'c        ec'        fcr      Tension Stiffening
   Number       [Mpa]   [Milli-Strain] [Mpa]    Factor
       1     39.10    -2.000      2.06       1.00
Number of Rebar Types  (1-5):                3
   Type  Elastic Modulus    fy         esh       esrupt       fu
   Number     [Mpa]          [Mpa]     [---Milli-Strain--]  [Mpa]
       1    209400        430     72.300   200.000        680
       2    200000        430      7.500   200.000        630
       3    200340        407      7.500   200.000        630
Number of Tendon Types  (1-5):               0
Height of Section:                           400      mm
Distance to Moment Axis:                     264      mm
Shear Y/N 'Yes/No':                             Y
   Web width  (bw)  :                        200      mm
   Shear depth (jd) :                        283      mm
   Distance to web strain ex :                94      mm
   Distance to center of web :               236      mm
   Longitudinal crack spacing:               324      mm
   Maximum Aggregate size    :                20      mm
Stirrups Y/N 'Yes/No':                          Y
   Transverse crack spacing  :               286      mm
   Area of Stirrups (Av)     :               142      mm^2
   Stirrup Spacing  (s)      :               120      mm
   Stirrup (Rebar) Type      :               3
Number of Concrete Layers (1-20):           16
   Layer      y       bottom width  top width   height      Type
   Number     [mm]        [mm]        [mm]        [mm]      Number
       1        0        200        200         25         1
       2       25        200        200         25         1
       3       50        200        200         25         1
       4       75        200        200         25         1
       5      100        200        200         25         1
       6      125        200        200         25         1
       7      150        200        200         25         1
       8      175        200        200         25         1
       9      200        200        200         25         1
      10      225        200        200         25         1
      11      250        200        200         25         1
      12      275        200        200         25         1
      13      300        800        800         25         1
      14      325        800        800         25         1
      15      350        800        800         25         1
      16      375        800        800         25         1
Number of Rebar Layers  (0-10) :             4
   Layer      y          Area       Type
   Number     [mm]       [mm^2]    Number
       1      374        200       2
       2      363        200       2
       3      124       1400       1
       4       64       1400       1
Consider displaced Concrete Y/N:                N
Thermal & Shrinkage Strains Y/N :               N
Initial Strains             Y/N :               N
```

A6. "RESPONSE" Data File for Beam A - Region 2

```
Response Version 1 Data-File
Copyright 1990 A. Felber
Name of Section:                          A-WEST
Units M/U 'Metric/U.S.Customary':            M
Number of Concrete Types (1-5):              1
   Type          f'c        ec'        fcr      Tension Stiffening
   Number       [Mpa]  [Milli-Strain] [Mpa]     Factor
       1     39.10    -2.000       2.06        1.00
Number of Rebar Types  (1-5):                3
   Type  Elastic Modulus   fy        esh       esrupt       fu
   Number     [Mpa]          [Mpa]     [---Milli-Strain--]  [Mpa]
       1    209400        430    72.300    200.000        680
       2    200000        430     7.500    200.000        630
       3    200340        407     7.500    200.000        630
Number of Tendon Types  (1-5):               0
Height of Section:                           400      mm
Distance to Moment Axis:                     264      mm
Shear Y/N 'Yes/No':                            Y
   Web width  (bw)  :                        200      mm
   Shear depth (jd) :                        283      mm
   Distance to web strain ex :                94      mm
   Distance to center of web :               236      mm
   Longitudinal crack spacing:               324      mm
   Maximum Aggregate size    :                20      mm
Stirrups Y/N 'Yes/No':                         Y
   Transverse crack spacing  :               378      mm
   Area of Stirrups (Av)     :               142      mm^2
   Stirrup Spacing  (s)      :                80      mm
   Stirrup (Rebar) Type      :               3
Number of Concrete Layers (1-20):           16
   Layer      y       bottom width  top width   height      Type
   Number     [mm]        [mm]        [mm]        [mm]      Number
       1        0        200         200         25         1
       2       25        200         200         25         1
       3       50        200         200         25         1
       4       75        200         200         25         1
       5      100        200         200         25         1
       6      125        200         200         25         1
       7      150        200         200         25         1
       8      175        200         200         25         1
       9      200        200         200         25         1
      10      225        200         200         25         1
      11      250        200         200         25         1
      12      275        200         200         25         1
      13      300        800         800         25         1
      14      325        800         800         25         1
      15      350        800         800         25         1
      16      375        800         800         25         1
Number of Rebar Layers  (0-10) :             4
   Layer       y          Area       Type
   Number     [mm]        [mm^2]    Number
       1      374         200       2
       2      363         200       2
       3      124        1400       1
       4       64        1400       1
Consider displaced Concrete Y/N:               N
Thermal & Shrinkage Strains Y/N :              N
Initial Strains             Y/N :              N
```

A7. "RESPONSE" Data File for Beam B - Region 1

```
Response Version 1 Data-File
Copyright 1990 A. Felber
Name of Section:                    B-WEST
Units M/U 'Metric/U.S.Customary':      M
Number of Concrete Types (1-5):        1
   Type          f'c        ec'       fcr     Tension Stiffening
   Number       [Mpa]  [Milli-Strain] [Mpa]   Factor
       1     39.10    -2.000      2.06      1.00
Number of Rebar Types  (1-5):          3
   Type  Elastic Modulus   fy        esh      esrupt      fu
   Number    [Mpa]          [Mpa]     [---Milli-Strain--]  [Mpa]
       1    209400       430    72.300   200.000       680
       2    200000       430     7.500   200.000       630
       3    200340       407     7.500   200.000       630
Number of Tendon Types  (1-5):         0
Height of Section:                     400     mm
Distance to Moment Axis:               264     mm
Shear Y/N 'Yes/No':                      Y
   Web width  (bw)  :                  200     mm
   Shear depth (jd) :                  283     mm
   Distance to web strain ex :          94     mm
   Distance to center of web :         236     mm
   Longitudinal crack spacing:         324     mm
   Maximum Aggregate size    :          20     mm
Stirrups Y/N 'Yes/No':                   Y
   Transverse crack spacing  :         363     mm
   Area of Stirrups (Av)     :         142     mm^2
   Stirrup Spacing  (s)      :         170     mm
   Stirrup (Rebar) Type      :         3
Number of Concrete Layers (1-20):      16
   Layer      y       bottom width  top width   height      Type
   Number     [mm]       [mm]         [mm]        [mm]       Number
       1        0       200       200         25        1
       2       25       200       200         25        1
       3       50       200       200         25        1
       4       75       200       200         25        1
       5      100       200       200         25        1
       6      125       200       200         25        1
       7      150       200       200         25        1
       8      175       200       200         25        1
       9      200       200       200         25        1
      10      225       200       200         25        1
      11      250       200       200         25        1
      12      275       200       200         25        1
      13      300       800       800         25        1
      14      325       800       800         25        1
      15      350       800       800         25        1
      16      375       800       800         25        1
Number of Rebar Layers  (0-10) :       4
   Layer       y          Area       Type
   Number      [mm]       [mm^2]     Number
       1       374       200       2
       2       363       200       2
       3       124      1400       1
       4        64      1400       1
Consider displaced Concrete Y/N:          N
Thermal & Shrinkage Strains Y/N :         N
Initial Strains             Y/N :         N
```

A8. "RESPONSE" Data File for Beam B - Region 2

```
Response Version 1 Data-File
Copyright 1990 A. Felber
Name of Section:                        B-WEST
Units M/U 'Metric/U.S.Customary':            M
Number of Concrete Types (1-5):              1
   Type          f'c        ec'        fcr     Tension Stiffening
   Number       [Mpa]  [Milli-Strain] [Mpa]    Factor
       1     39.10    -2.000      2.06      1.00
Number of Rebar Types  (1-5):                3
   Type  Elastic Modulus   fy        esh      esrupt       fu
   Number     [Mpa]          [Mpa]     [---Milli-Strain--]  [Mpa]
       1    209400        430    72.300   200.000        680
       2    200000        430     7.500   200.000        630
       3    200340        407     7.500   200.000        630
Number of Tendon Types  (1-5):               0
Height of Section:                           400      mm
Distance to Moment Axis:                     264      mm
Shear Y/N 'Yes/No':                            Y
   Web width  (bw)  :                        200      mm
   Shear depth (jd) :                        283      mm
   Distance to web strain ex :                94      mm
   Distance to center of web :               236      mm
   Longitudinal crack spacing:               324      mm
   Maximum Aggregate size    :                20      mm
Stirrups Y/N 'Yes/No':                         Y
   Transverse crack spacing  :               455      mm
   Area of Stirrups (Av)     :               142      mm^2
   Stirrup Spacing  (s)      :               230      mm
   Stirrup (Rebar) Type      :               3
Number of Concrete Layers (1-20):           16
   Layer      y       bottom width  top width   height      Type
   Number     [mm]        [mm]         [mm]       [mm]       Number
       1        0        200        200          25         1
       2       25        200        200          25         1
       3       50        200        200          25         1
       4       75        200        200          25         1
       5      100        200        200          25         1
       6      125        200        200          25         1
       7      150        200        200          25         1
       8      175        200        200          25         1
       9      200        200        200          25         1
      10      225        200        200          25         1
      11      250        200        200          25         1
      12      275        200        200          25         1
      13      300        800        800          25         1
      14      325        800        800          25         1
      15      350        800        800          25         1
      16      375        800        800          25         1
Number of Rebar Layers  (0-10) :             4
   Layer       y          Area       Type
   Number      [mm]       [mm^2]     Number
       1       374        200        2
       2       363        200        2
       3       124       1400        1
       4        64       1400        1
Consider displaced Concrete Y/N:               N
Thermal & Shrinkage Strains Y/N :              N
Initial Strains             Y/N :              N
```